

CRITICAL BEHAVIOUR OF THE THERMODYNAMIC QUANTITIES CLOSE  
TO PHASE TRANSITIONS IN MOLECULAR CRYSTALS USING RAMAN  
DATA

A THESIS SUBMITTED TO  
THE GRADUATE SCHOOL OF NATURAL AND APPLIED SCIENCES  
OF  
MIDDLE EAST TECHNICAL UNIVERSITY

BY

HİLAL ÖZDEMİR

IN PARTIAL FULFILLMENT OF THE REQUIREMENTS  
FOR  
THE DEGREE OF DOCTOR OF PHILOSOPHY  
IN  
PHYSICS

FEBRUARY 2017



Approval of the thesis:

**CRITICAL BEHAVIOUR OF THE THERMODYNAMIC QUANTITIES  
CLOSE TO PHASE TRANSITIONS IN MOLECULAR CRYSTALS USING  
RAMAN DATA**

submitted by **HİLAL ÖZDEMİR** in partial fulfillment of the requirements for the degree of **Doctor of Philosophy in Physics Department, Middle East Technical University** by,

Prof. Dr. Gülbin Dural Ünver  
Dean, Graduate School of **Natural and Applied Sciences**

Prof. Dr. Altuğ Özpineci  
Department, **Physics**

Prof. Dr. Hamit Yurtseven  
Supervisor, **Physics Dept., METU**

**Examining Committee Members:**

Prof. Dr. Barış Akaoğlu  
Physics Eng. Dept., Ankara University

Prof. Dr. Hamit Yurtseven  
Physics Dept., METU

Prof. Dr. Nizami Hasanlı  
Physics Dept., METU

Assoc. Prof. Dr. İsmail Rafatov  
Physics Dept., METU

Assoc. Prof. Dr. Emre Taşcı  
Physics Eng. Dept., Hacettepe University

Date:

**I hereby declare that all information in this document has been obtained and presented in accordance with academic rules and ethical conduct. I also declare that, as required by these rules and conduct, I have fully cited and referenced all material and results that are not original to this work.**

Name, Last Name : HİLAL ÖZDEMİR

Signature :

## **ABSTRACT**

### **CRITICAL BEHAVIOUR OF THE THERMODYNAMIC QUANTITIES CLOSE TO PHASE TRANSITIONS IN MOLECULAR CRYSTALS USING RAMAN DATA**

Özdemir, Hilal

Ph.D., Department of Physics

Supervisor : Prof. Dr. Hamit Yurtseven

February 2017, 124 pages

In this thesis we investigate the pressure and temperature dependence of the Raman frequencies for different modes of benzene at ambient conditions ( $P=0$  GPa and  $T=300$  K). By using the experimental data we calculated the volume and frequency as a function of pressure at constant temperature and as a function of temperature at constant pressure, thus isothermal and isobaric mode Grüneisen parameter has been inferred in the different modes. Our calculations show that calculated Raman frequencies agree well with the observed data for each mode in solid benzene. In a more generalized way, Raman frequencies were calculated as a function of pressure and temperature for different modes of solid naphthalene and anthracene. Our calculations are in a good agreement with the observed data.

Thermodynamic quantities such as heat capacity  $C_p$ , entropy  $S$  was analyzed using the experimental data at various temperatures and pressures through the Raman frequencies and crystal volume for the different modes in solid benzene, naphthalene and anthracene. Our results agree better with the observed data at higher pressures and temperatures.

Also, quasi-harmonic approximation is used to calculate thermodynamic quantities for solid benzene, naphthalene and anthracene. Quasi-harmonic vibrational energy is defined as a function of temperature to originate of deriving other thermodynamic quantities of solid benzene, naphthalene and anthracene. When the experimental data is available our calculations through the quasi-harmonic vibrational energy can be compared with the observed data for solid benzene, naphthalene and anthracene.

Keywords: Raman frequency, Grüneisen parameter, Thermodynamic quantities, Phase transitions, Quasi-harmonic approximation

## ÖZ

# MOLEKÜLER KRİSTALLERDE RAMAN VERİSİ KULLANARAK FAZ GEÇİŞLERİ YAKININDA TERMODİNAMİK NİCELİKLERİN KRİTİK DAVRANIŞI

Özdemir, Hilal

Doktora, Fizik Bölümü  
Tez Yöneticisi: Prof. Dr. Hamit Yurtseven

Şubat 2017, 143 sayfa

Bu tezde uygun ortam koşullarında ( $P=0$  GPa ve  $T=300$  K) benzenin farklı modları için Raman frekanslarının sıcaklık ve basınç bağımlılıkları incelendi. Kristal hacmi ve frekans, deneysel veriler kullanılarak, sabit sıcaklıkta basıncın ve sabit basınçta sıcaklığın fonksiyonu olarak hesaplandı, böylece farklı modlar için izotermal ve izobarik mod Grüneisen parametreleri tanımlanmış oldu. Farklı modlar için hesaplanan frekans değerleri deneysel verilerle uyumlu bulunmuştur. Genelleme yapılarak, Raman frekansları basıncın ve sıcaklığın fonksiyonu olarak farklı modlar için naftalin ve antrasen için de hesaplandı. Naftalin ve antrasen için yapılan hesaplamalar deneysel verilerle uyumlu bulunmuştur.

Isı kapasitesi  $C_p$ , entropi  $S$  gibi termodinamik nicelikler, katı benzen, naftalen ve antrasene ait farklı modlar için Raman frekansları ve kristal hacmi boyunca çeşitli sıcaklık ve basınçtaki deney verileri kullanılarak analiz edildi. Sonuçlarımız daha yüksek basınç ve sıcaklıklarda gözlenen verilerle daha iyi uyumaktadır.

Ayrıca, yarı-harmonik yaklaşım kullanılarak katı benzen, naftalin ve antrasene ait termodinamik nicelikler hesaplandı. Quasi harmonik titreşim enerjisi, katı benzen, naftalin ve antrasene ait diğer termodinamik niceliklerin basıncın ve sıcaklığın fonksiyonu olarak türetilmesinde kullanıldı. Literatürde deneysel veriler mümkün

olduğunda, yarı harmonik titreşim enerjisiyle hesaplamalarımız, katı benzen, naftalin ve antrasen için gözlemlenen verilerle karşılaştırılabilir.

Anahtar Kelimeler: Raman frekansı, Grüneisen parametresi, termodinamik nicelikler, faz geçişleri, yarı harmonik yaklaşım



To my dear family

## ACKNOWLEDGMENTS

I would like to express my deepest gratitude to my supervisor, Prof. Dr. Hamit Yurtseven, who have made this dissertation possible. His excellent supervision, patient guidance, encouragement, friendly attitude, being accessible and continuous support provided the impetus for successful completion of this work.

I would like to thank the members of my supervisory committee for their thoughtful comments during the course of my dissertation work; Assoc. Prof. Dr. BARIŞ AKAOĞLU and Assoc. Prof. Dr. İSMAİL RAFATOV. I would also want to thank Prof. Dr. NİZAMİ HASANLİ and Assoc. Prof. Dr. EMRE TAŞCI for serving as my committee members.

Over my graduate experience at Middle East Technical University, I owe my gratitude to all the people for the mentoring, support, encouragement, and contributions in my academic career.

The most importantly I would like to thank to my big family for their moral support, encouragement and patience during my study and throughout all my life. Their generosity will always be in my heart and encourage me to overcome any difficulties in my life.

## TABLE OF CONTENTS

ABSTRACT .....	v
ÖZ .....	vii
ACKNOWLEDGMENTS .....	x
TABLE OF CONTENTS .....	xi
LIST OF TABLES .....	xiv
LIST OF FIGURES .....	xviii
1. INTRODUCTION .....	1
1.1 Phase Transitions .....	4
1.2 Raman Effect .....	7
1.2.1 The Raman Effect on Crystals .....	8
1.3 Scattering Theory .....	10
2. THEORY .....	11
2.1. Phase Transition .....	11
2.1.1 Classification of Phase Transitions .....	11
2.2 GRUNEISEN PARAMETER .....	13
2.3 ORDER PARAMETER .....	14
2.4 PIPPARD RELATIONS .....	15
3. CALCULATIONS AND RESULTS .....	21
3.1.1. Calculation of the Raman Frequency as a Function of Pressure and Temperature for the Hydrocarbons: Benzene, Naphthalene and Anthracene .....	21
3.1.1 Pressure Dependence of the Raman Frequencies at Ambient Temperature for Solid Benzene .....	22

3.1.1.1 For the Modes I, II and III at Constant Temperatures in Phase II of Benzene	22
3.1.1.2 For Phonon Modes of Solid Benzene I at Room Temperature .....	29
3.1.2 <i>Naphtalene</i> .....	35
3.1.3 Anthracene .....	43
3.2 Calculation of the Raman Frequency as a Function of Temperature for the Hydrocarbons: Benzene, Naphthalene and Anthracene .....	51
3.2.1 Benzene .....	51
3.2.2 <i>Naphthalene</i> .....	56
3.2.3 Anthracene .....	64
3.3 <i>Calculation of the Specific Heat as a Function of Temperature Using the Raman Frequency Shifts for Hydrocarbons</i> .....	69
3.3.1 <i>Benzene</i> .....	69
3.3.1.1 Calculation of Heat Capacity at P=0.1 GPa .....	71
3.3.2 <i>Naphthalene</i> .....	75
3.3.3 Anthracene .....	78
3.4 <i>Calculation of the Specific Heat Under Pressure by Using the Raman Frequency Shifts for Hydrocarbons</i> .....	80
3.4.1 <i>Benzene</i> .....	80
3.4.1.1 Pressure Dependence of Heat Capacity for Benzene Close to the I-II Phase Transition at Room Temperature .....	83
3.4.2 Naphthalene.....	85
3.4.3 <i>Anthracene</i> .....	86
3.5 Calculation of Change in Entropy Under Temperature .....	89
3.5.1 Benzene .....	89
3.5.2 Naphthalene.....	90
3.5.3 Anthracene .....	92

3.6	Derived Thermodynamic Quantities by Quasi Harmonic Free Energy of Solid Benzene, Naphthalene and Anthracene as Hydrocarbon.....	94
3.6.1	Calculation of the Vibrational Free Energy for Benzene.....	95
3.6.2	Entropy Derived from the Vibrational Free Energy for Benzene ....	96
3.6.3	The Heat Capacity at Constant Volume Derived from the Vibrational Free Energy for Benzene .....	97
3.6.4	Analysis of Free Energy for Naphthalene.....	98
3.6.5	Derived Entropy by Free Energy for Naphthalene .....	99
3.6.6	The Heat Capacity at Constant Volume Derived from the Vibrational Free Energy for Naphthalene .....	100
3.6.7	Calculation of the Vibrational Free Energy for Anthracene .....	101
3.6.8	Entropy Derived from the Vibrational Free Energy for Anthracene	102
3.6.9	The Heat Capacity at Constant Volume ( $C_v$ ) Derived from the Vibrational Free Energy for Anthracene.....	103
3.7	Application of Vinet Equation of State for Benzene at Constant Temperatures.....	106
4.	CONCLUSIONS.....	113
	REFERENCES .....	117
	CURRICULUM VITAE .....	123

## LIST OF TABLES

### Tables

Table 2.1 Definitions of critical exponents .....	33
Table 3.1 Coefficients $a_0$ , $a_1$ and $a_2$ as determined by Equation (3.1) for the volume of solid benzene with the uncertainties. $V_0$ value is also given. ....	44
Table 3. 2 Coefficients $c_0$ , $c_1$ and $c_2$ which were found according to Equation (3.3) using the observed data [11,17] for the modes indicated with the uncertainties for the phase II of benzene. $\vartheta_0$ value is also given.....	44
Table 3. 3 Coefficients $a'$ , $b'$ and $c'$ which were determined according to Equation (3.5) using the observed frequencies [11] which were obtained at 300 K (modes I and II) and at 450 K for mode III of benzene. ....	45
Table 3. 4 Coefficients $c_0$ , $c_1$ and $c_2$ which were determined according to Eq. (3.3) using the observed data [12] for the phonon modes of solid benzene I . We also give here the uncertainties determined for the coefficients $c_0$ , $c_1$ and $c_2$ for six phonon modes of solid benzene I. Calculated Raman frequency shifts are also represented at $P= 0$ GPa and $T= 300$ K.....	50
Table 3. 5 Coefficients $a'$ , $b'$ and $c'$ which were determined according to Equation (3.5) using the observed frequencies [12] which were obtained at 300 K for six phonon modes of solid benzene I.....	50
Table 3. 6 Coefficients $a_0$ , $a_1$ and $a_2$ as determined according to Equation (3.1) by using observed volume data [35] of solid naphthalene at room temperature. We also give here the uncertainties determined in the coefficients $a_0$ , $a_1$ and $a_2$ . ....	56
Table 3. 7 Coefficients $c_0$ , $c_1$ and $c_2$ which were found according to Eq. (3.3) using the observed data [35] for the modes indicated for solid naphthalene. We also give here the uncertainties determined for the coefficients $c_0$ , $c_1$ and $c_2$ for six modes of solid naphthalene. Values of the Raman frequencies for six modes of solid naphthalene at $P= 0$ GPa and $T= 300$ K, are also given here. ....	57

Table 3. 8 Coefficients $a'$ , $b'$ and $c'$ which were found according to Equation (3.5) using the observed frequencies [35] which were obtained at 300 K for six phonon modes of solid naphthalene.....	57
Table 3. 9 Values of the isothermal mode Gruneisen parameter $\gamma^T$ (Equation (2.9)) for the Raman modes showed at constant temperatures ( $P = 0$ ) for solid naphthalene. ....	60
Table 3.10 The $a_0$ , $a_1$ and $a_2$ values which were found according to the Equation (3.1) by using the experimental volume data [49] for six phonon modes of solid anthracene. We also give here the uncertainties determined in the coefficients $a_0$ , $a_1$ and $a_2$ for the volume of anthracene. ....	65
Table 3. 11 Coefficients $c_0$ , $c_1$ and $c_2$ which were found according to Eq. (3.3) using the observed data [49] for the modes indicated for solid anthracene. We also give here the uncertainties determined for the coefficients $c_0$ , $c_1$ and $c_2$ for six modes of solid anthracene. The values of the Raman frequencies for six modes of solid anthracene at $P = 0$ GPa and $T = 300$ K, are also given here.....	66
Table 3. 4 Calculated isothermal mode Grüneisen parameter (Equation (2.10)) for the six phonon and nine vibron modes of solid anthracene ( $P = 0$ GPa). Observed data [49] is also given. ....	70
Table 3.12 Coefficients $b_0$ , $b_1$ and $b_2$ as determined by Eq. (3.2) for the phonon modes of solid benzene. We also give here the uncertainties determined in the coefficients $b_0$ , $b_1$ and $b_2$ for the mentioned modes of benzene. ....	74
Table 3.13 Coefficients $d_0$ , $d_1$ and $d_2$ which were found according to Eq. (3.4) using the observed data [12] for the phonon modes of solid benzene I. We also give here the uncertainties determined for the coefficients $d_0$ , $d_1$ and $d_2$ for six phonon modes of solid benzene I. Calculated Raman frequency shifts are also represented at $P = 0$ GPa and $T = 300$ K. ....	74
Table 3. 15 Coefficients $b_0$ , $b_1$ and $b_2$ as determined according to Equation (3.2) by using observed data [35] of solid naphthalene at room temperature. We also give here the uncertainties determined in the coefficients $b_0$ , $b_1$ and $b_2$ . ....	79

Table 3. 16 Coefficients $d_0$ , $d_1$ and $d_2$ which were found according to Eq. (3.4) using the observed data [35] for the modes indicated for solid naphthalene. We also give here the uncertainties determined for the coefficients $d_0$ , $d_1$ and $d_2$ for six modes of solid naphthalene. Values of the Raman frequencies for six modes of solid naphthalene at $P = 0$ GPa and $T = 300$ K, are also given here. ....	79
Table 3. 17 The $a$ , $b$ and $c$ coefficients which were found according to Equation (3.10) using the observed frequencies [35] which were obtained at zero pressure for six phonon modes of solid naphthalene. ....	80
Table 3. 18 The isobaric mode Gruneisen parameter $\gamma_p$ (Equation (2.9)) values for the Raman modes indicated as a function of temperature for solid naphthalene. .	84
Table 3. 19 Coefficients $b_0$ , $b_1$ and $b_2$ as determined according to Equation (3.2) by using observed data [49] for solid anthracene at room temperature. We also give here the uncertainties determined in the coefficients $b_0$ , $b_1$ and $b_2$ for the mentioned modes of naphthalene. ....	87
Table 3. 20 Coefficients $d_0$ , $d_1$ and $d_2$ which were found according to Eq. (3.4) using the observed data [49] for the modes indicated for solid anthracene. We also give here the uncertainties determined for the coefficients $d_0$ , $d_1$ and $d_2$ for six modes of solid anthracene. Values of the Raman frequencies for six modes of solid anthracene at $P = 0$ GPa and $T = 300$ K, are also given here. ....	87
Table 3. 21 Values of constant molar volume of benzene at $p = 0$ GPa ( $V_0$ ) and at $T = 300$ K ( $V_0'$ ) [12]. Values of constant thermal expansion (Equation (2.24)) at $p = 0$ GPa and constant isothermal compressibility (Equation (2.26)) at $T = 300$ K in the phases I-II of solid benzene. ....	92
Table 3. 22 Values of the cell volume at ambient pressure $V_0$ , the isothermal bulk modulus $B_0$ and $C_0$ which is the derivative of the isothermal bulk modulus with respect to the pressure at 450 K. ....	128



Table 3. 23 Values of the cell volume at ambient pressure  $V_0$ , the isothermal bulk modulus  $B_0$  and  $C_0$  (derivative of the isothermal bulk modulus with respect to the pressure at room temperature).....129

Table 3.67 Coefficients  $e_0, e_1$  and  $e_2$  as determined according to Equation (3.50) by using observed data [12] for six phonon modes of solid benzene. We also give here the difference between the calculated Raman frequency at zero pressure and room temperature.....131

## LIST OF FIGURES

### Figures

Figure 1. 1 Experimentally constructed phase diagrams of benzene, (a) [12] and (b) [11].....	26
Figure 1.2 Crystallographic simulation of orthorhombic Pbc <sub>a</sub> (a) and monoclinic P2 <sub>1</sub> /c structure (b) of solid benzene. ....	28
Figure 1. 3 Schematic diagram for Raman scattering process [61] .....	8
Figure 1. 4 Schematic diagram of Raman scattering arising with a created phonon or an absorbed phonon [61] .....	8
Figure 3.1 Raman spectra of modes I, II and III for solid benzene at 294 K studied from Thiery and Leger [12].....	23
Figure 3. 2 Isothermal mode Grüneisen parameter as a function of pressure (Equation (2.10)) for the Raman modes I, II (300 K) and III (450 K) for the phase II of solid benzene.....	25
Figure 3. 3 Calculated Raman frequencies for mode I at various pressures (T=300K) for phase II of benzene. Experimental data [12] are also plotted.....	25
Figure 3. 4 Found Raman frequencies of mode II at various pressures (T=300K) for phase II of benzene. Also the experimental data [12] are plotted. ....	26
Figure 3. 5 Found Raman frequencies of mode III at various pressures (T=450K) for phase II of benzene. Also experimental data [12] are plotted. ....	26
Figure 3. 6 Uncertainties in the Raman frequencies calculated for the modes I, II and III at various pressures for phase II of benzene. ....	29
Figure 3. 7 Isothermal mode Grüneisen parameter as a function of pressure (Equation (2.13)) for phonon modes of solid benzene I at room temperature.....	31
Figure 3. 8 <i>Calculated Raman frequencies as a function of pressure at room temperature according to Equation (2.12) by using the observed data [12] for six phonon modes of solid benzene I.....</i>	31

Figure 3. 9 Pressure dependence of the Raman frequencies (Equation (2.12)) at room temperature for solid benzene I are defined with black squares (Mode A), blue triangles (Mode B) and green squares (Mode C). Observed data [12] is also given with red circles (Mode A), purple triangles (Mode B) and navy blue triangles (Mode C), respectively. ....32

Figure 3. 10 Pressure dependence of the Raman frequencies (Equation (2.12)) at room temperature for solid benzene I are defined with black squares (Mode X), grey triangles (Mode Y) and grey squares (Mode Z). Observed data [12] is also given with green circles (Mode X), green triangles (Mode Y) and navy blue triangles (Mode Z), respectively. ....32

Figure 3.11 Uncertainties in the calculated Raman frequencies as a function of pressure for lattice modes for solid benzene according to Equation (2.10). ....35

Figure 3.12 The measured Raman frequencies as a function of pressure at room temperature for modes of symmetry  $A_g$  for solid naphthalene (filled squares) according to Equation (2.12) and the experimental data of  $A_g$  modes [35] for solid naphthalene (filled circles) is also given. ....37

Figure 3.13 The measured Raman frequencies as a function of pressure at room temperature for modes of symmetry  $B_g$  for solid naphthalene (filled squares) according to Equation (2.12) and the experimental data of  $B_g$  modes [35] for solid naphthalene (filled circles) is also given. ....38

Figure 3. 14 Uncertainties in the Raman frequencies calculated for modes of symmetry  $B_g$  for solid naphthalene according to Equation (2.12). ....42

Figure 3.16 The found Raman frequencies of six phonon modes of solid anthracene as a function of pressure according to Equation (2.12). ....45

Figure 3.17 The found Raman frequencies for the phonon modes as a function of pressure at room temperature according to Equation (3.6) for crystalline anthracene. ....45

Figure 3.18 The found Raman frequencies for the phonon modes as a function of pressure at room temperature according to Equation (3.6) for crystalline anthracene. ....46

Figure 3.19 The found Raman frequencies of nine vibron modes of solid anthracene as a function of pressure according to Equation (3.6).....	46
Figure 3.20 Uncertainties in the Raman frequencies calculated for modes of solid anthracene according to Equation (3.6).....	50
Figure 3.21 Uncertainties in the Raman frequencies calculated for modes of solid anthracene according to Equation (3.6).....	50
Figure 3.22 Calculated Raman frequencies as a function of temperature at zero pressure according to Equation (3.7) by using the observed data [12] for six phonon modes of solid benzene I.....	52
Figure 3. 23 Temperature dependence of the Raman frequencies (Equation (3.7)) at zero pressure for solid benzene I are defined with red circles (Mode A), purple triangles (Mode B) and green squares (Mode C). Observed data [12] are also given with black squares (Mode A), blue triangles (Mode B) and green squares (Mode C), respectively.....	53
Figure 3. 24 Temperature dependence of the Raman frequencies (Equation (3.7)) at zero pressure for solid benzene I are defined with red circles (Mode X), purple triangles (Mode Y) and green squares (Mode Z). Observed data [12] are also given with black squares (Mode X), blue triangles (Mode Y) and green squares (Mode Z), respectively.....	53
Figure 3. 25 Uncertainties in the Raman frequencies calculated for modes of solid benzene according to Equation (3.7).....	56
Figure 3. 26 The determined Raman frequencies as a function of temperature at atmospheric pressure for mode of symmetry $A_g$ for solid naphthalene (filled squares) according to Equation (2.11) and the experimental data of $A_g$ modes [33] for solid naphthalene (filled circles).....	58
Figure 3. 27 The determined Raman frequencies as a function of temperature at atmospheric pressure for mode of symmetry $B_g$ for solid naphthalene (filled squares) according to Equation (2.11) and the experimental data of $B_g$ modes [35] for solid naphthalene (filled circles).....	59

Figure 3. 28 Uncertainties in the Raman frequencies calculated for modes of symmetry $A_g$ for solid naphthalene according to Equation (2.11).....	63
Figure 3. 29 Uncertainties in the Raman frequencies calculated for modes of symmetry $B_g$ for solid naphthalene according to Equation (2.11).....	63
Figure 3. 30 Calculated Raman frequencies for the phonon modes as a function of temperature at $P=0$ GPa according to Equation (3.9) for crystalline anthracene..	66
Figure 3. 31 Calculated Raman frequencies for the nine vibron modes as a function of temperature at $P=0$ GPa according to Equation (3.9) for crystalline anthracene.	66
Figure 3. 32 Calculated heat capacity as a function of temperature according to Equation (2.44) for the I-II transition ( $p_c=0$ GPa, $T_c=300$ K) in benzene. ....	70
Figure 3. 33 Pressure dependence of heat capacity per unit volume $\rho C_p$ due to total six modes correspond to phase I-II of solid benzene at 0.1 GPa. ....	72
Figure 3. 34 Calculated heat capacity per unit volume due to the total six lattice modes in phases I-II of solid benzene at $p=0.1$ GPa according to Equation (2.45). Observed data [4] is also given here for comparison. ....	73
Figure 3. 35 Calculated heat capacity as a function of temperature according to Equation (2.54) for the I-II transition ( $p_c=0$ GPa, $T_c=300$ K) in benzene. ....	75
Figure 3. 36 Calculated total heat capacity of six lattice modes of solid naphthalene (Equation (3.44)) by using the observed data [35] as a function of temperature...	76
Figure 3. 37 Calculated heat capacity due to the total six lattice modes of solid naphthalene at $p=0$ GPa according to Equation (2.45). Observed data [24] is also given here for comparison.....	77
Figure 3. 38 Heat capacity determined as a function of temperature (Equation (2.44)) at zero pressure ( $P=0$ GPa) using the Raman frequencies of the total six phonon modes of solid anthracene.....	78
Figure 3. 39 Heat capacity determined as a function of temperature at zero pressure ( $P=0$ GPa) using the Raman frequencies of the total nine vibron modes of solid anthracene. ....	79

Figure 3. 40 The determined heat capacity due to the six phonon and nine vibron modes of solid naphthalene ( $P=0$ GPa) according to Equation (2.45). Observed data [68] are also given here for comparison. ....	79
Figure 3. 41 Total heat capacity due to the six modes of solid benzene which was calculated at various pressures at room temperature ( $T=300\text{K}$ ). ....	81
Figure 3. 42 Calculated heat capacity as a function of pressure according to Equation (2.55) for the I-II transition ( $p_C=1.3\text{GPa}$ , $T_C=300\text{K}$ ) in benzene. ....	82
Figure 3. 43 Calculated total heat capacity due to the six modes of benzene using the critical exponent ( $\phi_R=0.23$ ) as a function of pressure according to Equation (2.54) at room temperature ( $T=300\text{K}$ ). ....	84
Figure 3. 44 Calculated total heat capacity $C_p$ due to the six lattice modes as a function of pressure in the solid phases I-II of benzene at room temperature according to Equation (2.54). Observed $C_p$ data [4] for benzene are also plotted here for comparison.....	84
Figure 3. 45 Total heat capacity due to the six modes of solid naphthalene which was calculated at various pressures at room temperature ( $T=300\text{K}$ ). ....	86
Figure 3. 46 Total heat capacity due to the six phonon modes of solid anthracene, which was found as a function of pressure at room temperature ( $T=300\text{K}$ ). ....	87
Figure 3. 47 Total heat capacity due to the six vibron modes of solid anthracene, which was found as a function of pressure at room temperature ( $T=300\text{K}$ ). ....	87
Figure 3. 48 Change in the heat capacity $C_p$ due to the six lattice modes of solid anthracene as a function of pressure at room temperature ( $T=300\text{ K}$ ). ....	88
Figure 3. 49 Change in entropy due to the total six modes of the phases I-II of solid benzene (Equation (3.12)) from $T_{\min}$ to $T_{\max}$ at various temperatures. ....	89
Figure 3. 50 Change in entropy due to the total six modes of solid naphthalene (Equation (3.12)) from $T_{\min}$ to $T_{\max}$ at various temperatures. ....	90
Figure 3. 51 Change in entropy due to the total six modes of solid naphthalene (Equation (3.12)) is given in comparison with the observed data [24]. ....	91

Figure 3. 52 Change in the entropy ( $\Delta S$ ) due to the six phonon and nine vibron modes of solid anthracene (Equation (3.12)) at various temperatures ( $P=0$ ).....	92
Figure 3. 53 Change in the entropy ( $\Delta S$ ) due to the six vibron modes of solid anthracene (Equation (3.12)) at various temperatures ( $P=0$ ). ....	93
Figure 3. 54 Change in the entropy calculated (Equation (3.12)) due to the total six modes of solid anthracene. The observed data [69] are also shown for comparison.	93
Figure 3. 55 Calculated total free energy of six lattice modes (A,B,C and X,Y,Z) of solid benzene under temperature.....	95
Figure 3. 56 Total entropy (Equation (3.16)) due to the six lattice modes (A,B,C and X,Y,Z) of solid benzene as a function of temperature. ....	96
Figure 3. 57 Calculated total heat capacity (Equation (3.48)) of six lattice modes (A,B,C and X,Y,Z) of solid benzene as a function of temperature.....	98
Figure 3. 58 Free energy due to the six lattice modes of solid naphthalene at various temperatures. ....	99
Figure 3. 59 Derived total entropy (Equation (3.16)) due to the six lattice modes of solid naphthalene as a function of temperature.....	100
Figure 3. 60 Calculated heat capacity as a function of temperature (Equation (3.48)) of solid naphthalene. ....	101
Figure 3. 61 Vibrational free energy due to the six phonon and nine vibron modes of solid anthracene as a function of temperature according to Equation (3.14).....	102
Figure 3. 62 The total entropy derived (Equation 3.16) due to the six phonon and nine vibron modes of solid anthracene as a function of temperature.....	103
Figure 3. 63 The heat capacity $C_v$ calculated as a function of temperature (Equation 3.48) oduo to six phonon and nine vibron modes of solid anthracene.....	104
Figure 3. 64 The total entropy derived (Eq. 23) due to the six phonon and nine vibron modes of solid anthracene as a function of temperature. Solid naphthalene and benzene are also given in this figure for comparison. Squares are used for solid anthracene due to the six phonon and nine vibron modes, circles are used for solid	

naphthalene due to six lattice modes and triangles are used for solid benzene due to the six lattice modes. .... 105

Figure 3. 65 Heat capacity calculated (Equation (3.48)) as a function of temperature for solid anthracene, naphthalene and benzene. Squares are used for solid anthracene due to the six phonon and nine vibron modes, circles are used for solid naphthalene due to six lattice modes and triangles are used for solid benzene due to the six lattice modes..... 106

Figure 3. 66 Calculated equation of state according to Equation (3.49) of crystalline benzene at 540 K. Calculated equation of state (Equation (3.49)) is given with the solid line, experimental data [11] are given with the squares. .... 108

Figure 3. 67 Calculated equation of state according to Equation (3.49) of crystalline benzene at 300 K. Calculated equation of state (Equation (3.49)) is given with the solid line, experimental data [15] are given with the squares. .... 109

Figure 3.68 Suggested phase diagram due to Equation (3.50) for six phonon modes in phases I-I' in solid benzene. .... 111

Figure 3.69 Calculated temperature as a function of pressure according to Equation (3.50) for six phonon modes in phases I-I' of solid benzene. Observed data [12] is also given comparison in here. .... 111



## CHAPTER I

### INTRODUCTION

Hydrocarbons, as their name indicates, are known the simplest organic compounds containing just hydrogen and carbon atoms [1]. They are good fuels which generally occur naturally. Hydrocarbons have a carbon backbone which can be linear chain, ring or both of linear chain and ring with the attached hydrogen atoms [2]. In this thesis, we carried out our calculations for solid benzene, naphthalene and anthracene as in the same hydrocarbone groups. Hydrocarbons are commonly studied as aromatic compounds which require high pressures and temperatures to activate the reaction in aromatic rings. In this way, it is feasible to investigate the physical properties of hydrocarbons under a wide range of pressure and temperature. Since benzene, naphthalene and anthracene are composed of only hydrogen and carbon, they are hydrocarbons and are commonly investigated in the literature.

Benzene with a molecular formula  $C_6H_6$  is an organic chemical compound which contains a ring of six carbon atoms accompanied by one hydrogen atom bound to each carbon atom. In benzene as the prototype aromatic compound, pressures of some tenths of gigapascals and/or temperatures as high as hundreds of degrees Celcius are necessary for the reaction to occur [3]. Therefore, it is commonly used among the aromatic compounds to investigate the stability of the crystalline forms.

Both experimental and theoretical studies have been conducted to reveal thermodynamic properties of benzene. In addition to the measurements of volume as a function of pressure in the liquid and solid phases of benzene [4], the heat capacity and thermal conductivity of the solid phases I and II of benzene have been measured [5]. Thermal expansivity was measured in solid benzene close to the melting point [6]. Molar volume as functions of pressure [7] and temperature [8] has been

investigated in benzene close to the melting point. Based on the experimental data [6], the Pippard relations [9] close to the melting point in solid benzene were also demonstrated in a previous study [10]. Particularly, the pressure and temperature dependence of the thermodynamic quantities including the heat capacity, isothermal compressibility and thermal expansivity was calculated for the solid phase II of benzene in that study [10]. As noted above, many spectroscopic studies on the phase transitions of the solid phases and also near the melting point in benzene have been reported in the literature. Raman [3,11-15] and infrared [11,16,17] studies have been focused on the solid phases of benzene. We have also studied the pressure dependence of the Raman frequencies in benzene [18].

Numerous physical characteristics of naphthalene have been widely studied and different techniques have been used to investigate its structure [19-23]. In addition, thermodynamic properties of naphthalene have been investigated experimentally [24,25]. Phonon frequencies of naphthalene have been widely examined through the spectroscopic studies [21,27-31]. The analysis of X-ray and neutron diffraction data has provided to study the molecular motion in crystalline naphthalene [31]. In some previous studies, anharmonic frequency shifts were calculated for naphthalene with the help of various potential models for hydrocarbons [19,32-34]. We have also calculated Raman frequency shifts in naphthalene [35]. It has been revealed [36] that crystallization of naphthalene occurs in the monoclinic system with the two molecules in the unit cell and its space group is  $C_{2h}$ . This crystalline system contains three acoustic modes ( $A_u + 2B_u$ ), six Raman active librational modes ( $3A_g + 3B_g$ ) and three infrared active translational modes ( $2A_u + B_u$ ) [37].

Anthracene ( $C_{14}H_{10}$ ) has also been widely studied as an example of the polycene family [38,39] and various experimental techniques have been used to obtain its isothermal compressibility [40], the Hugoniot [41] and other physical properties [39] by means of spectroscopic data [42,43]. Temperature and pressure dependence of the Raman frequency shifts have been calculated in anthracene in our previous study [44].

As benzene and naphthalene, anthracene is in the hydrocarbon group with the same structure. At ordinary pressure and temperature, its stable phase is monoclinic, space group  $P2_1/a$ , with the lattice parameters of  $a = 8.562$ ,  $b = 6.038$ ,  $c = 11.184$  Å,  $\beta = 124.7^\circ$  and  $V = 475.35$  Å<sup>3</sup> at room temperature (290 K) with two molecules to the unit cell [45]. A new phase of anthracene has been investigated in terms of its structure and dynamics [46]. In addition, its low-temperature elastic properties [47] and the thermal motion [48] have been examined in previous studies.

Crystal structure of anthracene [49-51] and its isothermal compressibility [52] up to 45 kbar have been given in the literature in regarding the high pressure effect on the physical properties of anthracene. The density functional theory was used to investigate the pressure effect on the interior molecular orientation and it has been calculated up to 10.2 GPa [53].

A number of studies correlating between quantities and the spectroscopic parameters for benzene, naphthalene and anthracene have been reported in the literature, as also stated above. Those studies have mainly focused on the correlations between the crystal volume and the vibrational frequencies through the mode Grüneisen parameter. From the temperature and pressure dependencies of the volume and frequency, the mode Grüneisen parameter has been determined. For various phases of benzene, naphthalene and anthracene, the values of the mode Grüneisen parameters can be determined as a function of temperature or pressure for those hydrocarbons. Using the temperature or pressure dependence of the mode Grüneisen parameters and the volume data, the frequencies can be calculated and then compared with the experimental measurements close to the phase transitions in benzene, naphthalene and anthracene. On that basis, from the variation of the frequency with temperature and with pressure, thermal expansion and the isothermal compressibility, respectively, can be predicted as functions of temperature and pressure through the mode Grüneisen parameter by means of the thermodynamic relations close to the phase transitions in those organic molecular systems. Additionally, entropy and the specific heat can be calculated as functions of temperature and pressure from the frequency shifts close to the phase transitions in benzene, naphthalene and anthracene. Finally, P-T (or T-P) phase diagrams of those crystalline systems can be constructed from the frequency ( $\nu$ ) shifts

spectroscopically ( $P\theta T$ ) as obtained thermodynamically (PVT) in benzene, naphthalene and anthracene. This is the motivation of our study given here. In this thesis, we investigate various physical properties of benzene, naphthalene and anthracene close to the phase transitions using the experimental data from the literature. Raman frequencies were calculated as functions of temperature and pressure. Thermodynamic properties of benzene, naphthalene and anthracene were investigated through the mode Grüneisen parameter. Consequently, those properties were presented in the  $P\theta T$  system spectroscopically in relation to the PVT system through the volume dependence of the frequency (Grüneisen parameter). Calculations were carried out for a  $P\theta T$  system by the Raman frequency shifts close to the phase transitions. Heat capacity and entropy were calculated through the Raman frequency shifts with the pressure and temperature for solid benzene, naphthalene and anthracene, as we have also reported for benzene in our earlier study [54]. Similarly, thermodynamic quantities were calculated by using the quasi-harmonic approximation for benzene, naphthalene and anthracene through the Raman frequency shifts. A phase diagram between phases I and I' was suggested by using the Raman frequency shifts of solid benzene.

## **1.1 Phase Transitions**

A phase defines the several arrangements of the atoms, molecules or particles of a solid or liquid corresponding to the different properties which are uniform at the macroscopic level of the same solid or liquid substance. A phase transition can take place when a phase changes to another one. In a crystal, the phase transition is the consequence of the change in lattice symmetry. In other words it is a structural phase transition. [55]

There are two common suggested phase diagrams of solid benzene in the literature constructed experimentally [11,12] as shown in Figures (1a) and(1b), respectively.

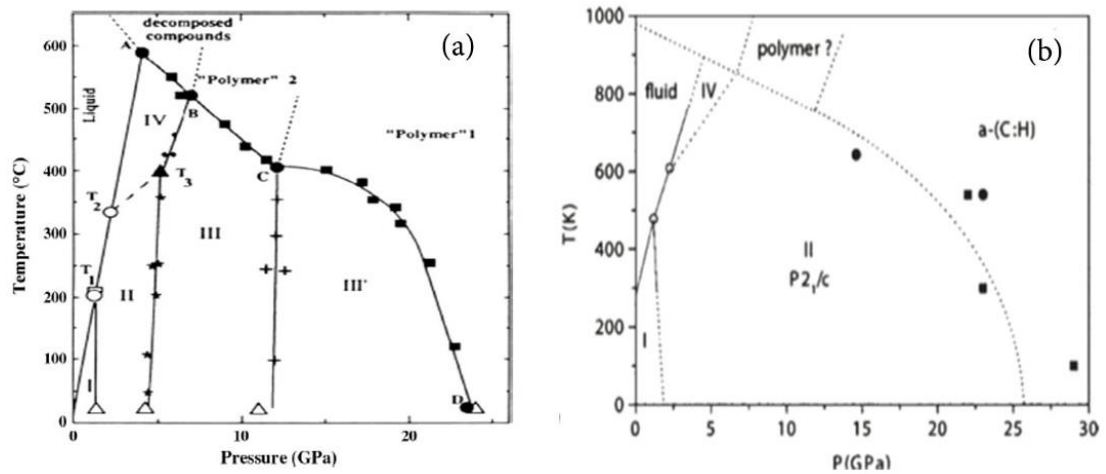


Figure 1. 1 Experimentally constructed phase diagrams of benzene, (a) [12] and (b) [11].

Suggested phase diagram of benzene possess five different solid phases as phases I, II, III [56,57], III' and IV [3,11,12]. Benzene crystallizes at normal pressure below 278.5 K with an orthorhombic Pbca structure (Figure 1.2a) and phase I occurs. Due to the discontinuities in the cell constants of phase I, Phase I' is suggested with the space group Cmca. Phase I is transformed into the phase II with the monoclinic P<sub>21/c</sub> structure (Figure 1.2b) at 1.2 GPa at 373 K [56]. The phase transition from benzene II to benzene III occurs at about 4 GPa and 373 K with the P<sub>21/c</sub> crystal structure (Figure 1.2a). The phase transition line between phase II and III is coarsely parallel to the temperature axis up to the point T<sub>3</sub> (340 °C and 5.1 GPa) (Figure 1.1a) and does not cross the melting line at the triple point T<sub>2</sub>. Up to the point B, this line diverges above the higher pressures. Phase III' with the same structure of phase III exists up to 11 GPa at 25°C. The transition line of phases III-III' is between 11 GPa at 25°C and 12 GPa at 410°C and it is stated that this line ends at point C (12 GPa at 410°C) [6]. Phase IV occurs at 24 GPa. From the existence of the triple point T<sub>2</sub> (335°C and 2.25 GPa) as the starting point and from this mild divergence of the equilibrium line of phases II and III, the point T<sub>3</sub> takes place, which can be considered as a triple point. Beyond the point C, an irreversible transformation of benzene occurs and thus the point C is not a triple point. Except the points A, B and C, the point D is placed at 25°C with the pressure of 24 GPa. Raman scattering [12], X-ray diffraction [11] and

infrared [11,58–62] were used to observe high pressure solid phases of benzene. The infrared spectroscopic study provided to obtain a chemical transformation of benzene under static pressurization to 30 GPa, as stated previously [3]. In a recent study, the pressure-induced phases of benzene have been examined through X-ray Raman spectroscopy [63].

Another phase diagram was constructed by Ciabini et al. [11] from infrared spectroscopy and X-ray analysis under high pressure (Figure 1b). At room temperature and above 0.07 GPa phase I occurs with the orthorhombic Pbca structure (Figure 1.2a). Phase I turns into phase II with the monoclinic  $P2_1/c$  structure (Figure 1.2b) at room temperature and 1.4 GPa and this phase is stable up to 20-25 GPa. There are three different solid phases as phase I (Pbca), phase II ( $P2_1/c$ ) and phase IV as a possible variant of phase II. Phase III occurs at room temperature and 4.8 GPa with the  $P2_1/c$  structure (Figure 1.2b) and the transition between phases III and III' occurs at room temperature and 11.2 GPa. A phase V was suggested through the higher temperatures [11].

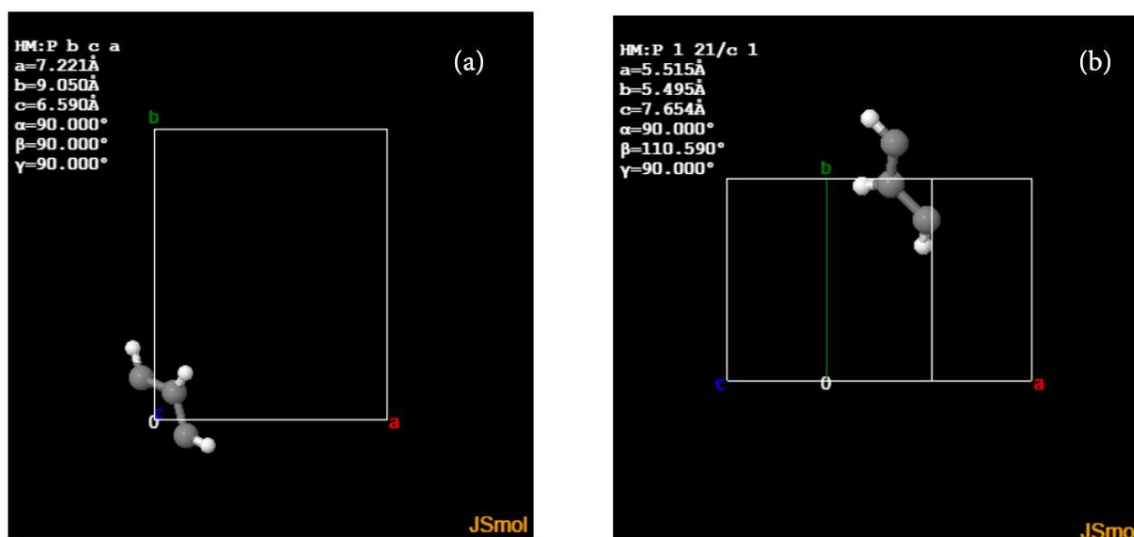


Figure 1.2 Crystallographic simulation of orthorhombic Pbca (a) and monoclinic  $P2_1/c$  structure (b) of solid benzene [64].

The difference between the two phase diagrams is originated from the technical improvements between the two experiments [65]. The first three phases of I, II and III as obtained experimentally are in good agreement with the theory. The other phases of solid benzene are more controversial. Phase III' may be only the distortion of phase III and phase IV, which can be formed with the new chemical bonds. It has been formed through the higher pressures. Remaining phases I' and V requires further experimental study in benzene.

## **1.2 Raman Effect**

Raman effect arises with a double transition of the three stationary levels, corresponding to the three levels are the initial k level, intermediate r level and final n level. In these levels, virtual level has an important situation to combine with other two levels; so if there isn't such a virtual level, we get a forbidden transition from k to n levels in Raman effect [66].

In Raman effect:

- I) the vibrations of a molecule produce changes in the induced electric moment of the molecule active
- II) the symmetrical oscillations of the molecule come out most prominently.

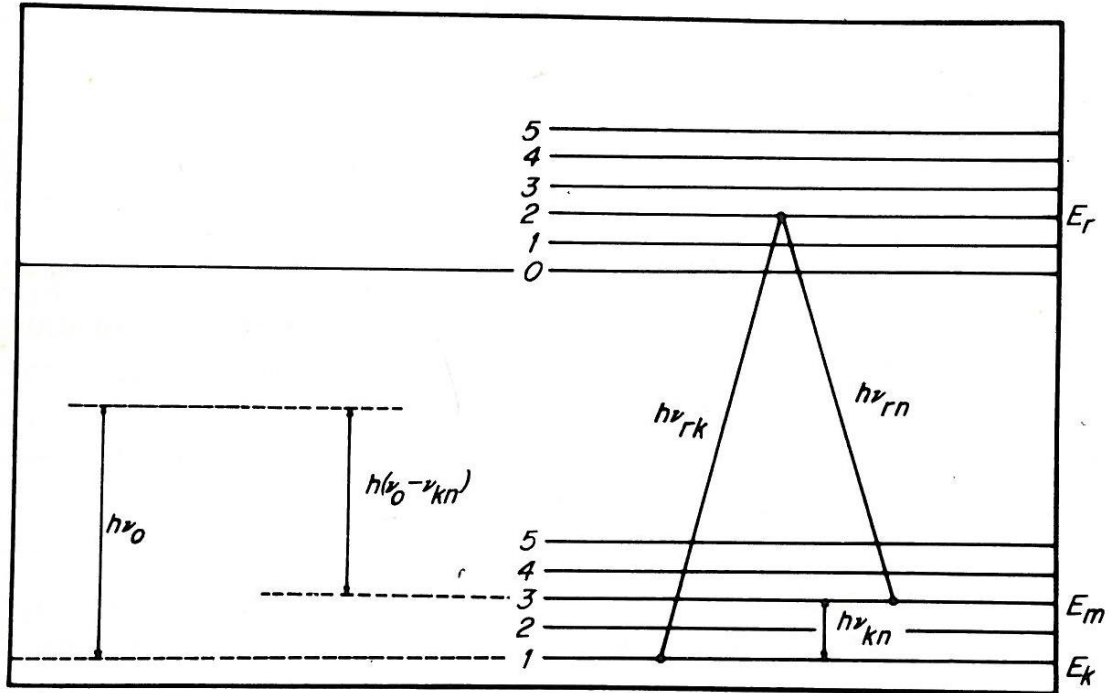


Figure 1. 3 Schematic diagram for Raman scattering process [66]

### 1.2.1 The Raman Effect on Crystals

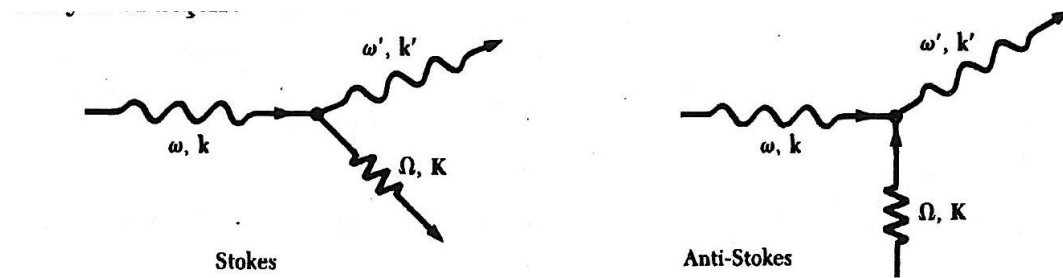


Figure 1. 4 Schematic diagram of Raman scattering arising with a created phonon or an absorbed phonon [66]

The Raman scattering includes two photons which are incident and scattered photons. The Raman effect gives rise to create a phonon with an inelastic scattering from crystal.



For the first order Raman effect;

$$w = w' \pm \Omega \quad (1.1)$$

$$\vec{k} = \vec{k}' \pm \vec{K} \quad (1.2)$$

$w, \vec{k}$  and  $w', \vec{k}'$  are the frequencies and wave vectors of incident and scattered photons.  $\Omega$  and  $\vec{K}$  are the frequency and wave vector of the created or annihilated phonon.

The Raman effect is possible with electronic polarizability which depends on stretch in lattice.

$$\alpha = \alpha_0 + \alpha_1 u + \alpha_2 u^2 + \dots \quad (1.3)$$

Equation (1.3) describes a series approximation of a phonon which has  $\alpha$ -polarization.  $u$  is the amplitude of phonon as given below:

$$u(t) = u_0 \cos \Omega t \quad (1.4)$$

and the incident electric field,

$$E(t) = E_0 \cos \omega t \quad (1.5)$$

Using Eqs. (1.4) and (1.5) in Eq. (1.3), we get;

$$\alpha_1 E_0 u_0 \cos \omega t \cos \Omega t = \frac{1}{2} \alpha_1 E_0 u_0 [\cos(\omega + \Omega)t + \cos(\omega - \Omega)t] \quad (1.6)$$

In Equation (1.6), a phonon with the  $\Omega$  frequency is created as photons with the frequencies of  $w+\Omega$  and  $w-\Omega$  frequencies. Here, photon with the  $w-\Omega$  frequency appears as a Stokes line in Raman spectra, while photon with the  $w+\Omega$  frequency appears as an anti-Stokes line. To make a simple choreography of the Raman effect, we can assume a collision that has energy conservation between a light quantum ( $\hbar\gamma$ ) and a molecule. If the incident light quantum has a loss of energy, the scattered radiation will appear as a Stokes line in the spectrum. Then the molecule excites to a higher level by taking up energy. If molecule is an excited state at first, then it can give its energy to the incident light quantum. It appears as an anti-Stokes line in the spectrum. So we can get the information about the rotational and vibrational frequencies of the molecule.

### 1.3 Scattering Theory

When photons scatter by a crystal inelastically, we get the Raman scattering. The probability of scattering by using golden rule of second order perturbation theory is given as,

$$w = \frac{2\pi}{\hbar} \rho(w_s) |H(\vec{k}_0, i; \vec{k}_s, f)|^2 \delta(\hbar w_0 + E_i - \hbar w_s - E_f) \quad (1.7)$$

where  $E_s$  is the energy of the initial state of crystal,  $E_f$  is the energy of final state and  $\rho(w_s)$  is the density of the states of photons. Incident photons have energy  $\hbar w_0$  with the momentum  $\vec{k}_0$  and the scattered photons have energy  $\hbar w_s$  with the momentum  $\vec{k}_s$  by a crystal. Hamiltonian  $H$  specifies the interaction between the photons and the crystal. The electric fields associated with the light almost result in Raman scattering cause of the sizes of atoms which are much smaller than the wavelength of the incident and scattered light [67].

## CHAPTER 2

### THEORY

#### 2.1. Phase Transition

A phase is defined as a state of material where its chemical properties are uniform and the physical properties are unique at macroscopic level. A phase transition is described as the change of the phase from one to another and energy is generally absorbed by or released from the system during a phase transition. The occurrence of a phase transition is a result of external condition such as pressure, temperature etc. changes and the value of these two external conditions at which the transformation occurs is defined as the phase transition point. As it is well known, matter has four phases which are called solid, liquid, gas and plasma.

##### 2.1.1 Classification of Phase Transitions

When the phase transition occurs between two different phases, three conditions must be satisfied as given below:

1. Temperature of the phase one ( $T_1$ ) must be equal to the temperature of the phase two ( $T_2$ ).

$$T_1 = T_2 \quad (2.1)$$

2. Pressure of the phase one ( $P_1$ ) must be equal to the pressure of the phase two ( $P_2$ ).

$$P_1 = P_2 \quad (2.2)$$

3. Chemical potential of the phase one ( $\mu_1$ ) must be equal to the chemical potential of the phase two ( $\mu_2$ ).

$$\mu_1 = \mu_2 \quad (2.3)$$

Under the condition of the two phases that have the same number of atoms, condition 3 can be generalized as the Gibbs free energy of the phase I must be equal to the phase II.

$$G_1(T, P) = G_2(T, P) \quad (2.4)$$

1. First Order Phase Transitions: First order phase transitions are induced by the first order derivatives of the thermodynamic potentials (i.e. volume and entropy) which are discontinuous with respect to the thermodynamical variables. So, the first order transitions occur with a density jump and a latent heat. Solid-liquid-gas transitions are the mentioned transitions and called the first kind phase transition or discontinuous phase transitions.

$$V = \left( \frac{\partial G}{\partial P} \right)_T \quad S = - \left( \frac{\partial G}{\partial T} \right)_P \quad (2.5)$$

2. Second Order Phase Transitions: The second derivative of the thermodynamic potential (i.e. isothermal compressibility  $\kappa_T$  and isobaric specific heat capacity  $C_P$ ) is discontinuous at the transition point while the first derivative of the free energy is continuous [68].

$$\kappa_T = - \frac{1}{V} \left( \frac{\partial V}{\partial P} \right)_T = - \frac{1}{V} \left( \frac{\partial^2 G}{\partial P^2} \right)_T \quad (2.6)$$

$$C_P = T \left( \frac{\partial S}{\partial T} \right)_P = - \left( \frac{\partial^2 G}{\partial T^2} \right)_P \quad (2.7)$$

## 2.2 GRUNEISEN PARAMETER

Grüneisen parameter as a dimensionless parameter is generally used to define the thermal and elastic features of solids at high pressures. Grüneisen parameter is useful to characterize the anharmonicity of solids in condensed matter and geophysics and predicting the Debye temperature for solids [69]. Grüneisen parameter has two definitions as macroscopic and microscopic Grüneisen parameter [70]. Macroscopic Grüneisen parameter is used to characterize the thermodynamic properties of solids with the anharmonic limitations and the microscopic Grüneisen parameter is useful to define in relation to the vibrational frequency of atoms in solids. Birch [71] presented a well known experimental research of the macroscopic Grüneisen parameter with the experimental thermodynamic characteristics at high temperatures and pressures. The microscopic Grüneisen parameter requires a comprehensive knowledge of the phonon dispersion spectrum of solids [71].

The Grüneisen parameter, characterizes the anharmonicity of a compound, can be depicted as

$$\gamma = \frac{V}{\vartheta} \cdot \frac{\partial \vartheta}{\partial V} \quad (2.8)$$

where  $\vartheta$  is the frequency and  $V$  is the crystal volume. As a function of temperature at the constant pressure, the isobaric mode Grüneisen parameter can be depicted as

$$\gamma_p = -\frac{V}{\vartheta} \frac{(\partial \vartheta / \partial T)_p}{(\partial V / \partial T)_p} \quad (2.9)$$

The isothermal mode Grüneisen parameter  $\gamma_T$  can also be defined as a function of pressure at constant temperature as

$$\gamma_T = \frac{V}{\vartheta} \frac{(\partial \vartheta / \partial p)_T}{(\partial V / \partial p)_T} \quad (2.10)$$

when both the frequency  $\vartheta$  and volume  $V$  depend on the pressure  $P$  at a constant temperature  $T$ . So, the vibrational frequency can be represented as a function of temperature through the definition of the isobaric mode Grüneisen parameter

$$\vartheta_p(T) = A(T) + \vartheta_1 \left[ -\gamma_p \ln \left( \frac{V_p(T)}{V_1} \right) \right] \quad (2.11)$$

The values of  $\vartheta_1$  and  $V_1$  at constant pressure represent the Raman frequency and the volume at ambient conditions, respectively.

Similarly, the vibrational frequency can be represented as a function of pressure  $P$  through the definition of isothermal mode Grüneisen parameter

$$\vartheta_T(p) = A(p) + \vartheta_1 \left[ -\gamma_T \ln \left( \frac{V_T(p)}{V_1} \right) \right] \quad (2.12)$$

The values of  $\vartheta_1$  and  $V_1$  at constant temperature represent the Raman frequency and the volume at ambient conditions, respectively. The terms of  $A(T)$  and  $A(p)$  in Eqs. (2.11) and (2.12) can be derived from the observed data in the literature.

## 2.3 ORDER PARAMETER

A continuous phase transition involves a discontinuous change at  $T_c$ . The properties of the system do not change but one of their rates changes. In this situation we can define a new quantity as an order parameter ( $\phi$ ) that has a discontinuity in thermal average which vanishes on one side of the transition and moves away from the zero on the other side. In particular,  $\alpha$ ,  $\beta$ ,  $\gamma$  and  $\delta$  are the symbols of indicating the critical exponents related to the temperature, magnetic field, pressure, etc. of the thermal average of  $\phi$ , as given in Table (2.1).

Table 2.1 Definitions of critical exponents

Exponent	Definition
$\alpha$	$C_B \sim \alpha^{-1}[(T - T_C)^{-\alpha} - 1], T \rightarrow T_C, B=0$
$\beta$	$m \sim (T_C - T)^\beta, T \rightarrow T_C \text{ from below}, B=0$
$\gamma$	$\chi_T \sim  T - T_C ^{-\gamma}, T=T_C, B \rightarrow 0$
$\delta$	$m \sim B^{1/\delta}, T=T_C, B \rightarrow 0,$

## 2.4 PIPPARD RELATIONS

Using the definition of the thermal expansion  $\alpha_p$  given by,

$$\alpha_p(T) = \frac{1}{V_p(T)} \cdot \left( \frac{\partial V}{\partial T} \right)_p \quad (2.13)$$

and substituting Equation (2.9) in Equation (2.13) gives

$$\alpha_p(T) = -\frac{1}{\gamma_p(T)} \cdot \frac{1}{\vartheta_p(T)} \cdot \left( \frac{\partial \vartheta}{\partial T} \right)_p \quad (2.14)$$

We can use the definition of the isothermal compressibility  $\kappa_T$ ,

$$\kappa_T(P) = -\frac{1}{V_T(P)} \cdot \left( \frac{\partial V}{\partial p} \right)_T \quad (2.15)$$

Using Equation (2.10) in Equation (2.15) gives,

$$\kappa_T(P) = -\frac{1}{\gamma_T(p)} \cdot \frac{1}{\vartheta_T(p)} \cdot \left( \frac{\partial \varphi}{\partial p} \right)_T \quad (2.16)$$

We can also use the thermodynamic relation,

$$C_p = \frac{TV\alpha_p^2}{\kappa_T} \quad (2.17)$$

Equation (2.17) can be expressed for the heat capacity  $C_p$  in terms of the frequency shifts  $(\partial\vartheta/\partial T)_p$  and  $(\partial V/\partial p)_T$ . Inserting Equations (2.14) and (2.16) into Eq.

(2.17) gives the heat capacity per unit volume.

$$\frac{C_p(T,p)}{V(T,p)} = -T \frac{\gamma_T(p)}{\gamma_p(T)^2} \cdot \frac{\vartheta_T(p)}{\vartheta_p^2(T)} \cdot \frac{(\partial\vartheta/\partial T)_p^2}{(\partial\vartheta/\partial p)_T^2} \quad (2.18)$$

Critical behaviour of the thermal expansivity  $\alpha_p$  can be described as

$$\alpha_p(T) = \alpha_0(T) \left( \frac{T-T_c}{T_c} \right)^{-\varphi} \quad (2.19)$$

where  $\varphi$  is the critical exponent for the thermal expansion,  $T_c$  is the critical temperature and  $\alpha_0$  is the thermal expansion at  $P=0$ .

Using the definition of the isobaric mode Grüneisen parameter  $\gamma_p$  as;

$$\gamma_p(T) = - \left( \frac{\partial \ln \vartheta(T)}{\partial \ln V(T)} \right)_p = - \frac{V_p(T)}{\vartheta_p(T)} \frac{(\partial\vartheta/\partial T)_p}{(\partial V/\partial T)_p} \quad (2.20)$$

the critical behaviour of the temperature –induced frequency shifts can be expressed as;

$$\frac{1}{\vartheta_p(T)} \left( \frac{\partial\vartheta}{\partial T} \right)_p = \frac{\gamma_p(T)}{\gamma_0(T)} \frac{1}{\vartheta_{p=0}(T)} \left( \frac{\partial\vartheta}{\partial T} \right)_{p=0} \left( \frac{T-T_c}{T_c} \right)^{-\varphi} \quad (2.21)$$

Define

$$\delta\vartheta_0(T) = \frac{1}{\vartheta_{p=0}(T)} \left( \frac{\partial\vartheta}{\partial T} \right)_{p=0} \quad (2.22)$$

and

$$\delta\vartheta_p(T) = \frac{1}{\vartheta_p(T)} \left( \frac{\partial\vartheta}{\partial T} \right)_p \quad (2.23)$$



Then, Eq. (2.21) can be expressed by using Eqs. (2.22) and (2.23) as;

$$\delta\vartheta_p(T) = \frac{\gamma_p(T)}{\gamma_0(T)} \delta\vartheta_0(T) \left(\frac{T-T_c}{T_c}\right)^{-\varphi} \quad (2.24)$$

where

$$\alpha_0(T) = \frac{1}{V_{p=0}(T)} \left(\frac{\partial V}{\partial T}\right)_{p=0} = -\frac{1}{\gamma_0(T)} \frac{1}{\vartheta_{p=0}(T)} \left(\frac{\partial \vartheta}{\partial T}\right)_{p=0} \quad (2.25)$$

as given in Eq. (2.19).

Likewise, the critical behaviour of the pressure-induced frequency shifts,  $\frac{1}{\vartheta} \left(\frac{\partial \vartheta}{\partial p}\right)_T$ , can be acquired from the pressure dependence of the isothermal compressibility  $\kappa_T$  as given below:

$$\kappa_T = \kappa_0(p) \left(\frac{p-p_c}{p_c}\right)^{-\phi} \quad (2.26)$$

where  $\phi$  is the critical exponent for the isothermal compressibility,  $p_c$  is the critical pressure and  $\kappa_0(p)$  is the isothermal compressibility at  $T=300K$ . Using the definition of the isothermal mode Grüneisen parameter  $\gamma_T(p)$ ,

$$\gamma_T(p) = \left(\frac{\partial \ln \vartheta(p)}{\partial \ln V(p)}\right)_T = \frac{V_T(p)}{\vartheta_T(p)} \cdot \frac{(\partial \vartheta / \partial p)_T}{(\partial V / \partial p)_T} \quad (2.27)$$

The pressure-induced frequency shifts can be obtained from Eq. (2.26) as,

$$\frac{1}{\vartheta_T(p)} \left(\frac{\partial \vartheta}{\partial p}\right)_T = \frac{\gamma_T(p)}{\gamma_{T=300K}} \frac{1}{\vartheta_{T=300K}(p)} \left(\frac{\partial \vartheta}{\partial p}\right)_{T=300K} \left(\frac{p-p_c}{p_c}\right)^{-\phi} \quad (2.28)$$

where

$$\kappa_0(p) = -\frac{1}{\vartheta_{T=300K}(p)} \left(\frac{\partial \vartheta}{\partial p}\right)_{T=300K} \quad (2.29)$$

and

$$\delta\vartheta_0(p) = -\frac{1}{\vartheta_{T=300K}(p)} \left( \frac{\partial\vartheta}{\partial p} \right)_{T=300K} \quad (2.30)$$

Similarly,

$$\delta\vartheta_T(p) = -\frac{1}{\vartheta_T(p)} \left( \frac{\partial\vartheta}{\partial p} \right)_T \quad (2.31)$$

Eq. (2.30) can be written by using Eqs. (2.30) and (2.31) .

$$\delta\vartheta_T(p) = \frac{\gamma_T(p)}{\gamma_{T=300K}(p)} \delta\vartheta_0(p) \left( \frac{p-p_c}{p_c} \right)^{-\Phi} \quad (2.32)$$

The slope  $dp/dT$  of the phase line in a  $p$ - $T$  phase diagram can be obtained using the thermodynamic relation.

$$\frac{dp}{dT} = \frac{\alpha_p(T)}{\kappa_T(p)} \quad (2.33)$$

which gives through Eqs. (2.19) and (2.26),

$$\frac{dp}{dT} = \frac{\alpha_0(T) \left( \frac{T-T_C}{T_C} \right)^{-\varphi}}{\kappa_0(p) \left( \frac{p-p_c}{p_c} \right)^{-\Phi}} \quad (2.34)$$

Eq. (2.34) can be emphasised in terms of the ratio of the frequency shifts.

$$\frac{dp}{dT} = \frac{\gamma_{T=300K}(p)}{\gamma_{p=0}(T)} \frac{\vartheta_{T=300K}(p)}{\vartheta_{p=0}(T)} \frac{(\partial\vartheta/\partial T)_{p=0}}{(\partial\vartheta/\partial p)_{T=300K}} \left( \frac{T-T_C}{T_C} \right)^{-\varphi} \left( \frac{p-p_c}{p_c} \right)^{\Phi} \quad (2.35)$$

This equation can be reduced with  $\delta\vartheta_0(T)$  and  $\delta\vartheta_0(p)$ .

$$\frac{dp}{dT} = -\frac{\gamma_{T=300K}(p)}{\gamma_{p=0}(T)} \frac{\delta\vartheta_0(T)}{\delta\vartheta_0(p)} \left( \frac{T-T_C}{T_C} \right)^{-\varphi} \left( \frac{p-p_c}{p_c} \right)^{\Phi} \quad (2.36)$$

The critical behaviour of the heat capacity can also be predicted according to

$$\frac{C_p(T,p)}{V(T,p)} = -\frac{T\gamma_T(p)}{\gamma_p^2(T)} \frac{\vartheta_T(p)}{\vartheta_p^2(T)} \frac{(\partial\vartheta/\partial T)_p^2}{(\partial\vartheta/\partial p)_T} \quad (2.37)$$

The temperature dependence of the volume at a constant pressure,  $V_p(T)$  near the critical temperature  $T_C$  can be obtained from Eq. (2.19) by integrating  $\alpha_p(T)$ .

$$\int \alpha_p(T) dT = \alpha_0 \int_0^T \left( \frac{T'-T_C}{T_C} \right)^{-\varphi} dT' \quad (2.38)$$

Since  $\alpha_p(T) \equiv \frac{1}{V_p(T)} \left( \frac{\partial V}{\partial T} \right)_p$ ,  $\alpha_0$  is assumed as a constant at  $T=0K$  and  $p=0GPa$ . This gives,

$$\int_0^T \left( \frac{T'-T_C}{T_C} \right)^{-\varphi} dT' = \frac{T_C}{\varphi-1} \left[ \left( \frac{T_C-T}{T_C} \right)^{1-\varphi} - 1 \right] \quad (2.39)$$

and finally,

$$\int_{V_0}^{V_p} \frac{1}{V} \left( \frac{\partial V}{\partial T} \right)_p dT = \ln V_p - \ln V_0 \quad (2.40)$$

where  $V_0$  is the volume at  $T=0K$  and  $p=0$ .

Thus, Eq. (2.32) is reduced by substituting Eqs.(2.39) and (2.40),

$$V_p(T) = V_0 \exp \left[ \alpha_0 \frac{T_C}{\varphi-1} \left[ \left( \frac{T_C-T}{T_C} \right)^{1-\varphi} - 1 \right] \right] \quad (2.41)$$

This formalism can be applied to the I-II phase transition in benzene. For this transformation at  $T_C=300K$  (room temperature) and  $p_C \cong 1.3GPa$  [1] by using Equation (2.41) in Equation (2.37), we get

$$C_p(T,p) = -TV_0 \exp \left[ \alpha_0 \frac{T_C}{\varphi-1} \left[ \left( \frac{T_C-T}{T_C} \right)^{1-\varphi} - 1 \right] \right] \frac{\gamma_T(p)}{\gamma_p^2(T)} \frac{\vartheta_T(p)}{\vartheta_p^2(T)} \frac{(\partial\vartheta/\partial T)_p^2}{(\partial\vartheta/\partial p)_T} \quad (2.42)$$

Equation (2.42) can be rearranged in terms of  $\delta\vartheta_0(p)$  and  $\delta\vartheta_0(T)$ ,

$$C_p(T, p) = TV_0 \exp \left[ \alpha_0 \frac{T_c}{\varphi - 1} \left[ \left( \frac{T_c - T}{T_c} \right)^{1-\varphi} - 1 \right] \right] \\ \times \frac{\gamma_{T=300K}(p)}{\gamma_{p=0}^2(T)} \frac{\delta\vartheta_0^2(T)}{\delta\vartheta_0(p)} \left( \frac{T-T_c}{T_c} \right)^{-2\varphi} \left( \frac{p_c-p}{p_c} \right)^\phi \quad (2.43)$$

$$C_p(T, p) = \sum_{i=1}^n TV_0 \exp \left[ \alpha_0 \frac{T_c}{\varphi - 1} \left[ \left( \frac{T_c - T}{T_c} \right)^{1-\varphi} - 1 \right] \right] \\ \times \frac{\gamma_{T=300K}(p)}{\gamma_{p=0}^2(T)} \frac{\delta\vartheta_0^2(T)}{\delta\vartheta_0(p)} \left( \frac{T-T_c}{T_c} \right)^{-2\varphi} \left( \frac{p_c-p}{p_c} \right)^\phi \quad (2.44)$$

where  $n$  is the number of modes of solid benzene for the phases I-II.

Similarly, heat capacity of the phases I-II of solid benzene near the critical pressure can be calculated in terms of  $\delta\vartheta_0(p)$ ,  $\delta\vartheta_0(p)$  and  $\kappa_0$ ,

$$C_p(T, p) = TV_0 \exp \left[ -\kappa_0 \left[ \frac{p_c}{\phi-1} \left( \frac{p_c-p}{p_c} \right)^{1-\phi} - 1 \right] \right] \frac{\gamma_{T=300K}(p)}{\gamma_{p=0}^2(T)} \frac{\delta\vartheta_0^2(T)}{\delta\vartheta_0(p)} \left( \frac{T-T_c}{T_c} \right)^{-2\varphi} \left( \frac{p-p_c}{p_c} \right)^\phi \quad (2.45)$$

Over all the total six modes Eq. (2.45) can be obtained as

$$C_p(T, p) = \sum_{i=1}^n TV_0 \exp \left[ -\kappa_0 \left[ \frac{p_c}{\phi-1} \left( \frac{p_c-p}{p_c} \right)^{1-\phi} - 1 \right] \right] \\ \times \frac{\gamma_{T=300K}(p)}{\gamma_{p=0}^2(T)} \frac{\delta\vartheta_0^2(T)}{\delta\vartheta_0(p)} \left( \frac{T-T_c}{T_c} \right)^{-2\varphi} \left( \frac{p-p_c}{p_c} \right)^\phi \quad (2.46)$$

## CHAPTER 3

### CALCULATIONS AND RESULTS

#### 3.1.1. Calculation of the Raman Frequency as a Function of Pressure and Temperature for the Hydrocarbons: Benzene, Naphthalene and Anthracene

The vibrational frequencies in the crisyalline systems can be calculated as a function of pressure and temperature related to the volume data through the Grüneisen parameter.

The crystal volume as a function of pressure at constant temperature can be interpreted in the form of quadratic equation defined as the following:

$$V_T(p) = a_0(T) + a_1(T)p + a_2(T)p^2 \quad (3.1)$$

Similarly, temperature dependence of the crystalline volume can be defined in a quadratic form at a constant pressure.

$$V_p(T) = b_0(p) + b_1(p)T + b_2(p)T^2 \quad (3.2)$$

Also, the vibrational frequency can be expressed as a function of pressure at ambient temperature related to the order parameter.

$$\vartheta_T(p) = c_0(T) + c_1(T)p + c_2(T)p^2 \quad (3.3)$$

The temperature dependence of the vibrational frequencies can be calculated at a constant pressure,

$$\vartheta_p(T) = d_0(p) + d_1(p)T + d_2(p)T^2 \quad (3.4)$$

The coefficients  $a_0, a_1, a_2$  and  $c_0, c_1, c_2$  in Eqs. (3.1) and (3.3) are in general temperature dependent at constant pressure and the coefficients  $b_0, b_1, b_2$  and  $d_0, d_1, d_2$  are the pressure dependent at ambient temperature.

### **3.1.1 Pressure Dependence of the Raman Frequencies at Ambient Temperature for Solid Benzene**

#### **3.1.1.1 For the Modes I, II and III at Constant Temperatures in Phase II of Benzene**

In the current study, first we found the pressure dependence of the isothermal mode Grüneisen parameter  $\gamma_T$  according to Equation (2.10) by using the observed frequencies of the Raman modes I, II and III [11,12,17] as the initial data and also the observed volume data [12] for the phase II of benzene. In this determination, we applied the functional forms of  $V(P)$  (Equation (3.1)) and  $\vartheta(P)$  (Equation (3.3)) with the coefficients  $a_0, a_1, a_2$  and  $c_0, c_1, c_2$ , respectively. The coefficients  $a_0, a_1, a_2$  and  $c_0, c_1, c_2$  are given in Tables 3.1 and 3.2, respectively, with the uncertainties of the six phonon modes for benzene. Values of the isothermal mode Grüneisen parameter  $\gamma_T$  were acquired at various pressures for the Raman modes I and II at 300 K and for the mode III at 450 K using the observed frequencies [11,17] and the volume [12].

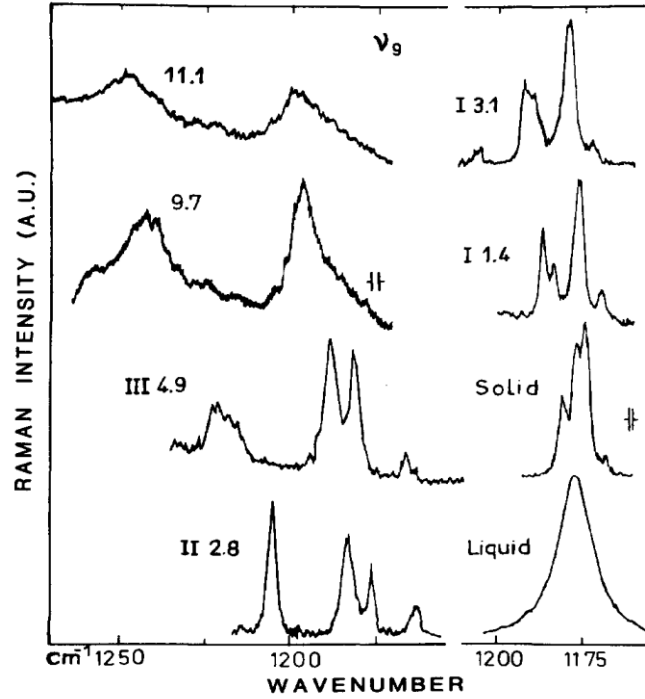


Figure 3.1 Raman spectra of modes I, II and III for solid benzene at 294 K studied from Thiery and Leger [12].

Once, we found the  $\gamma_T$  values for the Raman modes studied, then we were able to calculate the pressure dependence of Raman frequencies of modes I, II (at 300 K) and mode III (at 450 K) for the solid phase II of benzene. In Figure 3.2, the isothermal mode Grüneisen parameter is represented at different pressures for the Raman modes I and II (300 K) and mode III (450 K). This was completed through the pressure-dependent term  $A(P)$  whose coefficients (Eq. (2.12)) were determined by defining the pressure-dependent term in a quadratic form as given below:

$$A(p) = a' + b'p + c'p^2 \quad (3.5)$$

In order to find the coefficients  $a'$ ,  $b'$  and  $c'$  of the pressure-dependent  $A(P)$  term, we used the experimental data for the crystal volume  $V$  at constant pressures of 5, 10 and 15 GPa [12] at 300 K in Eq. (2.12). Also we used the experimental data for the Raman frequencies of the modes I and II at constant pressures of 5, 10 and 15 GPa at 300 K and for the Raman frequencies of the mode III at 450 K [11,17] in Eq. (2.12).

The  $V$  and  $\vartheta$  values used to determine the coefficients  $a'$ ,  $b'$  and  $c'$  are given in Table 3.3.

Table 3.1 Coefficients  $a_0$ ,  $a_1$  and  $a_2$  as determined by Equation (3.1) for the volume of solid benzene with the uncertainties.  $V_0$  value is also given.

BENZENE	$a_0(\text{cm}^3/\text{mole})$	$a_1(\text{cm}^3/\text{mole.GPa})$	$a_2(\text{cm}^3/\text{mole.GPa}^2)$	$V_0$
	$72.11 \pm 1.92$	$-2.62 \pm 0.5$	$0.06 \pm 0.02$	72.11

Table 3.2 Coefficients  $c_0$ ,  $c_1$  and  $c_2$  which were found according to Equation (3.3) using the observed data [11,17] for the modes indicated with the uncertainties for the phase II of benzene.  $\vartheta_0$  value is also given

Raman Modes	$c_0(\text{cm}^{-1})$	$c_1 (\text{cm}^{-1} / \text{GPa})$	$c_2 (\text{cm}^{-1} / \text{GPa}^2)$	$\vartheta_0 (\text{cm}^{-1})$
Mode I	$102.45 \pm 3.4$	$9.44 \pm 0.7$	$-0.16 \pm 0.04$	102.45
Mode II	$134.13 \pm 2.4$	$14.10 \pm 0.5$	$-0.27 \pm 0.03$	134.13
Mode III	$125.05 \pm 5.0$	$16.40 \pm 1.1$	$-0.31 \pm 0.06$	125.05

Table 3.3 Coefficients  $a'$ ,  $b'$  and  $c'$  which were determined according to Equation (3.5) using the observed frequencies [11] which were obtained at 300 K (modes I and II) and at 450 K for mode III of benzene.

A(P)	$a' (\text{cm}^{-1})$	$b' (\text{cm}^{-1} / \text{GPa})$	$c' (\text{cm}^{-1} / \text{GPa}^2)$
Mode I	-21.65	7.85	-0.30
Mode II	-27.99	10.40	-0.31
Mode III	-4.95	5.98	-0.38



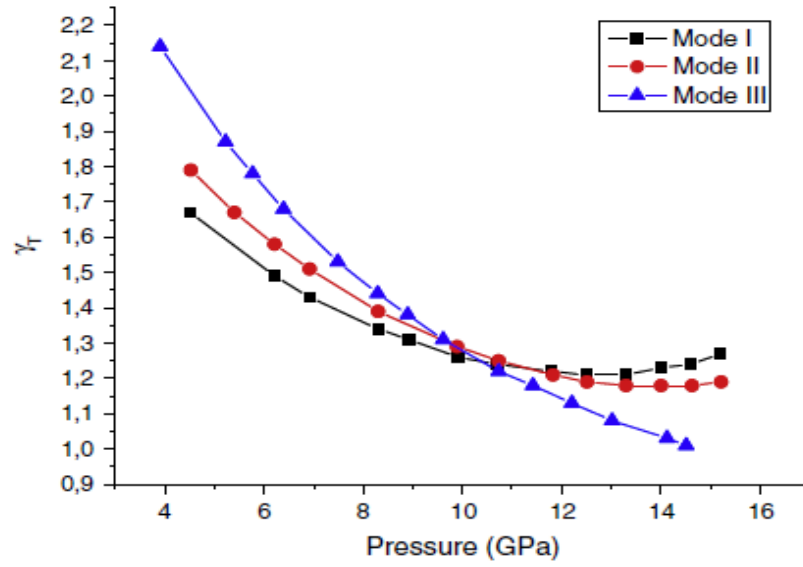


Figure 3.2 Isothermal mode Grüneisen parameter as a function of pressure (Equation (2.10)) for the Raman modes I, II (300 K) and III (450 K) for the phase II of solid benzene.

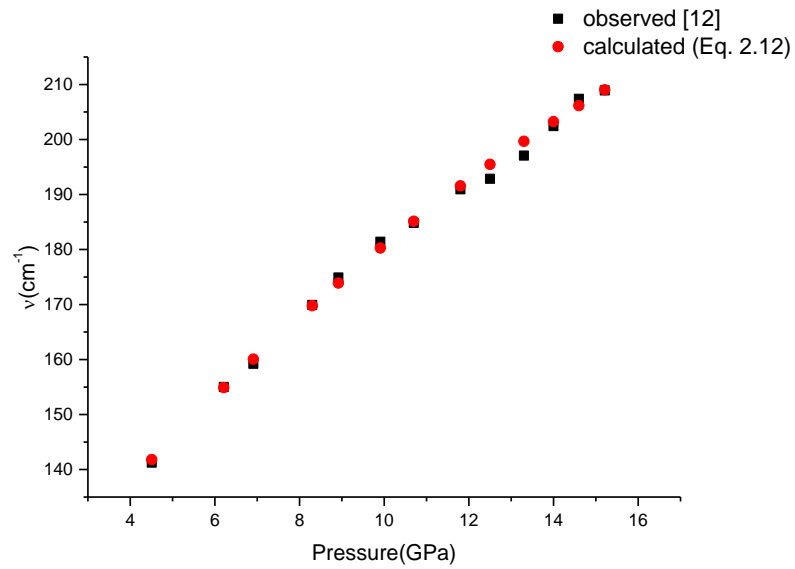


Figure 3.3 Calculated Raman frequencies for mode I at various pressures (T=300K) for phase II of benzene. Experimental data [12] are also plotted.

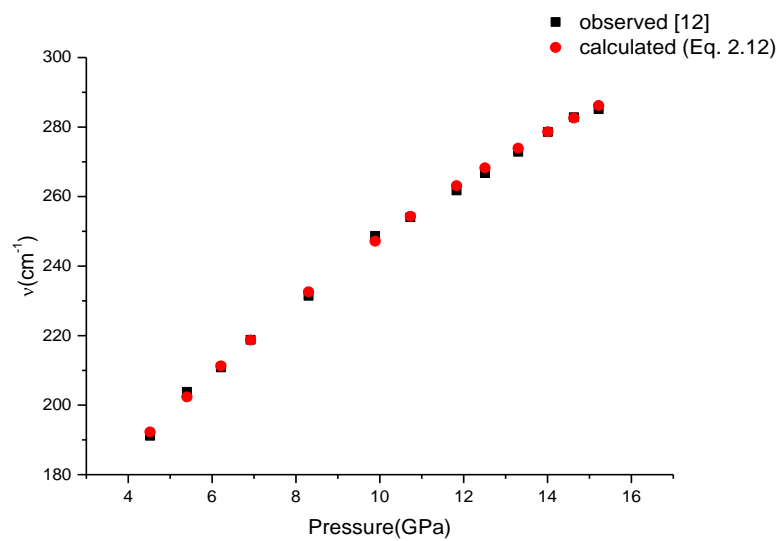


Figure 3.4 Found Raman frequencies of mode II at various pressures (T=300K) for phase II of benzene. Also the experimental data [12] are plotted.

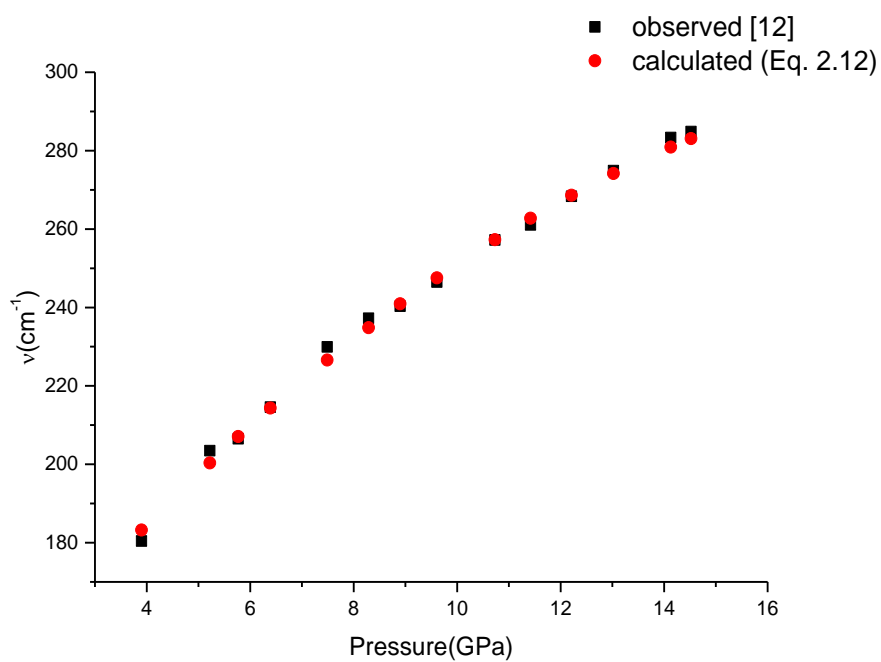


Figure 3.5 Found Raman frequencies of mode III at various pressures (T=450K) for phase II of benzene. Also experimental data [12] are plotted.

Raman frequency shifts as a function of pressure were calculated (Equation (2.12)) for modes I, II ( $T = 300$  K) and III ( $T = 450$  K) in phase II of solid benzene by using the observed data [12] through the isothermal mode Grüneisen parameter (Equation (2.13)). Calculated Raman frequencies of modes I, II ( $T = 300$  K) and III ( $T = 450$  K) are represented in Figures 3.3-3.5. Our calculated values are in good agreement with the observed data. Calculated Raman frequencies differ slightly from the observed Raman frequencies [12] through 12 to 13 GPa in Figure 3.3. This may be owing to the fact that the isothermal mode Grüneisen parameter  $\gamma_T$  which lowers with the pressure down to around 13 GPa (Figure (3.2)) where it starts increasing above that pressure. For the Raman mode II, agreement between the experimental data [12] and our calculated values is much better (Figure (3.4)). At various pressures, the isothermal mode Grüneisen parameter  $\gamma_T$  for this mode also decreases down to around 12.5 GPa as for the mode I, then it remains nearly constant with about 1.2 value (Fig. 3.2).

As the calculations of the Raman modes I and II at  $T = 300$  K, the pressure dependence of the Raman frequency for mode III was also calculated at  $T = 450$  K in phase II of benzene. As indicated in Figure 3.5, the calculated values agree with the experimental data [12]. The isothermal mode Grüneisen parameter  $\gamma_T$  for this mode also lowers with the pressure, which is steeper in comparison with the modes I and II (Figure 3.2). Possibly, it remains constant at around 15 GPa as for the Raman mode II. We note that we used the experimental volume data [12] at 300 K and the observed Raman frequency data [12,17] at 450 K for mode III (Equation (2.10)) and we predicted the Raman frequencies of this mode according to Equation (2.12). When the experimental volume data at 450 K are accessible in the literature, we need to recalculate the Raman frequencies of mode III by means the isothermal mode Grüneisen parameter (Equation (2.10)) through Equation (3.5). The Raman frequencies of the modes I, II and III increase with the increasing pressure, as shown in Figures 3.3–3.5. Their variation with the pressure is nonlinear (Equation (3.3)). This increase in the Raman frequencies of the modes indicate an increase in the ordering of the molecular orientations in the solid phase II of benzene. Change in the slopes of the  $\vartheta$ – $P$  curves of the modes I, II and III as lattice modes, is significant in

comparison with the internal modes in benzene, as also pointed out previously [12]. These pressure induced shifts are directly related to the large initial compressibility of benzene as a typical molecular crystal [12]. It has been pointed out that under the pressure applied to molecular solids such as benzene, the intermolecular interactions can be compared in magnitude to intramolecular ones [57]. To predict the Raman frequencies for the three modes (I, II and III), we used the isothermal mode Gruneisen parameter  $\gamma_T$  at various pressures at a constant temperature ( $T = 300$  K for modes I and II,  $T = 450$  K for mode III) as stated above (Figure (3.2)). The values of the mode Gruneisen parameter  $\gamma_T$  decreased from 1.67 ( $P = 4.5$  GPa) to 1.27 ( $P = 15.2$  GPa) for mode I, from 1.79 to 1.19 for mode II within the same pressure interval. Variation of  $\gamma_T$  for those two modes with the pressure ( $T = 300$  K) is similar within the same pressure range in the solid phase II of benzene (Figure 3.4). For the lattice mode III, the  $\gamma_T$  values decrease from 2.14 ( $P = 3.9$  GPa) to 1.01 ( $P = 14.5$  GPa) in this phase of benzene. Variation of the  $\gamma_T$  with the pressure ( $T = 450$  K) is much larger compared to the modes I and II in phase II of benzene. This may also be due to two constant temperatures of 300 K (modes I and II) and 450 K (mode III), which we considered in our treatment. Therefore, the temperature impacts on the frequency shifts can change the pressure dependence of the mode Grüneisen parameter.

In the present study, we found the uncertainties in our calculations due to the uncertainties in the experimental measurements [12]. It was indicated that in the X-ray diffraction works, the pressure uncertainty was usually  $\pm 0.3$  GPa with the slit width  $1\text{--}2\text{ cm}^{-1}$  [12]. Also, the uncertainties in the molar volume were estimated to be 1.5% for the solid I–II of benzene [12]. On that basis, we found the uncertainties in the molar volume  $V$ , in the Raman frequencies of the modes I, II and III and also in the isothermal mode Gruneisen parameter  $\gamma_T$  for the phase II of benzene. Uncertainties in the coefficients for the molar volume  $V$  and the Raman frequency  $\vartheta$  (for modes I, II and III) according to Equations (3.1) and (3.3) are given in Tables 3.1 and 3.2, respectively. They are plotted for modes I, II and III in Figure 3.6.

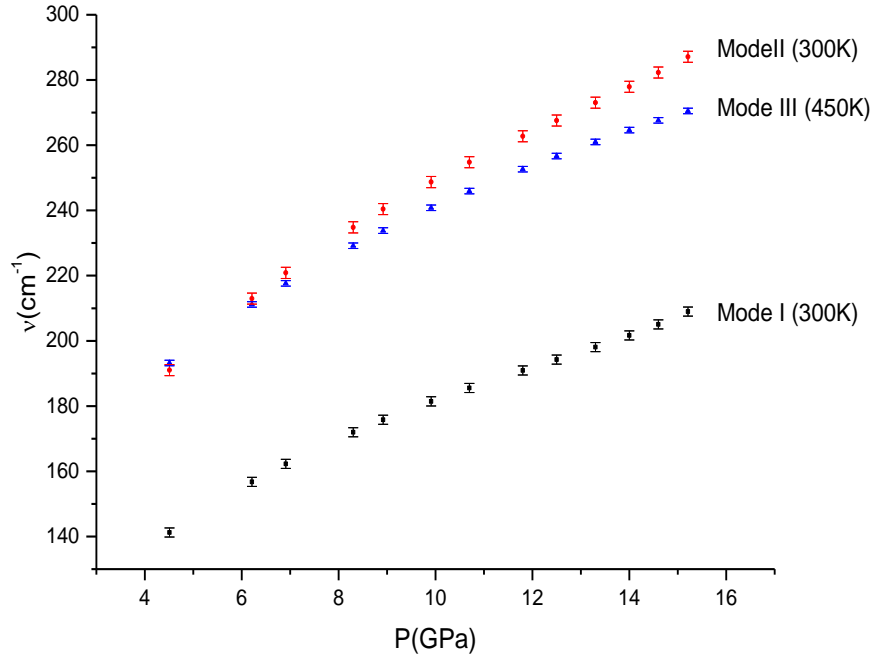


Figure 3.6 Uncertainties in the Raman frequencies calculated for the modes I, II and III at various pressures for phase II of benzene.

### 3.1.1.2 For Phonon Modes of Solid Benzene I at Room Temperature

Pressure dependence of the volume according to Equation (3.1) was determined by fitting the observed data [12] and the coefficients  $a_0$ ,  $a_1$ ,  $a_2$  in Equation (3.1) were given in Table 3.1 in Section 3.1.1.1. The Raman frequency shifts of six phonon modes of solid benzene I were defined as a function of pressure in Equation (3.3) and the coefficients are given in Table 3.4 with the uncertainties. Then, isothermal mode Grüneisen parameter was calculated according to Equation (2.10) for the six phonon modes of solid benzene I at room temperature as plotted in Figure 3.7. Finally, the pressure dependence of the Raman frequency shifts were defined by using Equation (2.12) for six phonon modes of solid benzene I. The coefficients  $a'$ ,  $b'$  and  $c'$  of the function of  $A(P)$  (Equation (3.5)) are given in Table 3.5.

Table 3. 4 Coefficients  $c_0$ ,  $c_1$  and  $c_2$  which were determined according to Eq. (3.3) using the observed data [12] for the phonon modes of solid benzene I . We also give here the uncertainties determined for the coefficients  $c_0$ ,  $c_1$  and  $c_2$  for six phonon modes of solid benzene I. Calculated Raman frequency shifts are also represented at P= 0 GPa and T= 300 K.

Benzene	$c_0(\text{cm}^{-1})$	$c_1 (\text{cm}^{-1}/\text{GPa})$	$c_2 (\text{cm}^{-1}/\text{GPa}^2)$	$\vartheta_0$
Mode A	$42.34 \pm 0.5$	$26.36 \pm 0.9$	$-4.37 \pm 0.3$	42.34
Mode B	$64.83 \pm 0.5$	$27.17 \pm 0.6$	$-3.62 \pm 0.2$	64.83
Mode C	$104.89 \pm 0.7$	$53.84 \pm 1.0$	$-8.10 \pm 0.3$	104.89
Mode X	$53.93 \pm 0.3$	$24.03 \pm 0.3$	$-3.18 \pm 0.1$	53.93
Mode Y	$79.46 \pm 0.3$	$34.69 \pm 0.4$	$-4.37 \pm 0.1$	79.46
Mode Z	$90.13 \pm 0.3$	$37.60 \pm 0.4$	$-4.97 \pm 0.1$	90.13

Table 3.5 Coefficients  $a'$ ,  $b'$  and  $c'$  which were determined according to Equation (3.5) using the observed frequencies [12] which were obtained at 300 K for six phonon modes of solid benzene I.

A(P)	$a'$	$b'$	$c'$
Mode A	0.	47.50	-13.43
Mode B	0.	50.78	-11.56
Mode C	0.	98.92	-25.48
Mode X	0.	44.72	-10.30
Mode Y	0.	64.71	-14.38
Mode Z	0.	70.30	-15.90

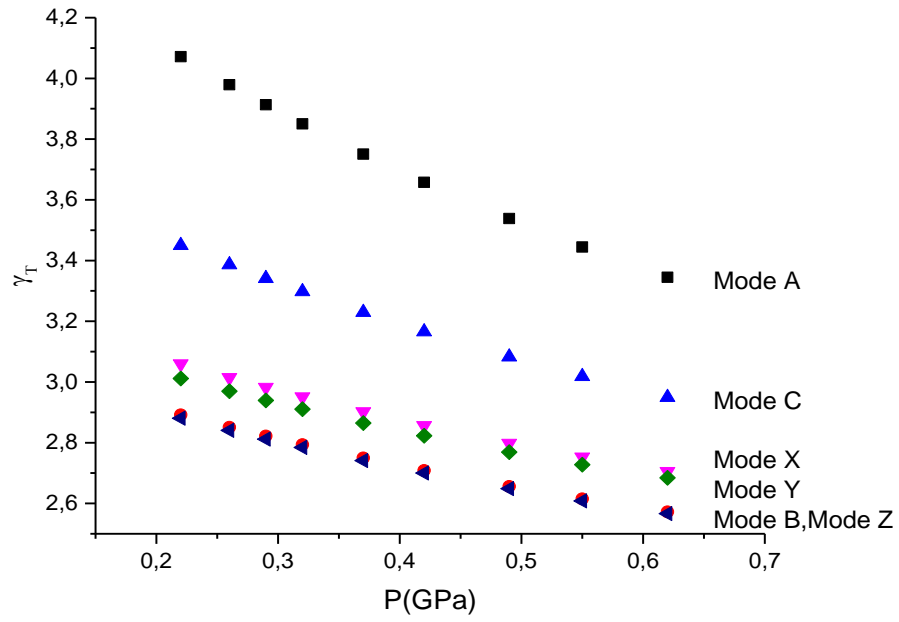


Figure 3.7 Isothermal mode Grüneisen parameter as a function of pressure (Equation (2.13)) for phonon modes of solid benzene I at room temperature.

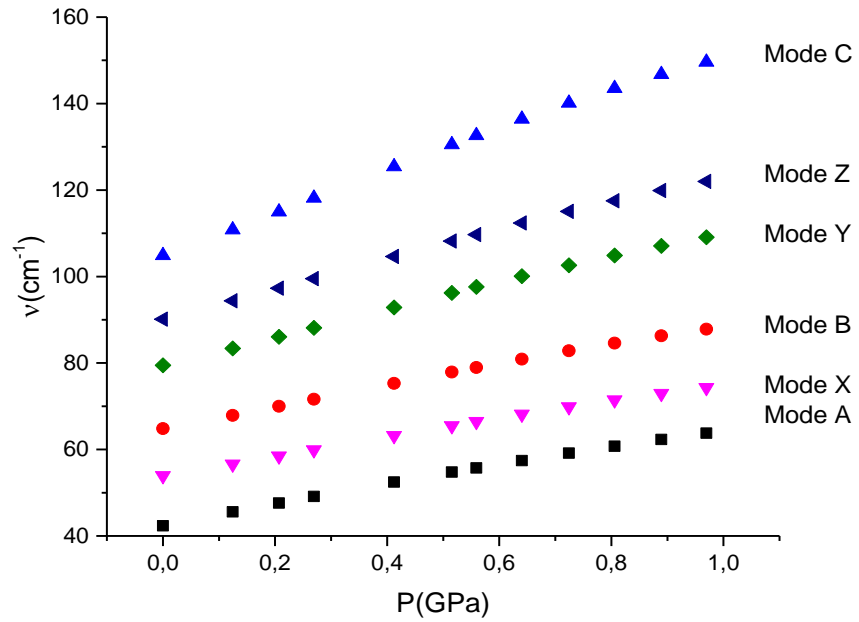


Figure 3.8 Calculated Raman frequencies as a function of pressure at room temperature according to Equation (2.12) by using the observed data [12] for six phonon modes of solid benzene I.

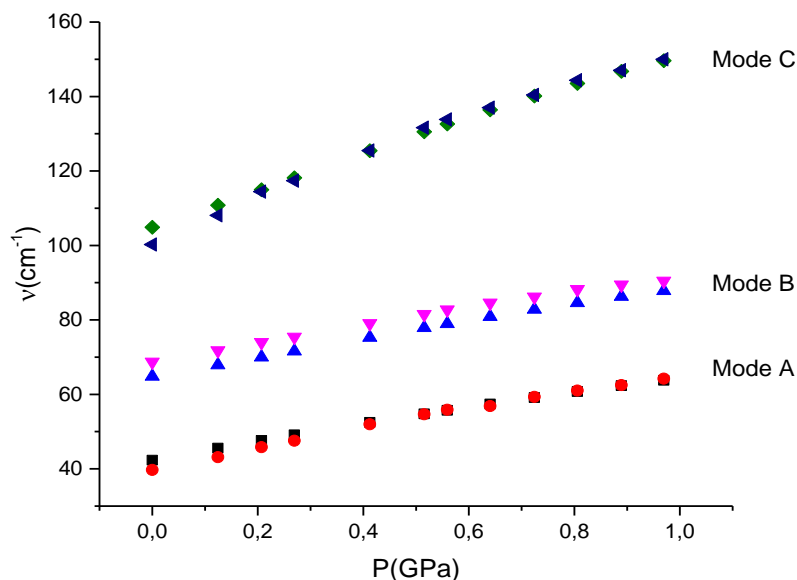


Figure 3.9 Pressure dependence of the Raman frequencies (Equation (2.12)) at room temperature for solid benzene I are defined with black squares (Mode A), blue triangles (Mode B) and green squares (Mode C). Observed data [12] is also given with red circles (Mode A), purple triangles (Mode B) and navy blue triangles (Mode C), respectively.

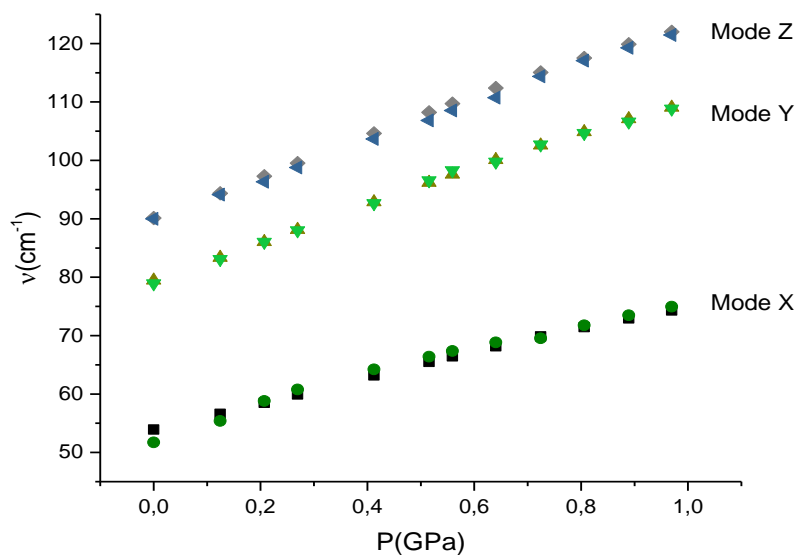


Figure 3.10 Pressure dependence of the Raman frequencies (Equation (2.12)) at room temperature for solid benzene I are defined with black squares (Mode X), grey triangles (Mode Y) and grey squares (Mode Z). Observed data [12] is also given with green circles (Mode X), green triangles (Mode Y) and navy blue triangles (Mode Z), respectively.



Crystal volume was defined as a function of pressure (Equation (3.1)) with the coefficients  $a_0$ ,  $a_1$  and  $a_2$  fitted to the experimental data [12]. To obtain the pressure dependence of the frequency shifts, the coefficients  $c_0$ ,  $c_1$  and  $c_2$  (Equation (3.3)) as given in Table 3.4 were calculated. Through the isothermal Grüneisen parameter which defines the change in frequency shifts with the change in crystal volume, the Raman frequencies were defined as a function of pressure for six phonon modes of solid benzene according to Equation (2.12) with the pressure dependence additional term  $A(P)$  (Table 3.5). Calculated Raman frequencies according to Equation (2.12) as given in Figure 3.7 for the six phonon modes of solid benzene increase with the increasing pressure range between 0 and 1 GPa. In Figure 3.8, we plot the calculated pressure dependence of the Raman frequencies of modes A, B and C with the experimental data [12]. There is a good agreement between the calculated Raman frequencies and the observed data [12]. There is a discrepancy in the range of 0 and 0.3 GPa between calculated mode A and the observed one [12], which occurs for the mode C. The discrepancy becomes more obvious for mode B between the calculated and the observed data. For the modes X, Y and Z which represented in Figure 3.9, there is a good match with the experimental data [12]. Small discrepancy occurs for mode C between 0.5 and 0.7 GPa pressure range and occurs at first two pressure values for mode X. The discrepancy between the calculated and observed data for the mentioned modes above can be attributed to the isothermal compressibility. Since, our frequency calculations (Equation (2.12)) have the volume dependency through the isothermal mode Grüneisen parameter, the Raman frequencies are not contributed by the isothermal compressibility at low pressure ranges.

Thiery and Leger [12] calculated the values of the isothermal mode Gruneisen parameter ( $\gamma_T$ ) for the lattice modes A, B and C in the orthorhombic phase I as  $\gamma_1 = 3.0$ , 2.5 and 3.0, respectively. Also the researchers determined those values in the monoclinic phase II as  $\gamma_2 = 2.9$ , 3.1 and 2.6 for the lattice modes of A, B and C, respectively [12]. Our  $\gamma_T$  values for those modes (A, B and C) in average, fall in the same range as we used the same observed data [12] to find the  $\gamma_T$  values for the I–II transition in benzene. Our  $\gamma_T$  values for the I–II transition in benzene, can also be compared with the experimental values of the Gruneisen parameters for  $q = 0$  phonons of crystalline naphthalene. As obtained by Dows et al. [26] and Backer et al.

[30], the  $\gamma_2$  and  $\gamma_3$  values differ from 3 to 4 at 300 K, as also reported previously [28]. Likewise, for anthracene the observed and calculated  $\gamma$  values vary from 3 to 6 for the Ag and Bg modes [26]. This shows that the values of the mode Gruneisen parameter lead to the similar physical features of benzene, naphthalene and anthracene.

We determined the uncertainties in the Raman frequency calculated as a function of pressure (Equation (2.10)) of the lattice modes (A,B,C and X,Y,Z) through the experimental data [12] at  $P=0$  GPa which is given in Table 3.2. We used the uncertainties in the Raman frequency calculated as a function of pressure through the coefficient  $c_0$ . The pressure uncertainty for the lattice modes was usually between  $\pm 0.3$  and  $\pm 0.7$  GPa with the slit width  $1-2 \text{ cm}^{-1}$ . Also, the uncertainties in the molar volume were estimated to be  $\pm 1.5 \text{ cm}^3/\text{mol}$  for the solid benzene [12]. On that basis, we determined the uncertainties in the molar volume  $V$ , in the Raman frequencies  $\nu$  of the modes, in the isothermal mode Gruneisen parameter  $\gamma_T$  and also the pressure-dependent term  $A(P)$  ( $P=0$  GPa) for benzene I. Using the calculated terms with the uncertainties in Equation (2.10), the Raman frequencies of the lattice modes of solid benzene were calculated. Uncertainty in the mode A with for solid benzene I was estimated to be 1.2% (or  $0.5 \text{ cm}^{-1}$ ) at zero pressure (Figure 3.10). Similarly, uncertainties in the mode B and mode C for benzene were estimated to be 0.8% (or  $0.5 \text{ cm}^{-1}$ ) and 0.7% (or  $0.7 \text{ cm}^{-1}$ ) at zero pressure (Figure 3.10). For the lattice modes of solid benzene, uncertainties in the Raman frequency calculated as a function of pressure were estimated as 0.6% (or  $0.3 \text{ cm}^{-1}$ ) for mode X with, 0.4% (or  $0.3 \text{ cm}^{-1}$ ) for mode Y and 0.3% (or  $0.3 \text{ cm}^{-1}$ ) for mode Z at zero pressure, as plotted in Figure 3.11.

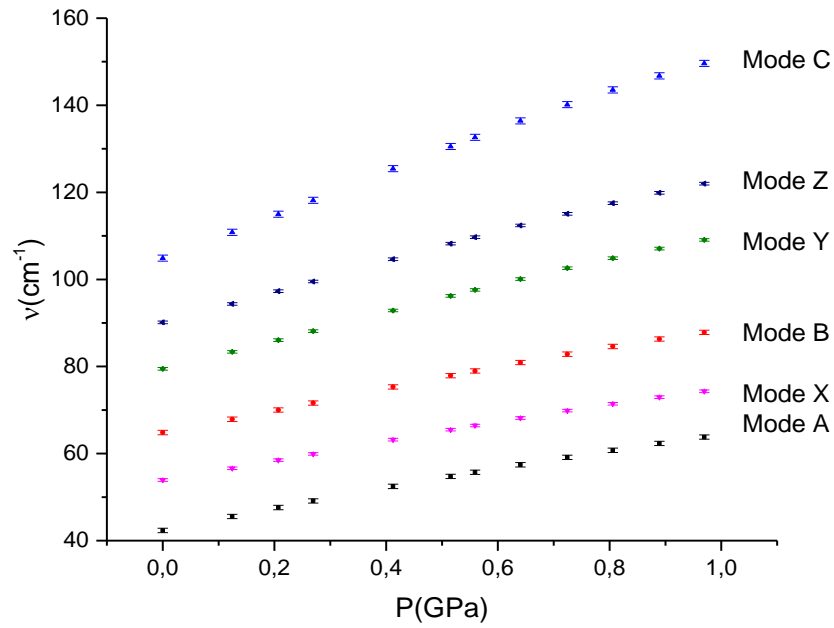


Figure 3.11 Uncertainties in the calculated Raman frequencies as a function of pressure for lattice modes for solid benzene according to Equation (2.10).

### 3.1.2 *Naphtalene*

The coefficients  $a_0$ ,  $a_1$  and  $a_2$  referred to the Equation (3.1) were determined for volume as a function of pressure (at room temperature), as given in Table 3.6. The coefficients  $c_0$ ,  $c_1$  and  $c_2$  were also analyzed according to Equation (3.3) by using the observed Raman frequencies of the  $A_g$  and  $B_g$  modes [37] at room temperature for naphthalene as given in Table 3.7.

The isobaric mode Grüneisen parameter  $\gamma_P$  of the six phonon modes of solid naphthalene were determined as a function of temperature at zero pressure according to Equations (3.2) and (3.4) by using the temperature dependence of the observed volume [72,73] and the observed Raman frequencies [37]. The coefficients of the temperature dependent function  $A(P)$  given in Equation (3.5) were obtained through

Equation (2.11) for the phonon modes of naphthalene at zero pressure. Determined coefficients  $a'$ ,  $b'$  and  $c'$  of A(P) for the phonon modes are given in Table 3.8. Also, the Raman frequencies of the  $A_g$  and  $B_g$  modes as a function of pressure were calculated through Equation (2.12) by using the observed volume data [20,74] and the observed Raman frequencies [37]. Table 3.6 gives the values of those coefficients. For naphthalene, we determined the coefficients in Equations (3.1) and (3.3) with the uncertainties through the experimental data by recalculating the A(P) parameters for six phonon modes.

Table 3. 6 Coefficients  $a_0$ ,  $a_1$  and  $a_2$  as determined according to Equation (3.1) by using observed volume data [37] of solid naphthalene at room temperature. We also give here the uncertainties determined in the coefficients  $a_0$ ,  $a_1$  and  $a_2$ .

NAPHTHALENE	$a_0$ (cm <sup>-1</sup> )	$a_1$ (cm <sup>-1</sup> /mole.GPa)	$a_2$ (cm <sup>3</sup> /mole.GPa <sup>2</sup> )	$V_0$
	360.18±0.4	-63.37±3.0	30.34±0.5	360.18

Table 3. 7 Coefficients  $c_0$ ,  $c_1$  and  $c_2$  which were found according to Eq. (3.3) using the observed data [37] for the modes indicated for solid naphthalene. We also give here the uncertainties determined for the coefficients  $c_0$ ,  $c_1$  and  $c_2$  for six modes of solid naphthalene. Values of the Raman frequencies for six modes of solid naphthalene at P= 0 GPa and T= 300 K, are also given here.

NAPHTHALENE	$c_0$ (cm <sup>-1</sup> )	$c_1$ (cm <sup>-1</sup> /GPa)	$c_2$ (cm <sup>-1</sup> /GPa <sup>2</sup> )	$\vartheta_0$
Mode $A_{g1}$	49.38±0.60	31.91±1.00	-3.86±0.30	49.38
Mode $A_{g2}$	73.96±0.40	35.92±1.00	-3.68±0.30	73.96
Mode $A_{g3}$	108.14±0.40	44.66±0.90	-5.59±0.30	108.14
Mode $B_{g1}$	45.10±0.40	26.04±0.81	-2.05±0.30	45.10
Mode $B_{g2}$	70.62±0.70	43.66±3.90	-13.32±0.40	70.62
Mode $B_{g3}$	124.26±0.70	52.41±1.50	-6.35±0.50	124.26

Table 3.8 Coefficients  $a'$ ,  $b'$  and  $c'$  which were found according to Equation (3.5) using the observed frequencies [37] which were obtained at 300 K for six phonon modes of solid naphthalene.

A(P)	$a'$	$b'$	$c'$
Mode A <sub>g1</sub>	0.14	19.59	42.56
Mode A <sub>g2</sub>	-0.79	68.30	-6.85
Mode A <sub>g3</sub>	0.55	38.27	68.88
Mode B <sub>g1</sub>	2.14	58.56	-6.88
Mode B <sub>g2</sub>	-0.54	95.00	-58.27
Mode B <sub>g3</sub>	-3.14	131.13	-58.29

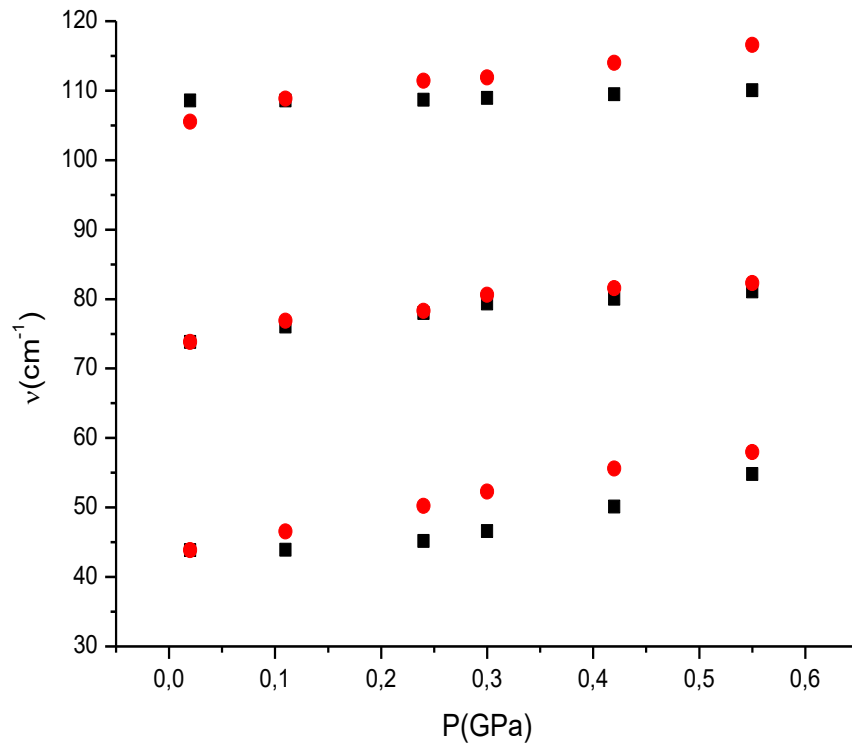


Figure 3.12 The measured Raman frequencies as a function of pressure at room temperature for modes of symmetry A<sub>g</sub> for solid naphthalene (filled squares) according to Equation (2.12) and the experimental data of A<sub>g</sub> modes [37] for solid naphthalene (filled circles) is also given.

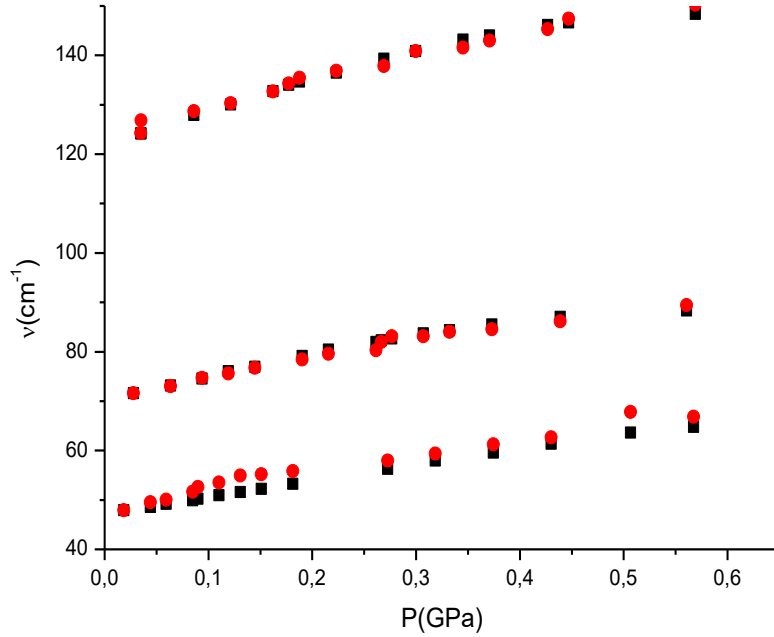


Figure 3.13 The measured Raman frequencies as a function of pressure at room temperature for modes of symmetry  $B_g$  for solid naphthalene (filled squares) according to Equation (2.12) and the experimental data of  $B_g$  modes [37] for solid naphthalene (filled circles) is also given.

The Raman frequencies were estimated for the  $3A_g$  and  $3B_g$  modes using the observed volume data by determining their mode Gruneisen parameters in naphthalene. Increase in the Raman frequencies of six lattice modes with increasing pressure (Figures 3.12 and 3.13) can be ascribed to the isothermal compressibility in naphthalene. For the  $A_g$  and  $B_g$  modes, increase in their Raman frequencies (Figures 3.12 and 3.13), as also observed experimentally [37], can be directly related to the reduction in the isothermal compressibility as the pressure increases within the pressure range studied here up to 0.6 GPa for the solid naphthalene. There is a difference between our calculated Raman frequencies of the  $A_{g1}$  mode and the observed data [37], which also occurs for the  $A_{g3}$  mode at comparatively higher pressures of above about 0.25 GPa (Figure 3.12). For the  $B_g$  modes, Equation (2.12) fits quite well to the experimental Raman frequencies [37] within the pressure range

of 0–0.6 GPa as for the  $A_{g2}$  mode (Figure 3.13). Consider that as the volume data were obtained in the pressure region up to 0.6 GPa [20,48], our calculated Raman frequencies of the  $A_g$  and  $B_g$  modes (Equation (2.12)) were restricted to that pressure range.

Table 3. 9 Values of the isothermal mode Gruneisen parameter  $\gamma_T$  (Equation (2.9)) for the Raman modes showed at constant temperatures ( $P = 0$ ) for solid naphthalene.

T(K)	Mode $A_{g1}$ ( $\gamma_T$ )	Mode $A_{g2}$ ( $\gamma_T$ )	Mode $A_{g3}$ ( $\gamma_T$ )	Mode $B_{g1}$ ( $\gamma_T$ )	Mode $B_{g2}$ ( $\gamma_T$ )	Mode $B_{g3}$ ( $\gamma_T$ )
7	4.58	1.86	1.22	2.88	2.45	2.10
79	4.66	2.62	1.67	3.88	2.77	2.14
83	4.67	2.65	1.68	3.92	2.78	2.14
197	5.24	3.35	2.06	5.03	3.20	2.29
297	6.27	4.03	2.37	6.35	3.69	2.51

Our values for the isothermal mode Gruneisen parameter  $\gamma_T$  of the  $A_g$  and  $B_g$  modes, which we determined at constant temperatures for zero pressure (Table 3.9), also can be compared with those given in the earlier works. Dows et al. [26] obtained from the pressure dependence of the Raman lattice modes the values of the Gruneisen parameters between 3.6 and 6.3 for the highest ( $B_{g3}$ ,  $125\text{ cm}^{-1}$ ) and lowest ( $B_{g1}$ ,  $46\text{ cm}^{-1}$ ) for anthracene and naphthalene within the pressure range of 0 and 10 kbar. From the measurements of the Raman active lattice modes, the  $\gamma$  values were obtained as 2.9 for the  $B_{g3}$  ( $126\text{ cm}^{-1}$ ) mode and 5.1 for the  $B_{g1}$  ( $46\text{ cm}^{-1}$ ) mode at room temperature [29]. From the incoherent inelastic scattering measurements on d8-naphthalene, it was obtained that the  $\gamma$  values are between 3.2 and 5.0 for the 12 branches of the external phonon dispersion curves at 100 K [26], as also stated previously [31]. The  $\gamma_1$  values were found [21] to be between 2.8 and 4.2 for the same phonons at 100 K (using the experimental data of Ref. [26]),  $\gamma_2$  values between 2.75 and 3.90 (using the data of Ref. [29]) at 300 K and the  $\gamma_T$  values between 3.85 and 4.08 (using the data of Ref. [30]) in the solid naphthalene. Our  $\gamma_T$  values for the highest ( $B_{g3}$  mode) and the lowest ( $B_{g1}$  mode) vary from 2.5 to 6.4 at room

temperature (297 K) (Table 3.9), which are almost in the same interval as given by Dows et al. [26], which can also be compared with the values of Ref. [29], as stated above.

Also, our  $\gamma_T$  values can be compared with the above given values of Refs. [42] and [75]. For the  $\gamma_T$  values which we obtained for the  $A_g$  modes (Table 3.9) of solid naphthalene, the comparison can be made with those  $\gamma_{obs}$  and  $\gamma_{cal}$  values of the  $A_g$  modes for anthracene [75] that is also the same hydrocarbon as naphthalene. Our findings of  $\gamma_T = 6.3, 4$  and  $2.4$  for the  $A_{g1}, A_{g2}$  and  $A_{g3}$  modes, respectively, ( $T = 297$  K, Table 3.9) can then be compared with those values of  $\gamma_{obs} = 6.2$  ( $51 \text{ cm}^{-1}$ ),  $4.9$  ( $74 \text{ cm}^{-1}$ ) and  $3.7$  ( $109 \text{ cm}^{-1}$ ), and also  $\gamma_{cal} = 5.1$  ( $51 \text{ cm}^{-1}$ ),  $4.1$  ( $74 \text{ cm}^{-1}$ ) and  $3.7$  ( $109 \text{ cm}^{-1}$ ) for the lattice modes of anthracene [26]. The pressure dependence of the isothermal compressibility  $\gamma_T$  can be predicted from the frequency shifts at a constant temperature (room temperature). For a compressible crystal under pressure, its isothermal compressibility can then be calculated using the normal mode frequency shifts with pressure by knowing a constant isothermal mode Gruneisen parameter  $\gamma_T$  (Equation (2.10)). When the  $\gamma_T$  varies with pressure, as in the case of the Raman lattice modes ( $A_g$  and  $B_g$  modes), then the pressure dependence of the isothermal compressibility  $\gamma_T$  can be calculated from the Raman frequency shifts by using the initial data for  $\gamma_T$ , as we worked here for naphthalene. Since the Raman frequency shifts  $\left(\frac{\partial\theta}{\partial p}\right)_T$  can be determined to high accuracy spectroscopically, the pressure dependence of the isothermal compressibility  $\kappa_T$  (Equation (2.15)), can be measured reasonably well. The calculated  $\kappa_T$  can then be compared with the experimental data for naphthalene. The temperature dependence of the isothermal compressibility  $\kappa_T$  (at a constant pressure) can also be estimated from the vibrational frequency shifts  $\left(\frac{\partial\theta}{\partial p}\right)_T$  by means of the isothermal  $\gamma_T$  mode Gruneisen parameters for naphthalene.

Uncertainties in the Raman frequencies calculated for the  $A_g$  and  $B_g$  modes of solid naphthalene were determined because of the uncertainties in the experimental measurements [35]. Uncertainties in the  $A_g$  mode with the frequency of  $\theta_0 =$



$89 \text{ cm}^{-1}$  and with  $\vartheta_0 = 123 \text{ cm}^{-1}$  for naphthalene were estimated to be 0.7% (or  $0.61 \text{ cm}^{-1}/\text{mole.K}$ ) and 0.5% (or  $0.6 \text{ cm}^{-1}/\text{mole.K}$ ), respectively, at room temperature (Fig. 3.14). For the symmetry  $B_g$  modes of solid naphthalene, uncertainties in the Raman frequency calculated as a function of temperature calculations were estimated as 6.8% (or  $3.9 \text{ cm}^{-1}/\text{mole.GPa}$ ) for mode  $B_g$  with  $\vartheta_0 = 57 \text{ cm}^{-1}$ , 0.4% (or  $0.3 \text{ cm}^{-1}/\text{mole.GPa}$ ) for mode  $B_g$  with  $\vartheta_0 = 74 \text{ cm}^{-1}$  and 0.7% (or  $0.98 \text{ cm}^{-1}/\text{mole.GPa}$ ) for mode  $B_g$  with  $\vartheta_0 = 142 \text{ cm}^{-1}$  at room temperature. We determined the uncertainties in the Raman frequency calculated as a function of pressure (Equation (2.12)) of the  $A_g$  and  $B_g$  modes through the experimental data [76] at  $P=0$  GPa. We used the uncertainties in the Raman frequency calculated as a function of pressure through the coefficient  $c_0$ . The pressure uncertainty for the  $A_g$  and  $B_g$  modes was usually between  $\pm 0.4$  and  $\pm 0.7$  GPa with the slit width  $1-2 \text{ cm}^{-1}$ . Also, the uncertainties in the molar volume were predicted to be  $\pm 1.4 \text{ cm}^3/\text{mol}$  for the solid naphthalene [20,76]. On that basis, we determined the uncertainties in the molar volume  $V$ , in the Raman frequencies  $\vartheta$  of the modes, in the isothermal mode Gruneisen parameter  $\gamma_T$  and also the pressure-dependent term  $A(P)$  ( $P=0$  GPa) for the naphthalene. Using the calculated terms with the uncertainties in Equation (2.12), the Raman frequencies of the  $A_g$  and  $B_g$  modes of solid naphthalene were calculated. Uncertainty in the  $A_g$  mode with  $\vartheta_0 = 49 \text{ cm}^{-1}$  for naphthalene was estimated to be 2.6% (or  $1.3 \text{ cm}^3/\text{mole}$ ) at zero pressure (Fig. 3.14). Similarly, uncertainties in the  $A_g$  mode with  $\vartheta_0 = 74 \text{ cm}^{-1}$  and with  $\vartheta_0 = 109 \text{ cm}^{-1}$  for naphthalene were estimated to be 1.7% (or  $1.26 \text{ cm}^3/\text{mole}$ ) and 0.7% (or  $0.8 \text{ cm}^3/\text{mole}$ ) at zero pressure (Figure 3.14). For the  $B_g$  modes of solid naphthalene, uncertainties in the Raman frequency calculated as a function of pressure were estimated as 3.8% (or  $1.9 \text{ cm}^3/\text{mole.GPa}$ ) for mode  $B_g$  with  $\vartheta_0 = 48 \text{ cm}^{-1}$ , 1.5% (or  $1.1 \text{ cm}^3/\text{mole}$ ) for mode  $B_g$  with  $\vartheta_0 = 71 \text{ cm}^{-1}$  and 1.6% (or  $1.9 \text{ cm}^3/\text{mole}$ ) for mode  $B_g$  with  $\vartheta_0 = 123 \text{ cm}^{-1}$  at zero pressure, as plotted in Figure 3.15.

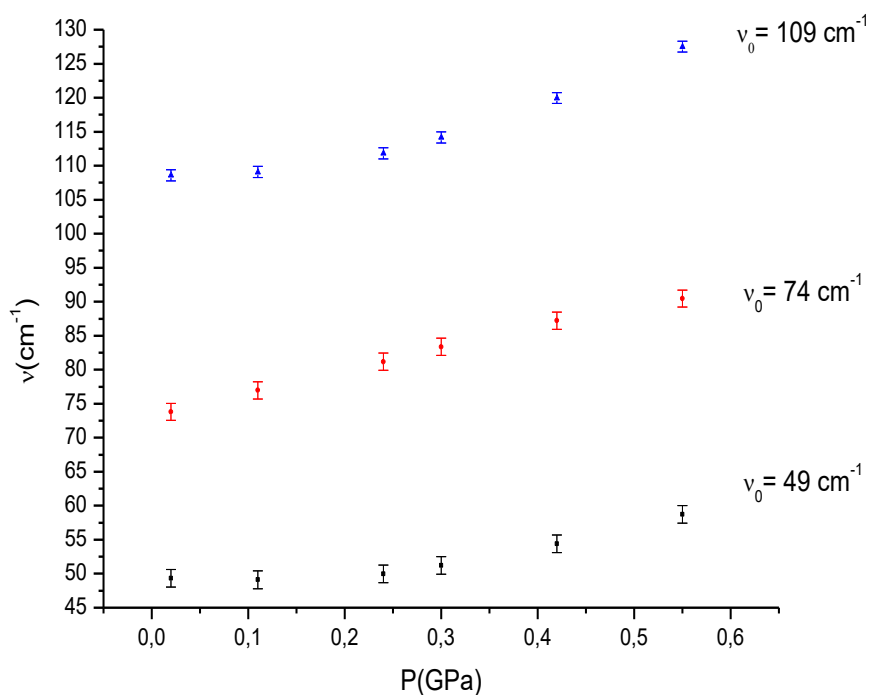


Figure 3. 1 Uncertainties in the Raman frequencies calculated for modes of symmetry  $A_g$  for solid naphthalene according to Equation (2.12).

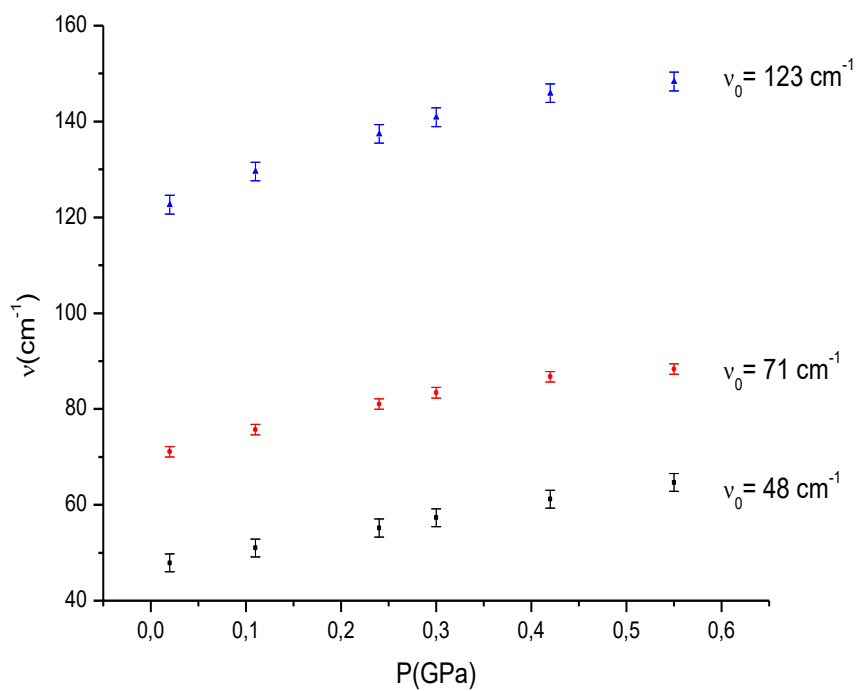


Figure 3. 2 Uncertainties in the Raman frequencies calculated for modes of symmetry  $B_g$  for solid naphthalene according to Equation (2.12).

### 3.1.3 Anthracene

Temperature and pressure dependence of the crystalline volume was found by fitting Equations (3.1) and (3.3) to the observed data and the coefficients  $a_0$ ,  $a_1$ ,  $a_2$  and  $c_0$ ,  $c_1$ ,  $c_2$  which were determined, are represented in Tables 3.10 and 3.11 with the uncertainties. The Raman frequencies of the six phonon and nine vibron modes of solid anthracene were obtained as a function of pressure and temperature by using the observed data [48,52] according to Equations (3.3) and (3.4) through the isothermal mode Grüneisen parameter  $\gamma_T$ . The coefficients  $b_0$ ,  $b_1$ ,  $b_2$  and  $d_0$ ,  $d_1$ ,  $d_2$  in Equations (2.11) and (2.12) are given in Tables 3.12 and 3.13 with the uncertainties. The isothermal and isobaric mode Grüneisen parameters were calculated for anthracene due to Equations (2.9) and (2.10) as given in Table 3.14. From the definition of the mode Grüneisen parameter, pressure and temperature dependence of the Raman frequency shifts of the six phonon and nine vibron modes of solid anthracene can be calculated through Equations (2.9) and (2.10) as

$$\vartheta_T(p) = \vartheta_1 \left[ -\gamma_T \ln \left( \frac{V_T(p)}{V_1} \right) \right] \quad (3.6)$$

$$\vartheta_p(T) = \vartheta_1 \left[ -\gamma_p \ln \left( \frac{V_p(T)}{V_1} \right) \right] \quad (3.7)$$

Raman frequency values and the crystal volume are represented in terms of  $\vartheta_1$  and  $V_1$  at zero pressure and room temperature. The Raman frequency as a function of pressure at room temperature for the six phonon and nine vibron modes of solid anthracene was calculated by using the observed data [48] according to Equation (3.6), as plotted in Figures (3.16-3.19). Similarly, the Raman frequency as a function of temperature at zero pressure for the six phonon and nine vibron modes of solid anthracene was calculated by using the observed data [48] according to Equation (3.7), as plotted in.

Table 3.10 The  $a_0$ ,  $a_1$  and  $a_2$  values which were found according to the Equation (3.1) by using the experimental volume data [52] for six phonon modes of solid anthracene. We also give here the uncertainties determined in the coefficients  $a_0$ ,  $a_1$  and  $a_2$  for the volume of anthracene.

ANTHRACENE	$a_0$ (cm <sup>-1</sup> )	$a_1$ (cm <sup>-1</sup> /mole.GPa)	$a_2$ (cm <sup>3</sup> /mole.GPa <sup>2</sup> )	$V_0$
	$470.95 \pm 2.60$	$-48.95 \pm 3.60$	$7.05 \pm 1.00$	470.95

Table 3. 10 Coefficients  $c_0$ ,  $c_1$  and  $c_2$  which were found according to Eq. (3.3) using the observed data [52] for the modes indicated for solid anthracene. We also give here the uncertainties determined for the coefficients  $c_0$ ,  $c_1$  and  $c_2$  for six modes of solid anthracene. The values of the Raman frequencies for six modes of solid anthracene at P= 0 GPa and T= 300 K, are also given here.

ANTHRACENE	$c_0$ (cm <sup>-1</sup> )	$c_1$ (cm <sup>-1</sup> /GPa)	$c_2$ (cm <sup>-1</sup> /GPa <sup>2</sup> )	$\vartheta_0$
A <sub>g</sub>	$38.47 \pm 0.60$	$11.06 \pm 0.20$	$1.37 \pm 0.02$	38.47
B <sub>g</sub>	$46.00 \pm 1.20$	$17.86 \pm 1.60$	$1.33 \pm 0.50$	46.00
B <sub>g</sub>	$68.19 \pm 1.00$	$24.13 \pm 1.50$	$2.28 \pm 0.50$	68.19
A <sub>g</sub>	$73.59 \pm 1.10$	$27.94 \pm 1.70$	$3.24 \pm 0.50$	73.59
A <sub>g</sub>	$122.73 \pm 1.80$	$38.82 \pm 2.90$	$4.55 \pm 0.90$	122.73
B <sub>g</sub>	$129.70 \pm 1.80$	$43.58 \pm 2.90$	$4.89 \pm 0.90$	129.70
Vibrons	$c_0$ (cm <sup>-1</sup> )	$c_1$ (cm <sup>-1</sup> /GPa)	$c_2 \times 10^{-4}$ (cm <sup>-1</sup> /GPa <sup>2</sup> )	$\vartheta_0$
12A <sub>g</sub>	$396.95 \pm 2.71$	$0.53 \pm 0.32$	$19.1 \pm 0.08$	396.95
10B <sub>3g</sub>	$521.94 \pm 1.80$	$0.17 \pm 0.19$	$15.8 \pm 0.05$	521.95
10A <sub>g</sub>	$754.19 \pm 3.68$	$0.38 \pm 0.19$	$8.2 \pm 0.05$	754.19
9A <sub>g</sub>	$1008.78 \pm 2.16$	$0.33 \pm 0.69$	$14.3 \pm 0.04$	1008.78
8A <sub>g</sub>	$1164.81 \pm 3.30$	$0.21 \pm 0.38$	$13.8 \pm 0.01$	1164.81
7B <sub>3g</sub>	$1189.70 \pm 2.87$	$0.23 \pm 0.34$	$11.7 \pm 0.01$	1189.70
7A <sub>g</sub>	$1261.01 \pm 2.16$	$0.70 \pm 0.25$	$37.9 \pm 0.01$	1261.01
6A <sub>g</sub>	$1403.34 \pm 2.89$	$0.62 \pm 0.34$	$30.2 \pm 0.01$	1403.34
4A <sub>g</sub>	$1558.78 \pm 2.31$	$0.33 \pm 0.27$	$18.2 \pm 0.01$	1558.78

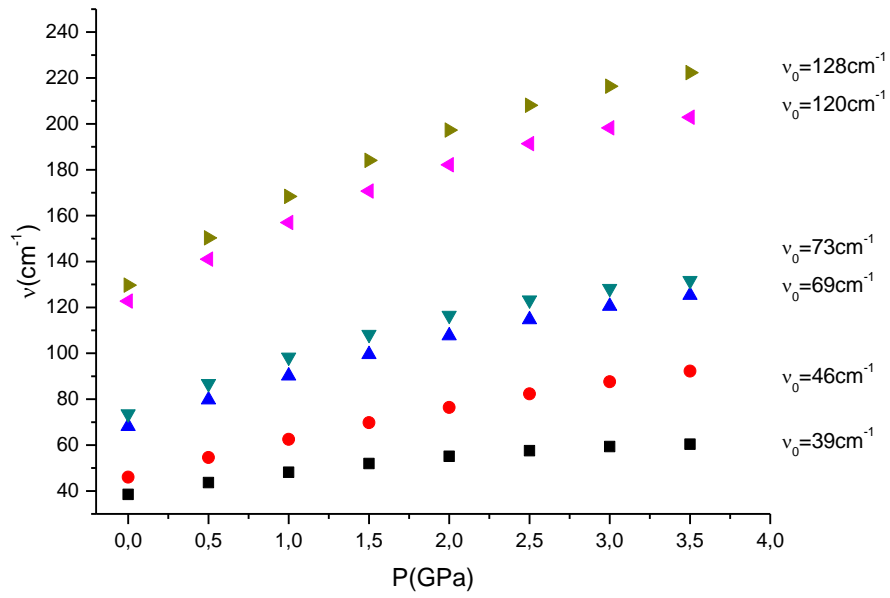


Figure 3.16 The found Raman frequencies of six phonon modes of solid anthracene as a function of pressure according to Equation (2.12).

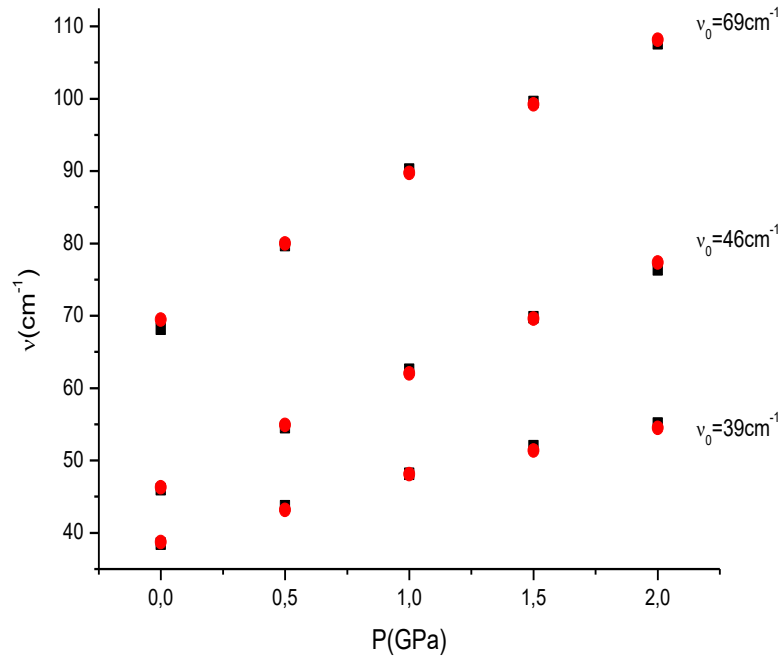


Figure 3.17 The found Raman frequencies for the phonon modes as a function of pressure at room temperature according to Equation (3.6) for crystalline anthracene.

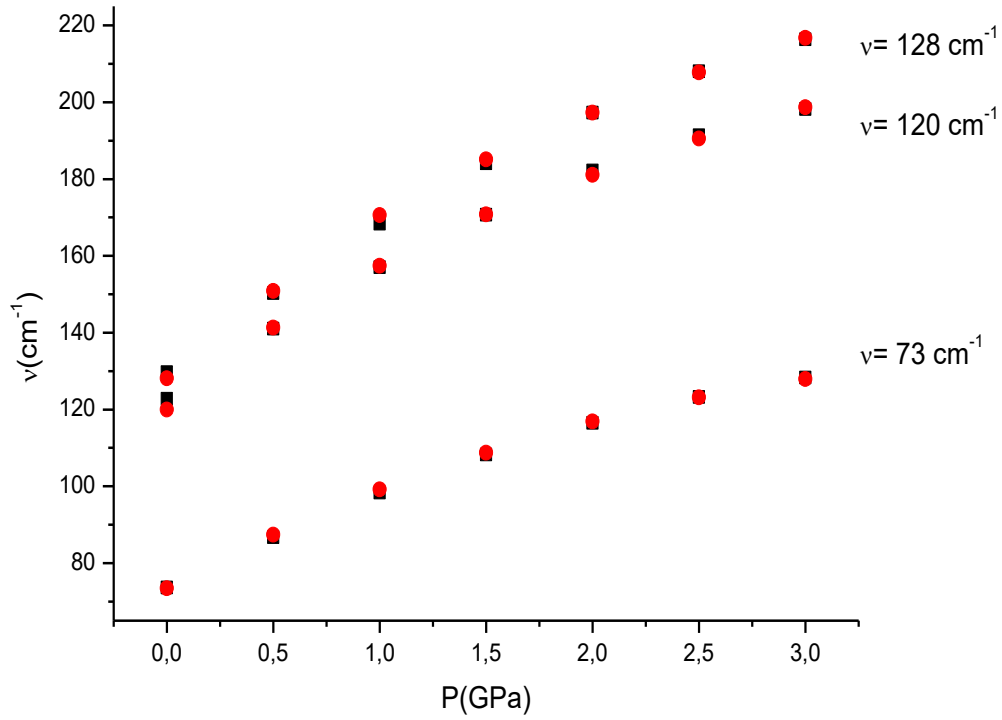


Figure 3.18 The found Raman frequencies for the phonon modes as a function of pressure at room temperature according to Equation (3.6) for crystalline anthracene.

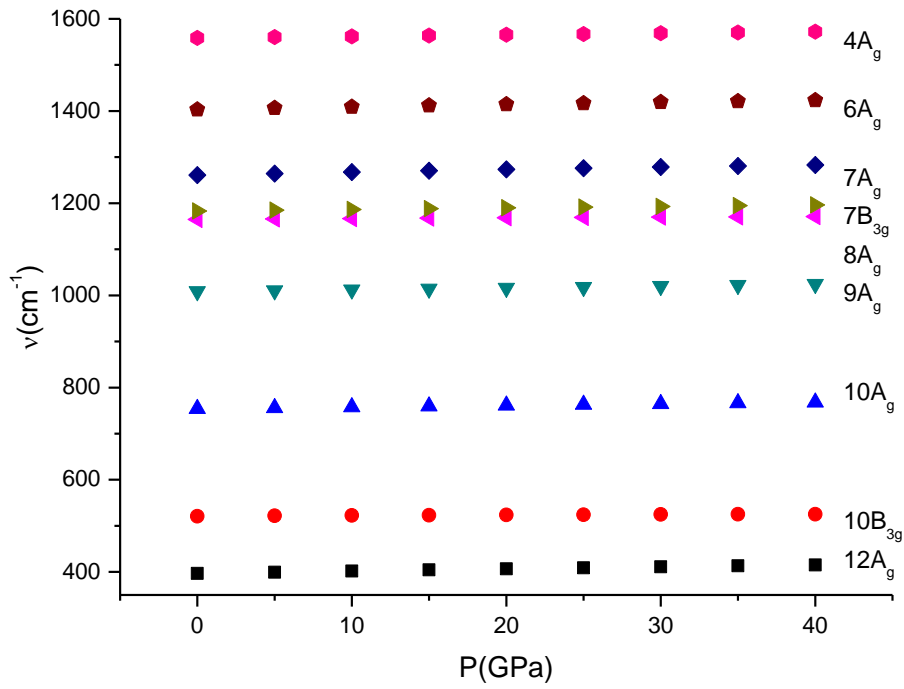


Figure 3.19 The found Raman frequencies of nine vibron modes of solid anthracene as a function of pressure according to Equation (3.6).

The Raman frequencies were calculated as functions of pressure with the observed volume data[48,52] for the six phonon and nine vibron modes of solid anthracene through the values of the isothermal mode Grüneisen parameter  $\gamma_T(P)$  at  $P = 0$  for those modes studied (Table 3.14). It has been found experimentally [52] that the vibron modes exhibit almost a linear shift with pressure, but the pressure-induced shifts in the phonon frequencies are nonlinear. In fact, increasing with pressure in the Raman frequencies are more apparent for the phonon modes, as shown in Figure 3.16. Increasing in the Raman frequencies with the pressure are significant for the phonon modes (Figure 3.16) as stated above. Pressure dependence of the vibron modes looks almost insignificant so that they are also independent of pressure (Figure 3.19).

It has been indicated that intra-molecular vibration (vibron) frequencies are uniformly much less pressure-sensitive, which involves the volume dependence only, whereas the temperature variation of the vibrational frequencies of crystal lattices involves both temperature and volume [48].

In order to estimate the Raman frequencies, we determined the values of the isothermal mode Grüneisen parameter  $\gamma_T$  at  $P=0$  for the six phonon and nine vibron modes of solid anthracene (Table 3.14). As seen from this table, our values of the mode Grüneisen parameter of those modes studied, are in good agreement with the observed ones [52]. Notice that the values of the mode Grüneisen parameter for the six phonon modes (external modes) are much larger than those of the nine vibrons (internal modes) of the solid anthracene, as expected in general for the molecular solids. A small difference in crystal volume causes a big change in frequency, which results in a large Grüneisen parameter, in particular, for the six lattice modes of anthracene. This small change in the unit cell parameters results in a weaker rearrangement of the molecules at higher pressure, as also pointed out previously [50]. It has been reported that the values of the Grüneisen parameters for the  $A_g$  and  $B_g$  modes of anthracene, which vary from 3 to 6 are higher than those obtained for ionic crystals [26]. This also applies to our calculated  $\gamma_T$  and the observed  $\gamma_T$  [6] (at  $P=0$ ) values of the mode Grüneisen parameter for the phonon modes (external modes) (Table 3). It has been explained that the relatively large  $\gamma$  values observed for

intermolecular phonon modes (external modes) are due to the comparatively large compression of the vibrational coordinate and also, comparatively small  $\gamma$  values observed for some intramolecular vibrons (internal modes) are due to the compression along intermolecular coordinates orthogonal to the vibron coordinate [43].

Table 3. 4 Calculated isothermal mode Grüneisen parameter (Equation (2.10)) for the six phonon and nine vibron modes of solid anthracene (P= 0 GPa). Observed data [52] is also given.

Phonon Modes	$\vartheta_0$ (cm <sup>-1</sup> )	$\gamma_T$ (Calculated)	$\gamma_T$ (Observed [52])
A <sub>g</sub>	38.47	3.61	4.01
B <sub>g</sub>	46.00	3.25	4.00
B <sub>g</sub>	68.19	3.43	2.96
A <sub>g</sub>	73.59	3.65	3.06
A <sub>g</sub>	122.73	3.04	2.78
B <sub>g</sub>	129.70	3.23	2.87
Vibron Modes	$\vartheta_0$ (cm <sup>-1</sup> )	$\gamma_T$ (Calculated)	$\gamma_T$ (Observed [52])
12A <sub>g</sub>	396.95	0.196	0.186
10B <sub>3g</sub>	521.95	0.048	0.035
10A <sub>g</sub>	754.19	0.074	0.073
9A <sub>g</sub>	1008.78	0.048	0.054
8A <sub>g</sub>	1164.81	0.026	0.021
7B <sub>3g</sub>	1189.70	0.043	0.042
7A <sub>g</sub>	1261.01	0.081	0.068
6A <sub>g</sub>	1403.34	0.065	0.057
4A <sub>g</sub>	1558.78	0.031	0.031

Due to the uncertainties in the experimental measurements, we determined the uncertainties in the parameters of our calculations [41]. We also determined the uncertainties in the Raman frequencies calculated of the six phonon modes through the experimental data [41] at P=0 GPa (Table 3.11). Since we take into account the smallest uncertainty in the coefficients in our calculations, the physical quantities we calculated become more meaningful physically. Very large uncertainties in the



coefficients we found, increase the values of those physical quantities considerably, which then become incomparable with the experimental values. We used the uncertainties through the coefficient  $c_0$ . The pressure uncertainty was usually between  $\pm 0.6$  and  $\pm 1.8$  GPa. Also, the uncertainties in the molar volume were predicted to be  $\pm 2.6$  cm<sup>3</sup>/mol for the six phonon modes. On that basis, we determined the uncertainties in the molar volume  $V$ , in the Raman frequencies  $\vartheta$  of the modes and in the isothermal mode Grüneisen parameter  $\gamma_T(P=0 \text{ GPa})$  for the six phonon modes of anthracene. Using the calculated terms with the uncertainties in Equation (3.6), the Raman frequencies of the six phonon modes of solid anthracene were calculated. We determined uncertainties in the Raman frequencies calculated at various pressures, as plotted for the six phonon modes of anthracene in Figures 20 and 21. Uncertainty in the Raman frequency of the mode with  $\vartheta_0 = 39 \text{ cm}^{-1}$  for anthracene was estimated to be 1.5 % (or  $0.6 \text{ cm}^{-1}/\text{mole}$ ) at zero pressure (Figure 3.20). Uncertainty in the Raman frequency of the mode with  $\vartheta_0 = 46 \text{ cm}^{-1}$  for anthracene was estimated to be 2.6 % (or  $1.2 \text{ cm}^{-1}/\text{mole}$ ) at zero pressure (Figure 3.20). Uncertainty in the Raman frequency of the mode with  $\vartheta_0 = 69 \text{ cm}^{-1}$  for anthracene was estimated to be 1.4 % (or  $1.0 \text{ cm}^{-1}/\text{mole}$ ) at zero pressure (Figure 3.20). Uncertainty in the mode with  $\vartheta_0 = 73 \text{ cm}^{-1}$  for anthracene was estimated to be 1.5 % (or  $1.1 \text{ cm}^{-1}/\text{mole}$ ) at zero pressure (Figure 3.21). Uncertainty in the Raman frequency of the mode with  $\vartheta_0 = 120 \text{ cm}^{-1}$  for anthracene was estimated to be 1.5 % (or  $1.8 \text{ cm}^{-1}/\text{mole}$ ) at zero pressure (Figure 3.21). Uncertainty in the Raman frequency of the mode with  $\vartheta_0 = 128$  for anthracene was estimated to be 1.4 % (or  $1.8 \text{ cm}^{-1}/\text{mole}$ ) at zero pressure (Figure 3.21). Uncertainty range verifies the agreement between the calculated and observed data of the mentioned modes for anthracene.

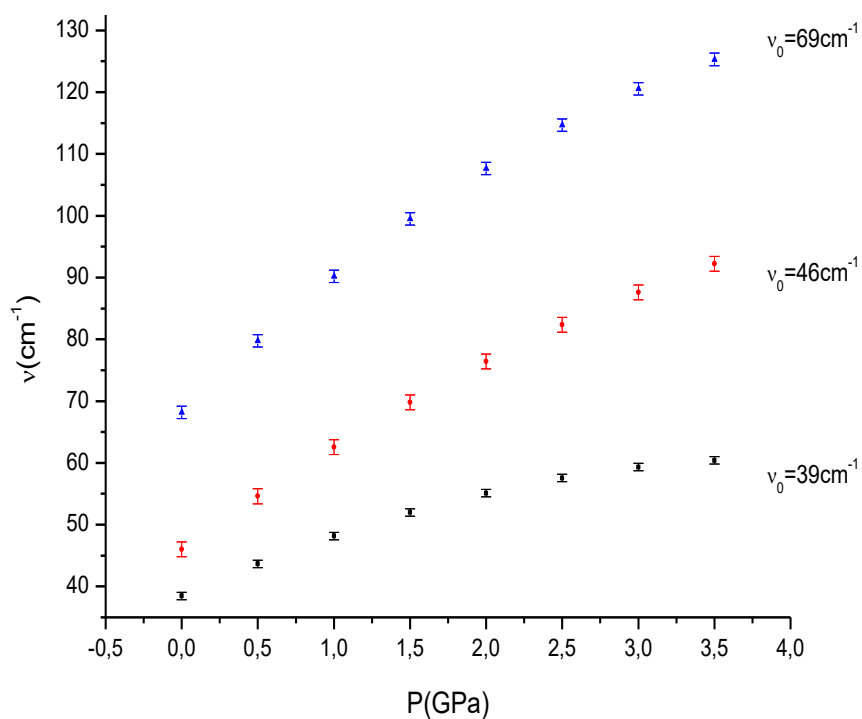


Figure 3.20 Uncertainties in the Raman frequencies calculated for modes of solid anthracene according to Equation (3.6).

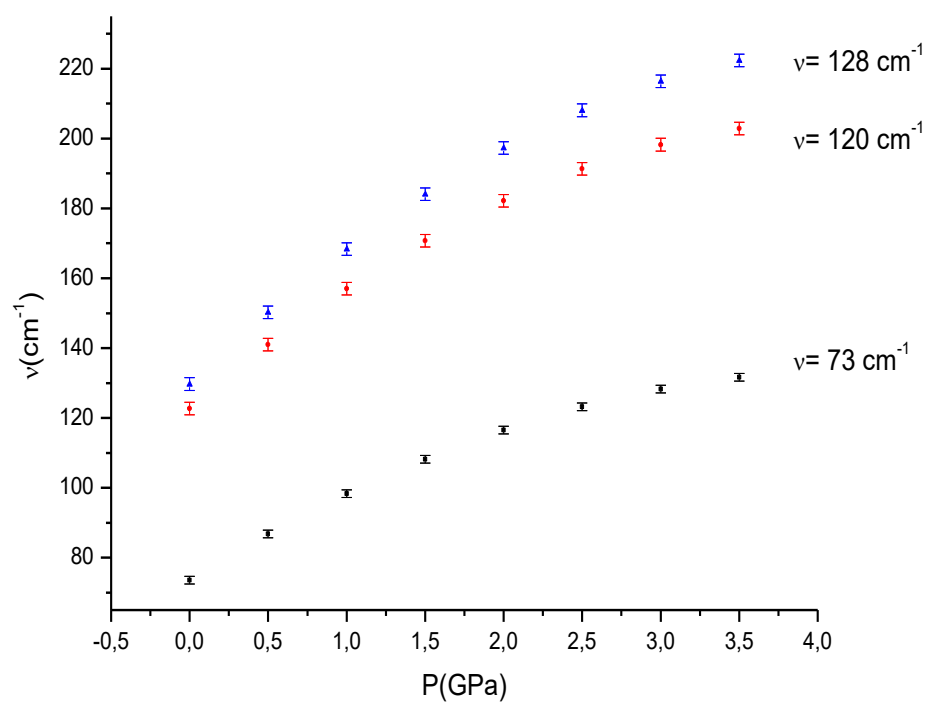


Figure 3.21 Uncertainties in the Raman frequencies calculated for modes of solid anthracene according to Equation (3.6).

## 3.2 Calculation of the Raman Frequency as a Function of Temperature for the Hydrocarbons: Benzene, Naphthalene and Anthracene

### 3.2.1 Benzene

Temperature dependence of the volume according to Equation (3.2) was determined by fitting the observed data [12] and the coefficients  $b_0$ ,  $b_1$ ,  $b_2$  in Equation (3.2) are given in Table 3.12. The Raman frequency shifts of six phonon modes of solid benzene I were obtained as a function of temperature in Equation (3.4) and the coefficients are given in Table 3.13 with the uncertainties. Then, isothermal mode Grüneisen parameter was calculated according to Equation (2.10) for the six phonon modes of solid benzene I at zero pressure. Finally, the temperature dependence of the Raman frequency shifts were obtained by using Equation (3.7) for six phonon modes of solid benzene I.

Table 3.12 Coefficients  $b_0$ ,  $b_1$  and  $b_2$  as determined by Eq. (3.2) for the phonon modes of solid benzene. We also give here the uncertainties determined in the coefficients  $b_0$ ,  $b_1$  and  $b_2$  for the mentioned modes of benzene.

BENZENE	$b_0(\text{cm}^3/\text{mole})$	$b_1 \times 10^{-2}(\text{cm}^3/\text{mole.K})$	$b_2 \times 10^{-5}(\text{cm}^3/\text{mole.K}^2)$	$V_0$
	$69.16 \pm 0.03$	$4.92 \pm 0.04$	$8.29 \pm 0.20$	78.10

Table 3.13 Coefficients  $d_0$ ,  $d_1$  and  $d_2$  which were found according to Eq. (3.4) using the observed data [12] for the phonon modes of solid benzene I . We also give here the uncertainties determined for the coefficients  $d_0$ ,  $d_1$  and  $d_2$  for six phonon modes of solid benzene I. Calculated Raman frequency shifts are also represented at P= 0 GPa and T= 300 K.

BENZENE	$d_0(\text{cm}^{-1})$	$d_1 \times 10^{-2} (\text{cm}^{-1}/\text{K})$	$d_2 \times 10^{-4} (\text{cm}^{-1}/\text{K}^2)$	$\vartheta_0$
Mode A	$61.42 \pm 0.1$	$-1.16 \pm 0.2$	$-2.12 \pm 0.1$	38.32
Mode B	$70.44 \pm 0.2$	$-6.46 \pm 0.4$	$0.87 \pm 0.1$	51.83
Mode C	$139.28 \pm 0.2$	$-6.58 \pm 0.4$	$-0.23 \pm 0.1$	99.02
Mode X	$68.79 \pm 0.2$	$-3.15 \pm 0.01$	$-0.28 \pm 0.5$	38.82
Mode Y	$100.30 \pm 0.3$	$-3.45 \pm 0.01$	$-2.66 \pm 0.2$	66.01
Mode Z	$110.91 \pm 0.3$	$-3.40 \pm 0.01$	$-2.89 \pm 0.6$	74.70

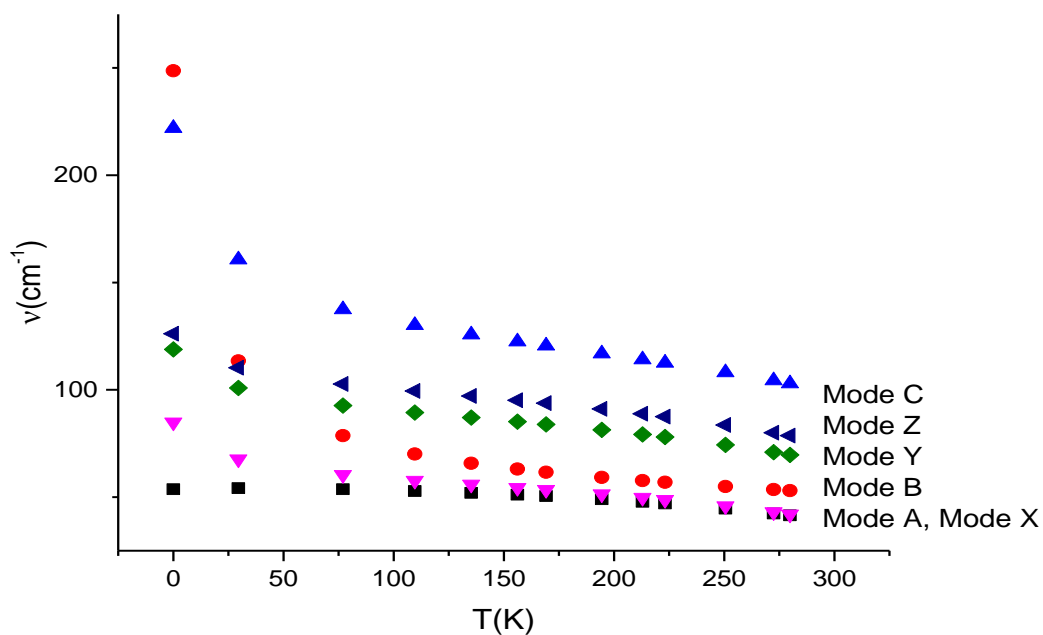


Figure 3.22 Calculated Raman frequencies as a function of temperature at zero pressure according to Equation (3.7) by using the observed data [12] for six phonon modes of solid benzene I.

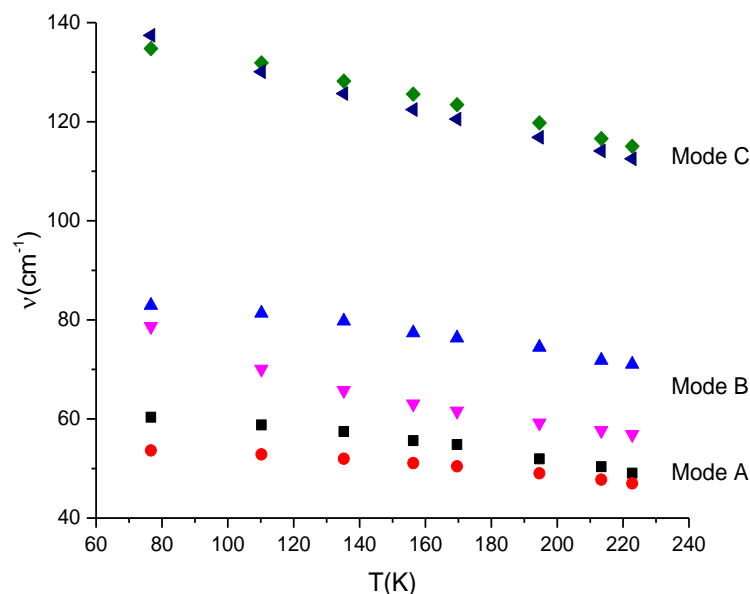


Figure 3. 23 Temperature dependence of the Raman frequencies (Equation (3.7)) at zero pressure for solid benzene I are defined with red circles (Mode A), purple triangles (Mode B) and green squares (Mode C). Observed data [12] are also given with black squares (Mode A), blue triangles (Mode B) and green squares (Mode C), respectively.

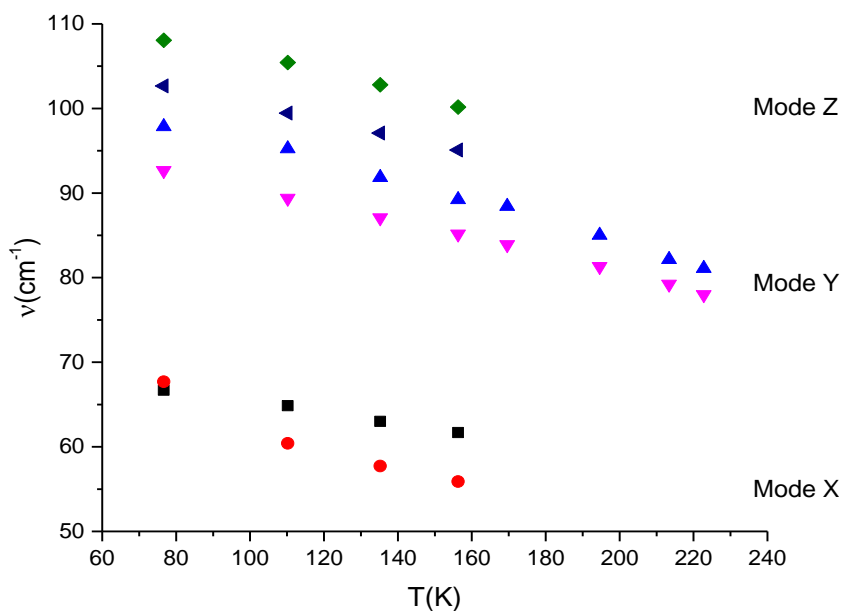


Figure 3. 24 Temperature dependence of the Raman frequencies (Equation (3.7)) at zero pressure for solid benzene I are defined with red circles (Mode X), purple triangles (Mode Y) and green squares (Mode Z). Observed data [12] are also given with black squares (Mode X), blue triangles (Mode Y) and green squares (Mode Z), respectively.

Calculated Raman frequencies (Equation (3.7)) for the six phonon modes of solid benzene decrease with the increasing temperature as seen in Figure 3.22, as expected. Calculated data exhibits the same behaviour with the observed data [12] for all phonon modes in Figures 3.23 and 3.24. There is a distinct discrepancy with the observed data [12] for all modes of benzene. The reason of the discrepancy may be due to the lack of experimental graph of Raman frequencies as a function of temperature in the literature. In this section, a graph is suggested for the Raman frequencies of six phonon modes of solid benzene in solid I-II transition through the experimental data [12]. When a direct experimental data is available in literature, an accurate comparison will be given between the calculated and observed data for this section.

The Raman frequencies of the six phonon modes (A,B,C and X,Y,Z) were calculated from the volume data through the isobaric mode Grüneisen parameter  $\gamma_p$  (Table 3.) at zero pressure. Calculated isobaric mode Grüneisen parameters differ slightly around the value of 3 except mode A. Grüneisen parameter differs between 3 and 4 for mode A. Consequently, the isobaric mode Grüneisen parameter  $\gamma_p$  seems to be independent of the change in this temperature range.

Calculated uncertainties in the Raman frequencies for the lattice modes (A,B,C and X,Y,Z) of solid benzene were determined because of the uncertainties in the experimental measurements [12]. We determined uncertainties in the Raman frequencies found as a function of temperature (Equation (3.4)) for the modes through the experimental data [34] at  $T=293$  K which is given in Table 3.13. Since we take into account the smallest uncertainty in the coefficients in our calculations, the physical quantities we calculated become more meaningful physically. Very large uncertainties in the coefficients we found, increase the values of those physical quantities considerably, which then become incomparable with the experimental values. We used the uncertainties in the Raman frequency as a function of temperature calculations through the coefficient  $d_1$ . The temperature uncertainty range is between  $\pm 0.1$  and  $\pm 0.3$ . Also, the uncertainties in the molar volume were predicted to be  $\pm 1.5$  cm<sup>3</sup>/mol for the solid benzene [12]. Equation (3.2) was used with the uncertainties in the volume as a function of temperature to determine the

uncertainties in our Raman frequencies which were calculated for the lattice modes (A,B,C and X,Y,Z) of solid benzene as plotted in Figure 3.24. Uncertainty in the mode A with the frequency of  $\vartheta_o = 38.32 \text{ cm}^{-1}$  for naphthalene was estimated to be 0.3% (or  $0.1 \text{ cm}^{-1}$ ) at room temperature (Figure 3.25). Similarly, uncertainties in the mode B with the frequency of  $\vartheta_o = 51.83 \text{ cm}^{-1}$  and with  $\vartheta_o = 99.02 \text{ cm}^{-1}$  for naphthalene were estimated to be 0.4% (or  $0.2 \text{ cm}^{-1}$ ) and 0.2% (or  $0.2 \text{ cm}^{-1}$ ), respectively, at ambient pressure (Figure 3.25). Uncertainties in the Raman frequency calculated as a function of temperature calculations were estimated as 0.5% (or  $0.2 \text{ cm}^{-1}$ ) for mode X with  $\vartheta_o = 38.82 \text{ cm}^{-1}$ , 0.4% (or  $0.3 \text{ cm}^3/\text{mole.GPa}$ ) for mode Y with  $\vartheta_o = 66.01 \text{ cm}^{-1}$  and 0.5% (or  $0.3 \text{ cm}^3/\text{mole.GPa}$ ) for mode Z with  $\vartheta_o = 74.70 \text{ cm}^{-1}$  at zero pressure. Both Figure 3.22 and Figure 3.23 have a discrepancy region for the A,B,C and X,Y,Z modes for solid benzene. As we mentioned before, uncertainty may arise from the weak contribution of the thermal expansion at low temperatures. Weak contribution of the thermal expansion effect of undefined or overlapped modes can also be reason for the uncertainties. This behaviour can be partly arised from the fitting the frequencies to the experimental structure rather than the relaxed structure.

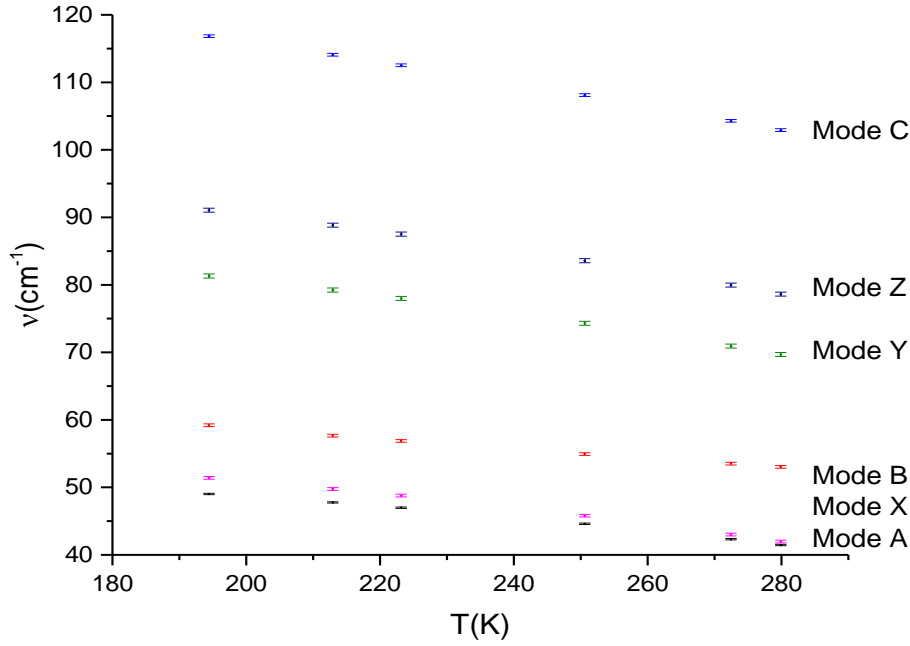


Figure 3. 25 Uncertainties in the Raman frequencies calculated for modes of solid benzene according to Equation (3.7).

### 3.2.2 Naphthalene

The coefficients  $b_0$ ,  $b_1$  and  $b_2$  referred to the Equation (3.2) were determined by using the experimental data [20,73] for volume as a function of temperature (at  $P = 0$  GPa), as given in Table 3.15. The coefficients  $d_0$ ,  $d_1$  and  $d_2$  were determined ( $P = 0$ ) by analyzing the temperature dependence of the Raman frequencies of the  $A_g$  and  $B_g$  modes by using the Equation (3.4) through the observed Raman frequencies [37] for solid naphthalene, as given in Table 3.16.

The isothermal mode Gruneisen parameter  $\gamma_T$  as a function of pressure at room temperature was also determined for the  $A_g$  and  $B_g$  modes by using the observed volume data [20,74] and the observed Raman frequencies [37], according to Equation (2.10). Equation (2.11) has the pressure-dependent term  $A(T)$  whose coefficients were determined by defining the pressure-dependent term in a quadratic form as given below:

$$A(T) = a + bT + cT^2 \quad (3.10)$$



The coefficients of the pressure dependent function  $A(T)$  defined in Equation (3.10) were defined through Equation (2.11) for the phonon modes of naphthalene at zero pressure. Determined coefficients  $a, b$  and  $c$  of  $A(T)$  for the phonon modes are given in Table 3.17. Also, the Raman frequencies of the  $A_g$  and  $B_g$  modes as a function of pressure and temperature were calculated through Equations (2.11) and (2.12) by using the observed volume data [20,74] and the observed Raman frequencies [37].

Table 3. 11 Coefficients  $b_0, b_1$  and  $b_2$  as determined according to Equation (3.2) by using observed data [37] of solid naphthalene at room temperature. We also give here the uncertainties determined in the coefficients  $b_0, b_1$  and  $b_2$ .

NAPHTHALENE	$b_0$ (cm <sup>-1</sup> )	$b_1$ (cm <sup>-1</sup> /mole.K)	$b_2 \times 10^{-4}$ (cm <sup>3</sup> /mole.K <sup>2</sup> )	$V_0$
	338.89±1.4	0.03±0.02	1.39±0.38	360.4

Table 3. 12 Coefficients  $d_0, d_1$  and  $d_2$  which were found according to Eq. (3.4) using the observed data [37] for the modes indicated for solid naphthalene. We also give here the uncertainties determined for the coefficients  $d_0, d_1$  and  $d_2$  for six modes of solid naphthalene. Values of the Raman frequencies for six modes of solid naphthalene at  $P=0$  GPa and  $T=300$  K, are also given here.

NAPHTHALENE	$d_0$ (cm <sup>-1</sup> )	$d_1 \times 10^{-2}$ (cm <sup>-1</sup> /K)	$d_2 \times 10^{-4}$ (cm <sup>-1</sup> /K <sup>2</sup> )	$\vartheta_0$
Mode $A_{g1}$	69.35±0.80	-2.82±0.01	-1.19±0.44	50.18
Mode $A_{g2}$	88.75±0.32	-1.37±0.02	-2.64±0.71	60.88
Mode $A_{g3}$	121.64±0.60	-1.24±0.01	-1.14±0.29	107.66
Mode $B_{g1}$	57.36±1.10	-2.26±0.02	-0.59±0.63	45.27
Mode $B_{g2}$	84.18±1.40	-1.79±0.02	-1.05±0.75	69.36
Mode $B_{g3}$	142.35±3.05	-2.65±0.05	-1.19±0.16	123.69

Table 3. 13 The a, b and c coefficients which were found according to Equation (3.10) using the observed frequencies [37] which were obtained at zero pressure for six phonon modes of solid naphthalene.

A(T)	a	$b \times 10^{-2}$	$c \times 10^{-4}$
Mode A <sub>g1</sub>	3.20	4.57	1.55
Mode A <sub>g2</sub>	6.29	8.10	2.48
Mode A <sub>g3</sub>	7.53	9.82	2.82
Mode B <sub>g1</sub>	3.71	4.70	1.41
Mode B <sub>g2</sub>	4.27	5.71	1.74
Mode B <sub>g3</sub>	10.37	13.71	3.75

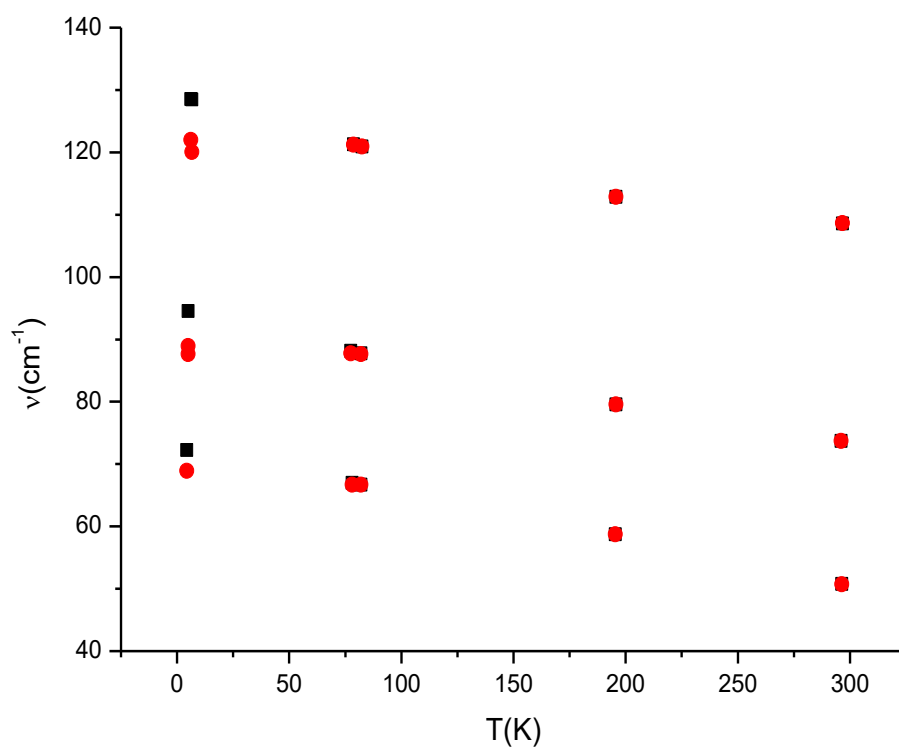


Figure 3. 26 The determined Raman frequencies as a function of temperature at atmospheric pressure for mode of symmetry A<sub>g</sub> for solid naphthalene (filled squares) according to Equation (2.11) and the experimental data of A<sub>g</sub> modes [34] for solid naphthalene (filled circles).

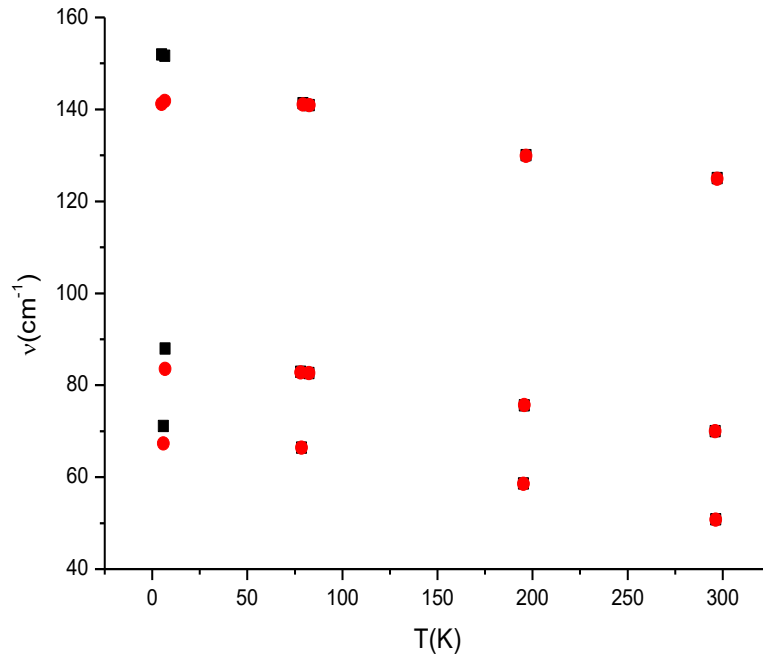


Figure 3. 27 The determined Raman frequencies as a function of temperature at atmospheric pressure for mode of symmetry  $B_g$  for solid naphthalene (filled squares) according to Equation (2.11) and the experimental data of  $B_g$  modes [37] for solid naphthalene (filled circles).

The Raman frequencies were estimated for the  $3A_g$  and  $3B_g$  modes using the observed volume data by finding their mode Gruneisen parameters in naphthalene. As shown in Figures 3.26 and 3.27, our found Raman frequencies (Equation (2.11)) for the  $A_g$  and  $B_g$  modes, respectively, reduce with increasing temperature, as observed experimentally [37]. There is a divergence between our computed and observed Raman frequencies of the  $A_g$  and  $B_g$  modes at a very low temperature (7 K) for the solid naphthalene. This is owing to the fact that decrease in the Raman frequencies of the six lattice modes ( $A_g$  and  $B_g$  modes) with increasing temperature can be ascribed to the thermal expansion in naphthalene. Subsequently we calculated the Raman frequencies using the volume data according to Equation (2.11), the Raman frequencies are not contributed by the thermal expansion at very low temperatures.

We determined the values of the isobaric mode Gruneisen parameter  $\gamma_p$  (Equation (2.9)) for the  $A_g$  and  $B_g$  modes of solid naphthalene as a function of temperature within the temperature interval of  $\sim 80\text{--}325$  K (Table 3.13). The average values of the  $\gamma_p$  which we obtained for the  $A_g$  modes, are between 5 and 7 ( $\gamma_p = 5.3$ ) for  $A_{g1}$ ,  $\gamma_p = 3.3$  for  $A_{g2}$  and  $\gamma_p = 2.0$  for the  $A_{g3}$  mode. For the  $B_g$  modes, we obtained as the average values,  $\gamma_p = 3.8$  for  $B_{g1}$ ,  $\gamma_p = 3.2$  for  $B_{g2}$  and  $\gamma_p = 2.3$  for the  $B_{g3}$  mode of solid naphthalene. The average values of the isobaric mode Gruneisen parameter  $\gamma_p$  for the  $A_g$  and  $B_g$  modes, show that the lower Raman frequency mode has the higher  $\gamma_p$  value for solid naphthalene. These are the  $\gamma_p$  values at zero pressure for the temperature interval of  $\sim 80\text{--}325$  K for this crystal (Table 3.18). Our  $\gamma_p$  values can be compared with those determined as reported in the literature. The temperature dependence of the Gruneisen parameter of the Raman active external modes in d8-naphthalene was determined as the mean values ranging from 2.7 to 3.5 for the temperature region 0–300 K [30]. Our average  $\gamma_p$  values for the  $A_g$  and  $B_g$  modes except the  $A_{g1}$  mode fall in the same interval as found for the Raman external modes given above.

Concerning the anharmonicity of a crystalline system, that gives rise to the thermal expansion and the deviation in frequency with temperature through the isobaric mode Gruneisen parameter  $\gamma_p$  (Equation (2.9)), the thermal expansion  $\gamma_p$  can be estimated from the Raman frequency shifts at a constant pressure (atmospheric pressure). By knowing a constant value of the mode Gruneisen parameter  $\gamma_p$ , the thermal expansion  $\alpha_p$  can be computed from the normal mode frequency shifts with temperature, which can be measured to high accuracy spectroscopically. When the  $\gamma_p$  varies with temperature as in the case of six lattice modes ( $A_g$  and  $B_g$  modes) for naphthalene, the thermal expansion can be computed from the Raman frequency shifts  $\alpha_p$  by using the initial data for the thermal expansion to determine the  $\alpha_p$  values as a function of temperature for naphthalene, as we studied here. The pressure dependence of the thermal expansion  $\alpha_p$  (at a constant temperature) can be estimated from the vibrational frequency shifts  $\left(\partial\vartheta/\partial T\right)_p$  by means of the isobaric  $\gamma_p$  mode Gruneisen parameter for naphthalene.

Table 3. 14 The isobaric mode Gruneisen parameter  $\gamma_p$  (Equation (2.9)) values for the Raman modes indicated as a function of temperature for solid naphthalene.

T(K) (P= 0 GPa)	Mode $A_{g1}$ ( $\gamma_p$ )	Mode $A_{g2}$ ( $\gamma_p$ )	Mode $A_{g3}$ ( $\gamma_p$ )	Mode $B_{g1}$ ( $\gamma_p$ )	Mode $B_{g2}$ ( $\gamma_p$ )	Mode $B_{g3}$ ( $\gamma_p$ )
79.0	4.66	2.62	1.67	3.81	2.77	2.14
84.4	4.68	2.66	1.69	3.80	2.79	2.14
93.3	4.70	2.72	1.73	3.76	2.82	2.15
110.5	4.76	2.84	1.79	3.73	2.88	2.17
118.7	4.80	2.89	1.82	3.72	2.91	2.18
124.6	4.82	2.92	1.84	3.71	2.93	2.18
142.9	4.91	3.03	1.90	3.70	2.99	2.21
144.2	4.92	3.04	1.90	3.70	3.00	2.21
157.7	4.99	3.12	1.95	3.70	3.05	2.23
182.0	5.14	3.27	2.02	3.72	3.14	2.26
185.1	5.16	3.28	2.03	3.72	3.15	2.27
240.8	5.61	3.63	2.19	3.84	3.39	2.37
273.3	5.96	3.85	2.30	3.96	3.55	2.45
294.7	6.23	4.02	2.37	4.05	3.68	2.50
298.3	6.28	4.04	2.38	4.06	3.70	2.51
314.8	6.53	4.18	2.44	4.15	3.80	2.56
325.0	6.69	4.27	2.47	4.20	3.87	2.59

Uncertainties in the Raman frequencies calculated for the  $A_g$  and  $B_g$  modes of solid naphthalene were determined because of the uncertainties in the experimental measurements [37]. We determined uncertainties in the Raman frequencies found as a function of temperature (Equation (3.4)) for the  $A_g$  and  $B_g$  modes through the experimental data [76] at T=293 K which is given in Table 3.16. Since we take into account the smallest uncertainty in the coefficients in our calculations, the physical quantities we calculated become more meaningful physically. Very large uncertainties in the coefficients we found, increase the values of those physical

quantities considerably, which then become incomparable with the experimental values. We used the uncertainties in the Raman frequency as a function of temperature calculations through the coefficient  $d_1$ . The temperature uncertainty range is between  $\pm 0.01$  and  $\pm 0.05$ . Also, the uncertainties in the molar volume were predicted to be  $\pm 0.02 \text{ cm}^3/\text{mol.K}$  for the solid naphthalene [20,74]. Equation (2.11) was used with the uncertainties in the Raman frequencies and the volume as a function of temperature to determine the uncertainties in our Raman frequencies calculated for the  $A_g$  and  $B_g$  modes of solid naphthalene as plotted in Figures 3.28 and 3.29. Uncertainty in the  $A_g$  mode with the frequency of  $\vartheta_o = 69 \text{ cm}^{-1}$  for naphthalene was estimated to be 2.3% (or  $1.6 \text{ cm}^3/\text{mole.K}$ ) at room temperature (Figure 3.28). Both in Figure 3.28 and Figure 3.29 have a discrepancy region through the lower temperatures for the  $A_g$  and  $B_g$  modes for solid naphthalene. As we mentioned before, uncertainty may arise from the weak contribution of the thermal expansion at low temperatures. Weak contribution of the thermal expansion effect of undefined or overlapped modes also be reason for the uncertainties. Weak contribution of the thermal expansion effect of undefined or overlapped modes also be reason for the uncertainties. This behaviour can be partly arisen from the fitting the frequencies to the experimental structure, rather than the relaxed structure. We determined uncertainties in the Raman frequency found as a function of temperature as plotted with the uncertainties for the  $A_g$  and  $B_g$  modes of solid naphthalene in Figures 3.28 and 3.29.

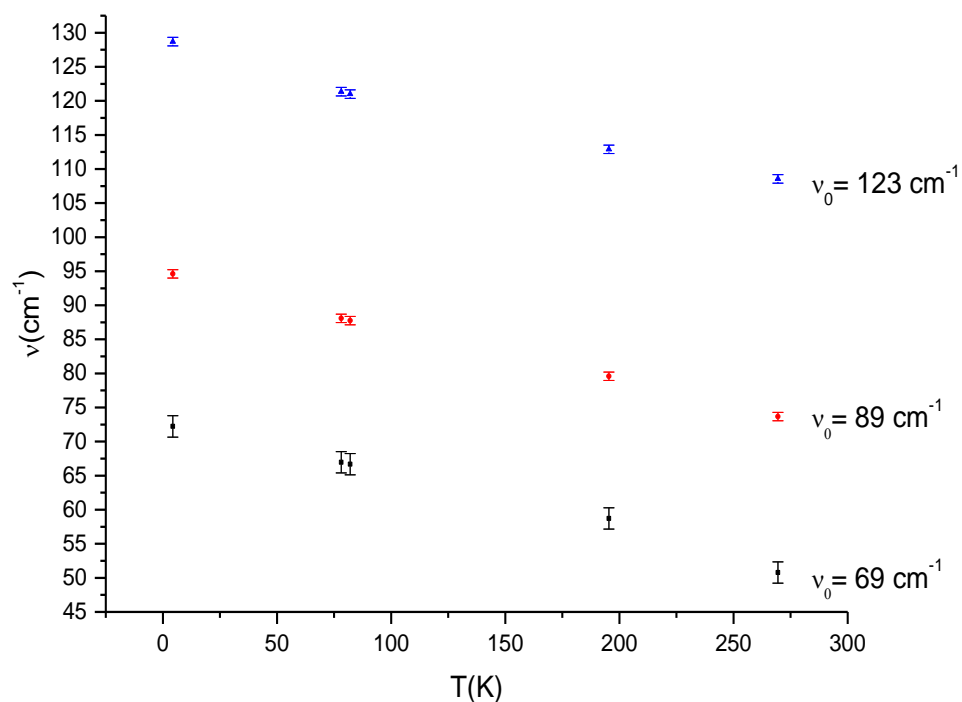


Figure 3. 28 Uncertainties in the Raman frequencies calculated for modes of symmetry  $A_g$  for solid naphthalene according to Equation (2.11).

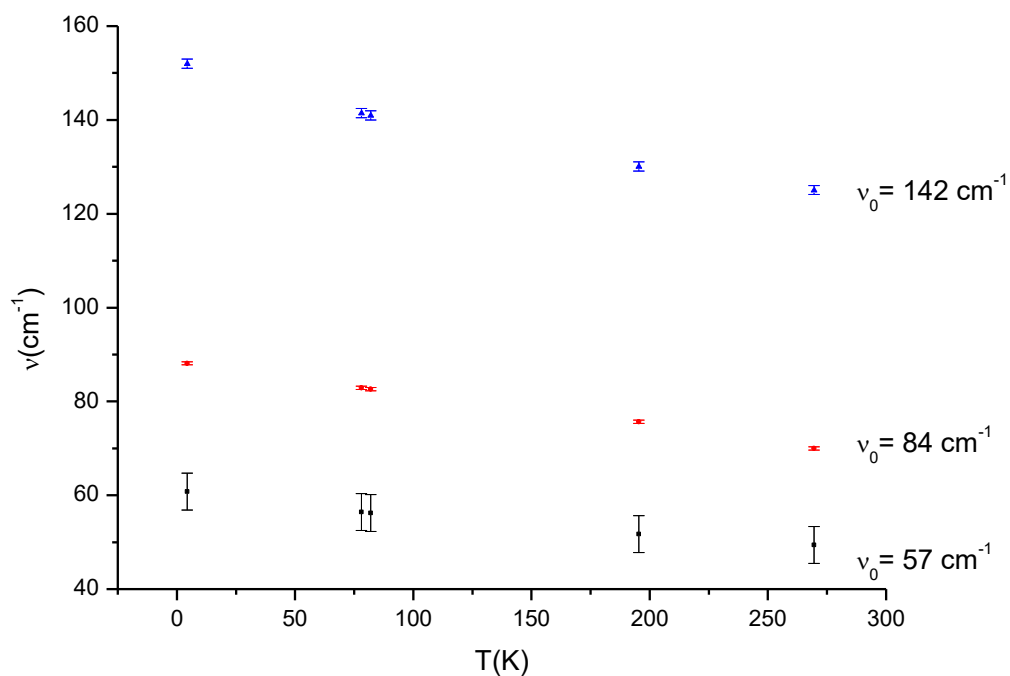


Figure 3. 29 Uncertainties in the Raman frequencies calculated for modes of symmetry  $B_g$  for solid naphthalene according to Equation (2.11).

### 3.2.3 Anthracene

Temperature dependence of the crystalline volume was calculated by fitting Equation (3.2) to the observed data and the coefficients  $b_0$ ,  $b_1$ ,  $b_2$  are represented in Table 3.19 with the uncertainties. The Raman frequencies of the six phonon and nine vibron modes of solid anthracene were obtained as a function temperature by using the observed data [48,52] according to Equation (3.9) through the isothermal mode Grüneisen parameter  $\gamma_T$ . The coefficients  $d_0$ ,  $d_1$ ,  $d_2$  in Equation (3.4) are given in Table 3.20 with the uncertainties.

The crystal volume and the Raman frequency values are represented in terms of  $\vartheta_1$  and  $V_1$  at zero pressure and room temperature. The Raman frequency as a function of temperature at zero pressure for the six phonon and nine vibron modes of solid anthracene was calculated by using the observed data [52] according to Equation (3.9), as plotted in Figures 3.30 and 3.31.

Table 3.15 Coefficients  $b_0$ ,  $b_1$  and  $b_2$  as determined according to Equation (3.2) by using observed data [52] for solid anthracene at room temperature. We also give here the uncertainties determined in the coefficients  $b_0$ ,  $b_1$  and  $b_2$  for the mentioned modes of naphthalene.

ANTHRACENE	$b_0$ (cm <sup>-1</sup> )	$b_1 \times 10^{-2}$ (cm <sup>-1</sup> /mole.K)	$b_2 \times 10^{-4}$ (cm <sup>3</sup> /mole.K <sup>2</sup> )	$V_0$
	451.72±0.3	4.14±0.4	1.06±0.1	473.7



Table 3.16 Coefficients  $d_0$ ,  $d_1$  and  $d_2$  which were found according to Eq. (3.4) using the observed data [52] for the modes indicated for solid anthracene. We also give here the uncertainties determined for the coefficients  $d_0$ ,  $d$  and  $d_2$  for six modes of solid anthracene. Values of the Raman frequencies for six modes of solid anthracene at  $P = 0$  GPa and  $T = 300$  K, are also given here.

ANTHRACENE	$d_0$ (cm <sup>-1</sup> )	$d_1 \times 10^{-2}$ (cm <sup>-1</sup> /K)	$d_2 \times 10^{-5}$ (cm <sup>-1</sup> /K <sup>2</sup> )	$\vartheta_0$
A <sub>g</sub>	46.26±0.03	-1.76±0.03	-2.35±0.07	38.87
B <sub>g</sub>	53.63±0.03	-1.83±0.03	-2.57±0.07	45.83
B <sub>g</sub>	81.15±0.04	-2.93±0.05	-4.01±0.12	68.75
A <sub>g</sub>	86.76±0.04	-3.35±0.06	-4.43±0.14	72.72
A <sub>g</sub>	138.52±0.06	-4.39±0.07	-6.37±0.17	119.62
B <sub>g</sub>	149.10±0.07	-5.04±0.08	-7.11±0.20	127.58
Vibrons	$d_0$ (cm <sup>-1</sup> )	$d_1 \times 10^{-2}$ (cm <sup>-1</sup> /K)	$d_2 \times 10^{-5}$ (cm <sup>-1</sup> /K <sup>2</sup> )	$\vartheta_0$
12A <sub>g</sub>	399.64±0.06	0.77±0.07	0.50±0.16	399.64
10B <sub>3g</sub>	523.17±0.02	0.24±0.02	0.50±0.50	523.17
10A <sub>g</sub>	756.61±0.04	0.54±0.05	1.16±0.11	756.61
9A <sub>g</sub>	1011.26±0.04	0.48±0.05	0.98±0.14	1011.26
8A <sub>g</sub>	1166.13±0.02	0.22±0.02	0.56±0.06	1166.13
7B <sub>3g</sub>	1190.35±0.04	0.45±0.04	1.20±0.11	1190.35
7A <sub>g</sub>	1265.75±0.09	0.97±0.09	2.19±0.24	1265.75
6A <sub>g</sub>	1407.31±0.06	0.92±0.07	1.84±0.17	1407.31
4A <sub>g</sub>	1560.26±0.04	0.47±0.05	1.02±0.12	1560.26

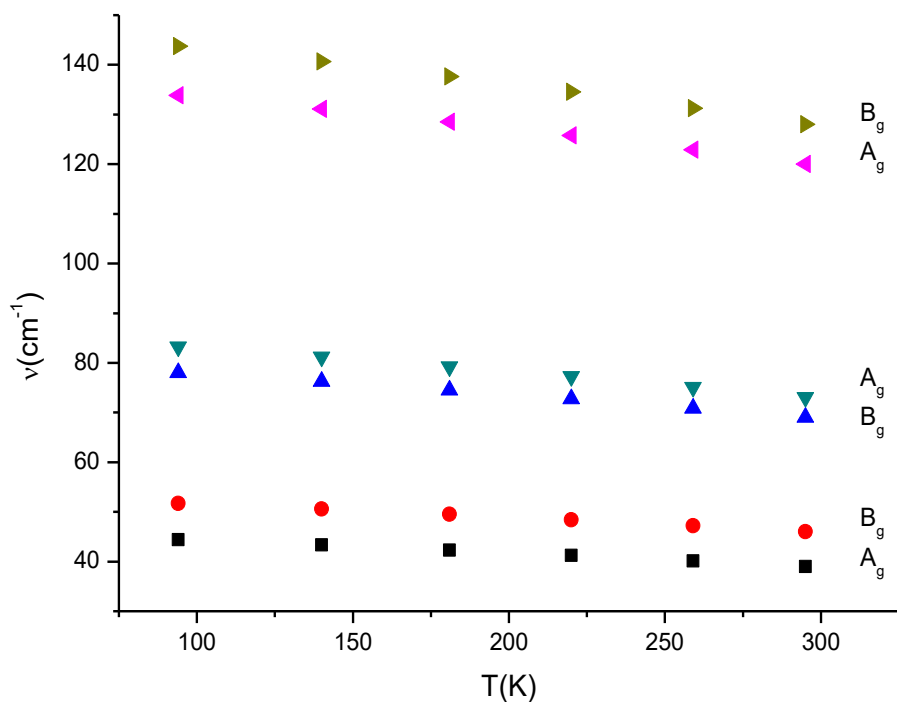


Figure 3. 30 Calculated Raman frequencies for the phonon modes as a function of temperature at  $P=0$  GPa according to Equation (3.9) for crystalline anthracene.

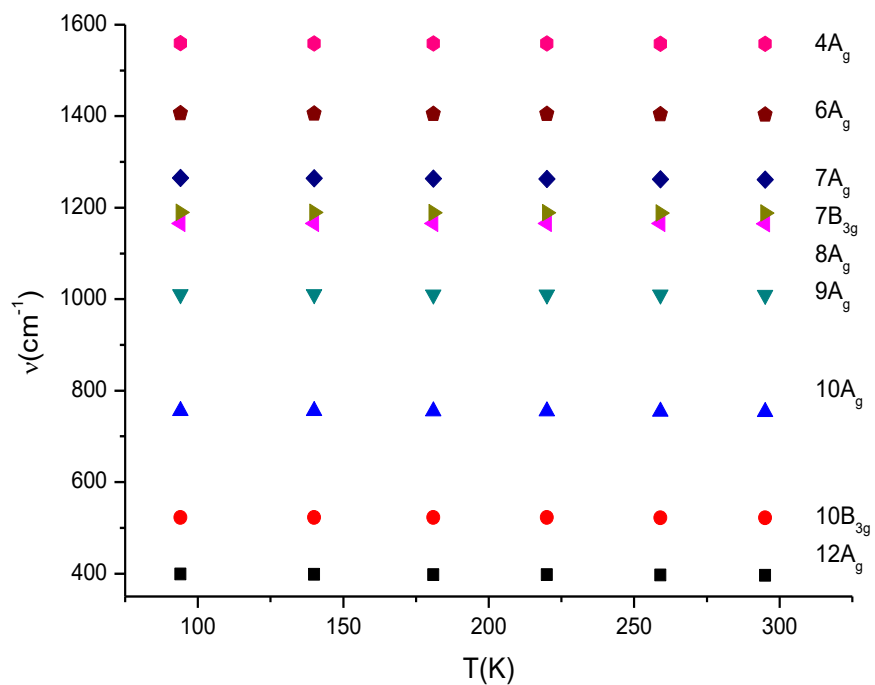


Figure 3. 31 Calculated Raman frequencies for the nine vibron modes as a function of temperature at  $P=0$  GPa according to Equation (3.9) for crystalline anthracene.

The Raman frequencies were found as functions of temperature and pressure with the observed volume data[48,52] for the six phonon and nine vibron modes of solid anthracene through the values of the isothermal mode Grüneisen parameter  $\gamma_T(P)$  at  $P = 0$  for those modes studied (Table 3.8). As shown in Figures 3.30 and 3.31, our calculated Raman frequencies for the six phonon and nine vibron modes, respectively, decrease with increasing temperature, due to the thermal expansion, whereas they increase with increasing pressure (Figures 3.30 and 3.31) as also observed experimentally [26,43]. As shown in Figures 3.30 and 3.31, our found Raman frequencies for the six phonon and nine vibron modes, respectively, reduce with increasing temperature, due to the thermal expansion. In fact, these decreases with temperature in the Raman frequencies are more apparent for the phonon modes, as shown in Figures 3.30 and 3.31, respectively. For vibrons, decreases in the Raman frequencies with temperature are very small so that the Raman frequencies are almost independent from the temperature within the frequency scale of vibrons (Figure 3.31). The temperature variation of the vibrational frequencies of crystal lattices involves both temperature and volume[26]. This indicates that fluctuation in phonon frequencies with temperature is due to both the deterioration of the unit cell with temperature and the phonon-phonon interaction [31].

Within large values of the isothermal mode Grüneisen parameter  $\gamma_T$  ( $P=0$ ) and relatively small  $\gamma_T$  ( $P=0$ ) values which we determined for the phonon modes (external modes) and the vibrons (internal modes), respectively, we calculated not only the pressure dependence of the Raman frequencies (Equation 2.9) but also their temperature dependence (Equation 3.1) using the observed volume data [48,52] (and also the observed  $\vartheta_T(p)$  data [43]), in anthracene, as stated above. When the Raman frequencies of six phonons and nine vibrons are measured experimentally as a function of temperature ( $P=0$ ) in anthracene, then the isobaric mode Grüneisen parameter  $\gamma_p(T)$  can be determined using the volume  $V_p(T)$  [48] according to Equation (2.9) at  $P=0$ . From the  $\gamma_p(T)$  values calculated at  $P=0$ , the temperature dependence of the Raman frequencies  $\vartheta_p(T)$  of the modes studied using the observed volume  $V_p(T)$  data [48] by means of Equation (3.2). By comparing with the observed

$\vartheta_p(T)$  data at  $P=0$  when available in the literature, this then examines our method of predicting the  $\vartheta_p(T)$  values for the Raman modes studied in anthracene.

By determining the Raman frequencies at different temperatures and pressures, in anthracene, its P-T phase diagram can be obtained, as also suggested for a P-T phase diagram of benzene ( $C_6H_6$ ) at high pressures [20]. By measuring the Raman frequencies of various modes at room temperature as a function of pressure up to 25 GPa, first order and second order phase transformations among the pressure-induced solid phases of benzene have been proposed and the phase boundaries have also been suggested in this molecular crystal [20].

In the case of anthracene, we calculated the Raman frequencies as functions of temperature (at normal pressure) and of pressure (at room temperature), as stated above. Thus, by predicting the Raman frequencies at different pressures (Figures 4 and 5) on the basis of the Raman measurements at ambient temperature up to 3.1 GPa [6], and also by predicting the Raman frequencies at different temperatures at normal pressure (Figures 2 and 3), various phase transformations in anthracene can be obtained and its P-T phase diagram can be determined from the Raman frequencies of the phonon modes and vibrons in this molecular crystal.

The Raman frequencies determined at different temperatures and pressures can then provide same applications for pressure/temperature sensing. As the thermodynamical PVT system, by means of the correlations between the volume  $V$  and the Raman frequency  $\vartheta$  through the mode Grüneisen parameter  $\gamma$ , spectroscopically  $P\vartheta T$  system can be used for various applications of the molecular crystals such as anthracene as exemplified here. Thus, various physical properties of molecular crystals, in particular, of anthracene can be investigated spectroscopically through the Raman frequency shifts which can be measured to high accuracy as compared to the thermodynamic PVT measurements in the phases or close to the phase transitions. Therefore, temperature and pressure dependences of the thermodynamic quantities such as the heat capacity, thermal expansivity and the isothermal compressibility can be predicted from the Raman frequency shifts in anthracene or in more general for the molecular crystals.

### 3.3 *Calculation of the Specific Heat as a Function of Temperature Using the Raman Frequency Shifts for Hydrocarbons*

#### 3.3.1 *Benzene*

Heat capacity as a function of temperature for each mode in the phases I-II of solid benzene is calculated according to Equation (2.43). Critical exponent for the thermal expansion  $\phi$  which was obtained from Equation (2.24) was assumed to be constant value of 0.8 for each mode in solid phases I-II of benzene. In the same way, critical exponent for the thermal compressibility  $\phi$  which was obtained from Equation (2.32) was assumed to be a constant value of -0.3 for the six modes of benzene. Constant molar volume of benzene as a function of temperature at zero pressure and as a function of pressure at room temperature was obtained by using the experimental data [12] and also constant thermal expansion in Equation (2.13) at zero pressure and constant isothermal compressibility in Equation (2.14) at room temperature. Isobaric mode Grüneisen parameter at  $p=0$  GPa and isothermal mode Grüneisen parameter at  $T=300$ K were calculated using Equations (2.9) and (2.10). Then, from the calculations for six modes in the solid phases I-II of benzene, total heat capacity of six modes is calculated according to Equation (2.44). Thus, the relationship between total heat capacity due to the six modes in phases I-II of solid benzene as a function of temperature is given in Figure 3.32.

Table 3. 17 Values of constant molar volume of benzene at  $p=0$  GPa ( $V_0$ ) and at  $T=300$  K ( $V_0'$ ) [12]. Values of constant thermal expansion (Equation (2.24)) at  $p=0$ GPa and constant isothermal compressibility (Equation (2.26)) at  $T=300$ K in the phases I-II of solid benzene.

$V_0(\text{cm}^3/\text{mol})$	$V_0'(\text{cm}^3/\text{mol})$	$\alpha_0 \times 10^{-4}(\text{K}^{-1})$	$\kappa_0 \times 10^{-2}(\text{GPa}^{-1})$
77.37	78.10	7.00	13.27

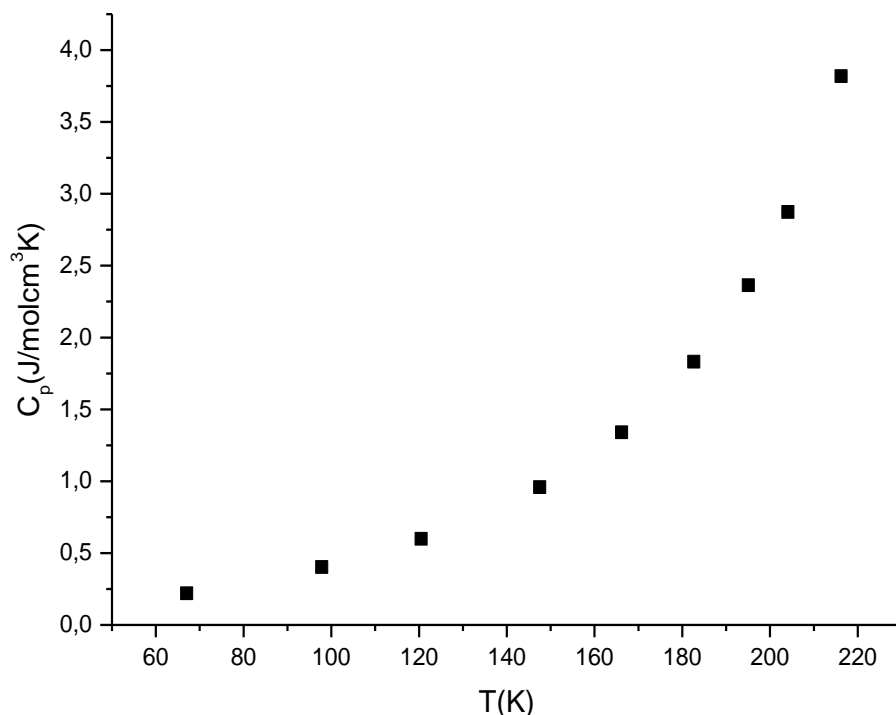


Figure 3.32 Calculated heat capacity as a function of temperature according to Equation (2.44) for the I-II transition ( $p_c=0$  GPa,  $T_c=300$  K) in benzene.

The specific heat  $C_P$  was determined as a function of temperature ( $P = 0$ ) and also as a function of pressure ( $T = 300$  K) according to Equation (2.44) for the phases I–II of solid benzene. For this computation, we used the observed data for the Raman frequencies of the six lattice modes (A, B, C and X, Y, Z) [12], which were obtained at various pressures ( $T = 300$  K) for the phases I–II of benzene. Contribution to the total specific heat  $C_P$  due to the six lattice modes was considered and also the observed volume data [12] were used in Equation (2.44). Table 3.8 gives the coefficients for the observed volume at various temperatures ( $P = 0$ ) [12] from our analysis according to Equation (3.2) for the phases II of solid benzene. The pressure dependence of the observed volume at constant temperature ( $T = 300$  K) [12] was also analyzed according to Equation (3.1) with the coefficients found for the solid phases I–II in benzene, as shown in Table 3.1. The Raman frequencies of the lattice modes (A, B, C and X, Y, Z), which were computed [12] as a function of pressure ( $T = 300$  K) were determined using Equation (3.3). Table 3.4 shows the values of the coefficients which we found for the six lattice modes for the phases I–II of solid

benzene. The investigation of the temperature dependence of the Raman frequencies for the six lattice modes ( $P = 0$ ) as observed experimentally [12], was also completed according to Equation (3.4) for the phases I–II of benzene. We represent the isothermal mode Grüneisen parameter ( $\gamma_T$ ) in Figure 3.6 (Equation (2.10)) for the six lattice modes studied. We then determined the temperature and pressure dependencies of the isobaric ( $\gamma_p$ ) and isothermal ( $\gamma_T$ ) mode Gruneisen parameter according to Equations (2.9) and (2.10), respectively, using the Raman frequency data [12] for the six lattice modes and also the observed volume data [12] for the phases I–II of solid benzene. Finally, using the temperature ( $P = 0$ ) and pressure ( $T = 300$  K) dependence of the six lattice modes with the frequency shifts  $\left(\frac{\partial \nu}{\partial T}\right)_P$  at  $P = 0$  and  $\left(\frac{\partial \nu}{\partial P}\right)_T$  at  $T = 300$  K, we found the specific heat  $C_P$  as a function of temperature ( $P = 0$ ) according to Equation (2.44) for the phases I–II of benzene. For this calculation, we used values of  $\gamma_p$  and  $\gamma_T$  at  $P = 0$  and  $T = 300$  K, respectively, for the six lattice modes in this equation. We plot in Figure 3.32 our found  $C_P$  as a function of temperature ( $P = 0$ ) due to the six lattice modes for the phases I–II of benzene. As predicted, the specific heat  $C_P$  increases as the temperature increases for both  $C_P$  vs.  $T$  (Figure 3.32) and  $\rho C_P / \rho C_{P_{max}}$  vs.  $T$  (Figure 3.33). For the finding of the specific heat  $C_P$  (Equation (2.44)), contributions due to the six lattice modes (denoted by A, B, C and X, Y, Z) were considered, for which the observed Raman frequency data [12] were used for the phase I–II of benzene. Our found  $\rho C_P$  values were compared with the observed data [12]. For this comparison, both the found and observed values were normalized with respect to the maximum  $C_P$  value (Figure 3.34). As given in the figure, there is a substantial discrepancy at low temperatures and they seem to agree as the temperature increases up to 200 K.

### 3.3.1.1 Calculation of Heat Capacity at $P=0.1$ GPa

Equation (2.45) is calculated at constant pressure of  $P=0.1$  GPa for six modes of solid benzene for various temperatures, calculated the temperature reliance of the specific heat  $C_P$  at a constant pressure of  $P = 0.1$  GPa, as measured experimentally

[4] for the solid phases I–II in benzene. Our finding of the specific heat  $C_P$  was performed by considering the contributions due to the six lattice modes (A, B, C and X, Y, Z) as in the  $C_P$  calculation for  $P = 0$  (Figure 3.33). By determining the Raman frequencies of the six lattice modes studied as a function of temperature at  $P = 0.1$  GPa according to Equation (3.3) and using the extrapolated values of  $\gamma_T$  for those modes at  $P = 0.1$  GPa, we were also able to compute  $C_P$  at several temperatures ( $P = 0.1$  GPa) by Equation (2.44). We give in Figure (3.34),  $\rho C_P$  values ( $q = 1/V$  is the density for the solid I–II phases in benzene) which were normalized with respect to the maximum value of  $\rho C_{Pmax}$ , as compared with the experimental data [4] at several temperatures for the solid I–II phases ( $P = 0.1$  GPa) in benzene. Behaviour of  $C_P$  ( $p=0.1\text{GPa}, T$ ) against the temperature as seen below.

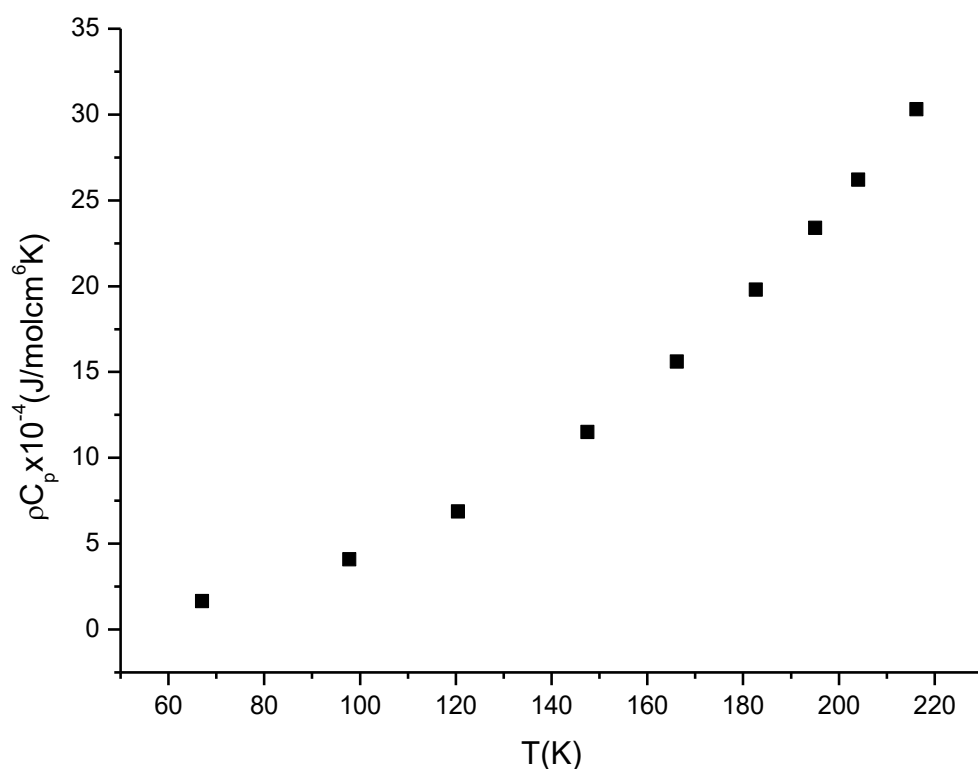


Figure 3. 33 Pressure dependence of heat capacity per unit volume  $\rho C_p$  due to total six modes correspond to phase I-II of solid benzene at 0.1 GPa.



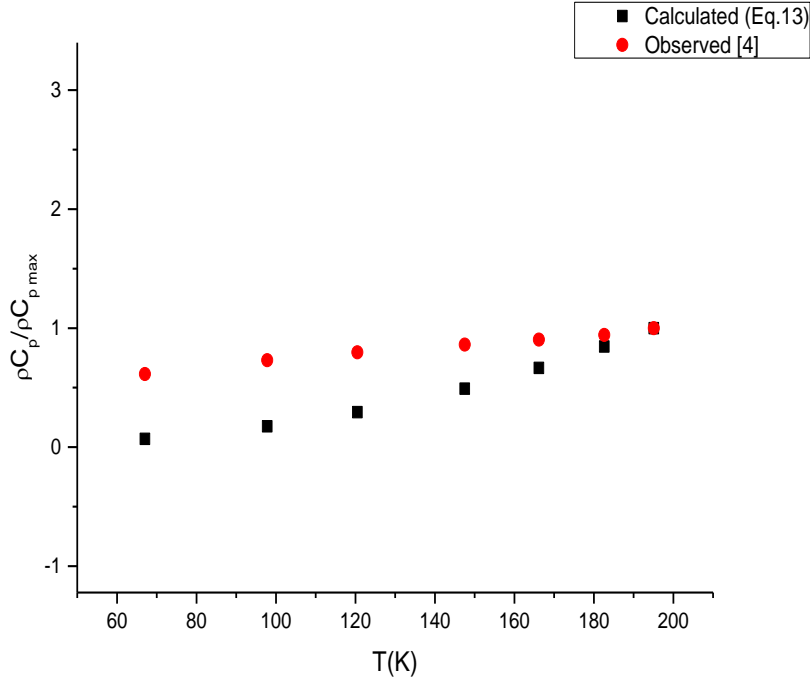


Figure 3. 34 Calculated heat capacity per unit volume due to the total six lattice modes in phases I-II of solid benzene at  $p=0.1$  GPa according to Equation (2.45). Observed data [4] is also given here for comparison.

When we found the specific heat  $C_p$  using the Raman frequency shifts (Equation (2.44)), we used the temperature dependence of the  $\gamma_p$  and the pressure dependence of the  $\gamma_T$  which we found for those phonon modes (A, B, C and X, Y, Z) studied for the I-II transition in benzene, as stated above. The  $\gamma_p$  values of six lattice modes do not differ significantly with the temperature and the  $\gamma_p$  value is around 3 for all the modes except the mode A which has the value between 3 and 4 within the temperature range of  $67 < T(K) < 216$  (Table 5). Remarkably, the  $\gamma_T$  as a negative value is about 3 for the lattice modes except the mode A as for cp and the pressure dependence of the  $\gamma_T$  is also unimportant (Table 6). In particular, the  $\gamma_T$  as a negative value fluctuates between 3 and 4 for the mode A. This shows that a constant  $\gamma_p$  for each mode can be used to estimate the frequency shifts  $\left(\frac{\partial \vartheta}{\partial T}\right)_p$  from the volume change  $\left(\frac{\partial \vartheta}{\partial T}\right)_p$  (Equation (2.20)) or a constant  $\gamma_T$  can be used to estimate

$\left(\partial\vartheta/\partial P\right)_T$  from the  $\left(\partial\vartheta/\partial P\right)_T$  (Equation (2.20)). A constant  $\gamma_P$  or  $\gamma_T$  value for each mode can also be used to calculate the temperature or pressure dependence, respectively, of the specific heat  $C_P$  according to Equation (2.44) for the I–II transition in solid benzene. Our calculated  $C_P$  as a function of temperature at zero pressure (Figure 3.32) and as a function of pressure at room temperature (Figure 3.33), can be compared with the experimental data. This then examines the validity of our method toward the determination of the specific heat  $C_P$  from the Raman frequency shifts  $\left(\partial\vartheta/\partial P\right)_T$  and  $\left(\partial\vartheta/\partial P\right)_T$  according to Equation (2.44).

### 3.3.1.2 Temperature Dependence of the Heat Capacity for Benzene Close to the I-II Phase Transition

Heat capacity as a function of temperature for each mode in the phases I-II of solid benzene is calculated according to Equation (2.54). Critical exponent for the thermal expansion  $\phi$  which was obtained from Equation (2.24) was assumed to be constant value of 0.8 for each mode in solid phases I-II of benzene. In the same way, critical exponent for the thermal compressibility  $\phi$  which was obtained from Equation (2.32) was assumed to be constant value of -0.3 for the six modes of benzene. Constant molar volume of benzene as a function of temperature at zero pressure and as a function of pressure at room temperature was obtained by using the experimental data [12] and also constant thermal expansion in Equation (2.13) at zero pressure and constant isothermal compressibility in Equation (2.15) at room temperature. Also, isobaric mode Grüneisen parameter at  $p=0$  GPa and isothermal mode Grüneisen parameter at  $T=300$ K were calculated using Equations (2.9) and (2.10) with the calculated values  $\delta\vartheta_p(T)$  (Equation (2.24)) at zero pressure and  $\delta\vartheta_T(p)$  (Equation (2.32)) at room temperature. Then, from the calculations for six modes in the solid phases I-II of benzene, total heat capacity of six modes is calculated according to Equation (2.54). Thus, relationship between total heat capacity due to the six modes in phases I-II of solid benzene as a function of temperature is given in Figure 3.35.

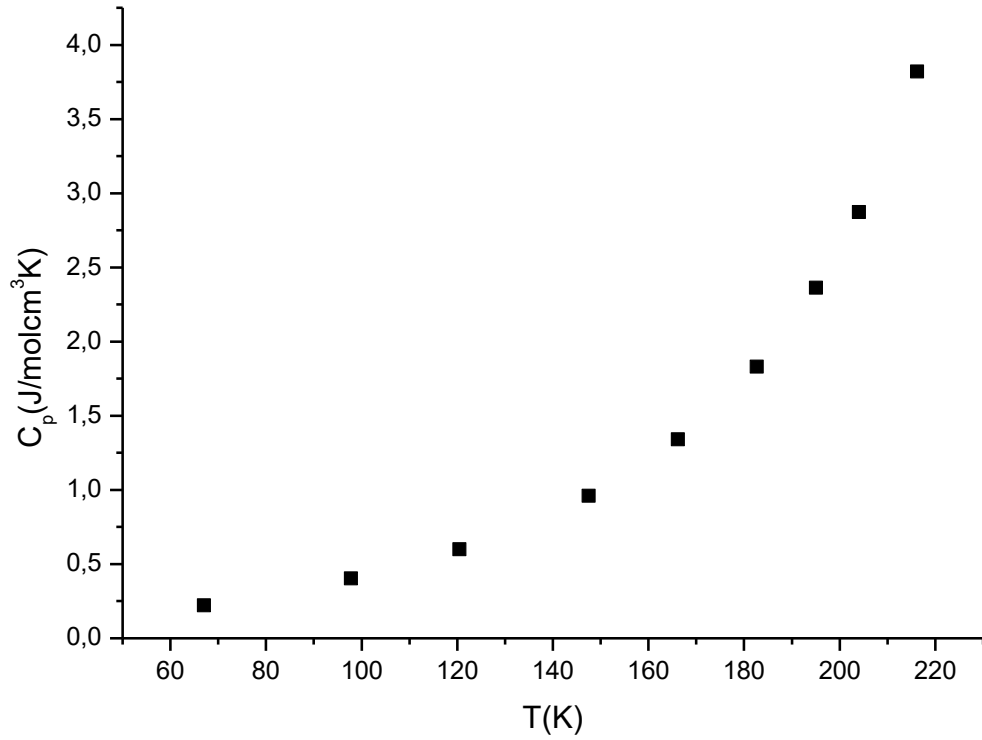


Figure 3. 35 Calculated heat capacity as a function of temperature according to Equation (2.54) for the I-II transition ( $p_C=0$  GPa,  $T_C=300$ K) in benzene.

Calculated heat capacity according to Equation (2.54) for six phonon modes in the phases I-II of solid benzene at zero pressure and room temperature increases with the increasing temperature range up to 220 K in Figure 3.35, as expected and exhibits the same behavior in Sections 3.3.1.1 and 3.3.1.2.

### 3.3.2 Naphthalene

The specific heat  $C_p$  was determined as a function of temperature at zero pressure according to Equation (2.44) for the six phonon modes of solid naphthalene by using the observed data [37]. For this calculation, we used the determined coefficients  $a_0, a_1$  and  $a_2$  (Equation (3.1)) and  $b_0, b_1$  and  $b_2$  (Equation (3.2)) at zero pressure as given in Tables in Section 3.1.2. To define the pressure and temperature dependence of the Raman frequency shifts, coefficients  $c_0, c_1$  and  $c_2$  (Equation (3.3)) and

$d_0, d_1$  and  $d_2$  (Equation (3.4)) at room temperature represented in Table 3.9 in Section 3.1.2 were used in this section, too. The isobaric and isothermal mode Grüneisen parameters in Equations (2.9) and (2.10) were used as given in Table in Section 3.1.2. Finally, specific heat was calculated as a function of temperature at  $P=0$  GPa of the six phonon modes for solid naphthalene according to Equation (2.44) and calculated specific heat  $C_p$  (Equation (2.44)) was plotted in Figure 3.36 as a function of temperature.

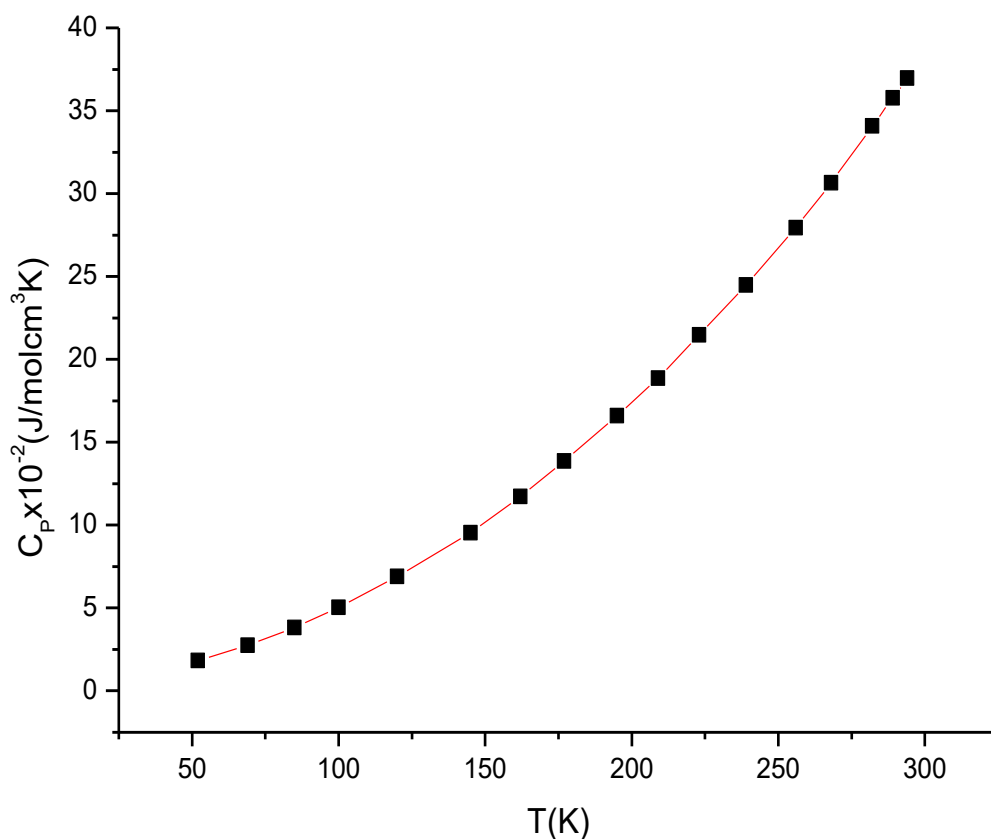


Figure 3. 36 Calculated total heat capacity of six lattice modes of solid naphthalene (Equation (3.44)) by using the observed data [37] as a function of temperature.

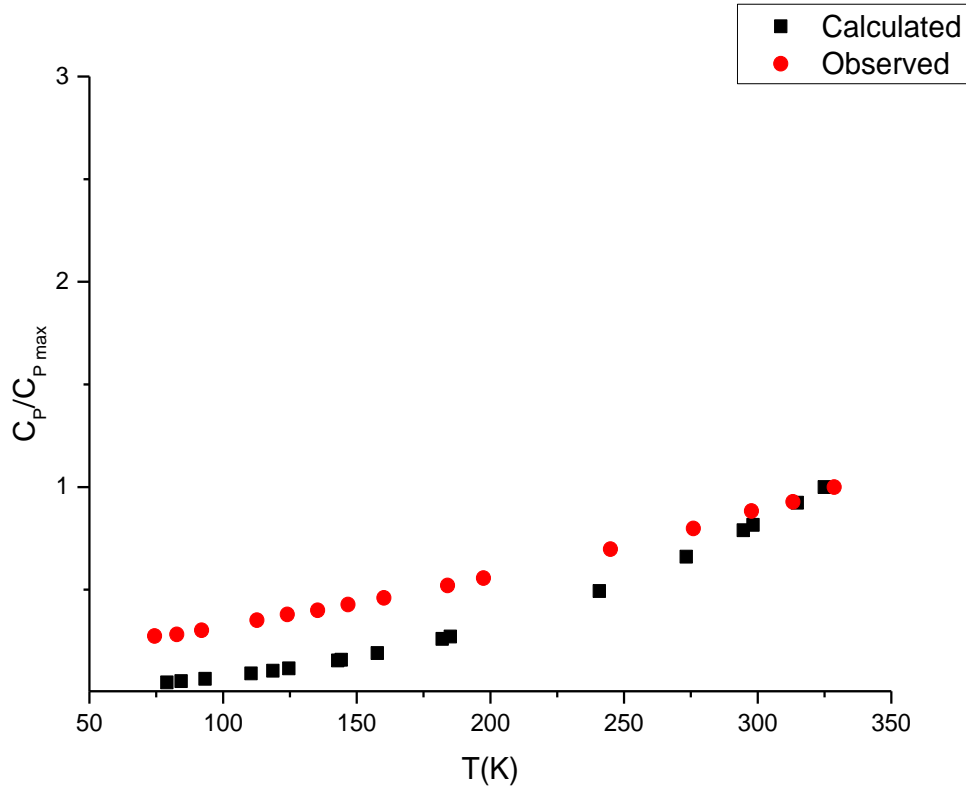


Figure 3. 37 Calculated heat capacity due to the total six lattice modes of solid naphthalene at  $p=0$  GPa according to Equation (2.45). Observed data [25] is also given here for comparison.

Heat capacity due to the contributions of six lattice modes of solid naphthalene was calculated according to Equation (2.45) by using the experimental volume data [25] through the isobaric ( $\gamma_p$ ) and the isothermal ( $\gamma_T$ ) mode Grüneisen parameter. We investigate the heat capacity as a function of temperature in Figure 3.36 with increasing values due to the increasing temperature values. Calculations were carried out at zero pressure and room temperature conditions. In Figure 3.37, both calculated and observed [25] heat capacity of six phonon modes of solid naphthalene are represented for comparison. Heat capacities were normalized with respect to the maximum heat capacity value. Calculated data are in good agreement through the higher temperature values up to 350 K with the observed data [25]. Discrepancy between the calculated and observed [25] data can be attributed to the isobaric compression.

### 3.3.3 Anthracene

The specific heat  $C_p$  was determined as a function of temperature at zero pressure according to Equation (2.44) for the six phonon modes of solid anthracene by using the observed data [48,52]. For this calculation, we used the determined coefficients  $a_0, a_1$  and  $a_2$  (Equation (3.1)) and  $b_0, b_1$  and  $b_2$  (Equation (3.2)) at zero pressure as given in Tables in Section 3.1.3. To define the pressure and temperature dependence of the Raman frequency shifts, coefficients  $c_0, c_1$  and  $c_2$  (Equation (3.3)) and  $d_0, d_1$  and  $d_2$  (Equation (3.4)) at room temperature represented in Table in Section 3.1.3 were used for six phonon modes of solid anthracene in this section, too. The isobaric and isothermal mode Grüneisen parameters in Equations (2.9) and (2.10) were used as given in Table in Section 3.1.3. Finally, specific heat was calculated as a function of temperature at  $P=0$  GPa of the six phonon modes for solid anthracene according to Equation (2.44) and the calculated specific heat  $C_p$  (Equation (2.44)) was plotted in Figure 3.38 as a function of temperature for solid anthracene.

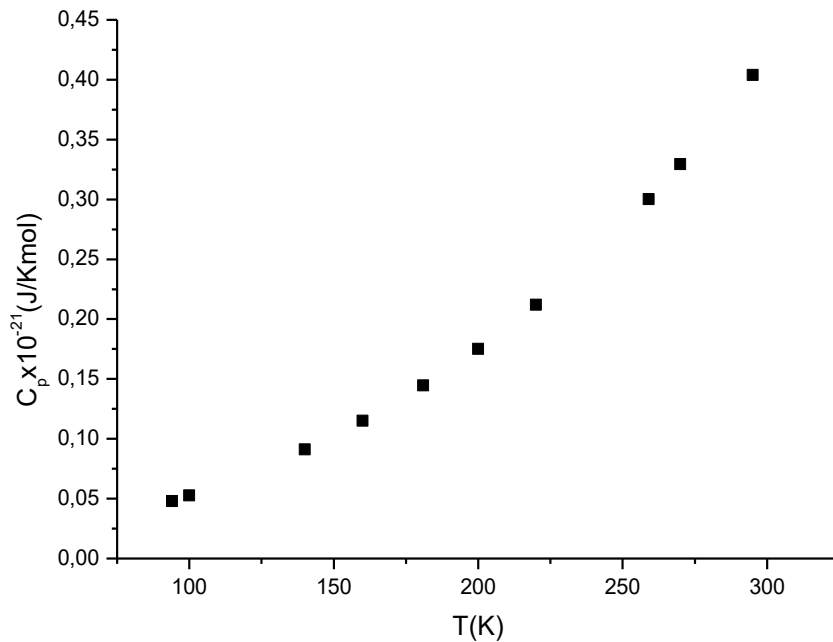


Figure 3. 38 Heat capacity determined as a function of temperature (Equation (2.44)) at zero pressure ( $P=0$  GPa) using the Raman frequencies of the total six phonon modes of solid anthracene.

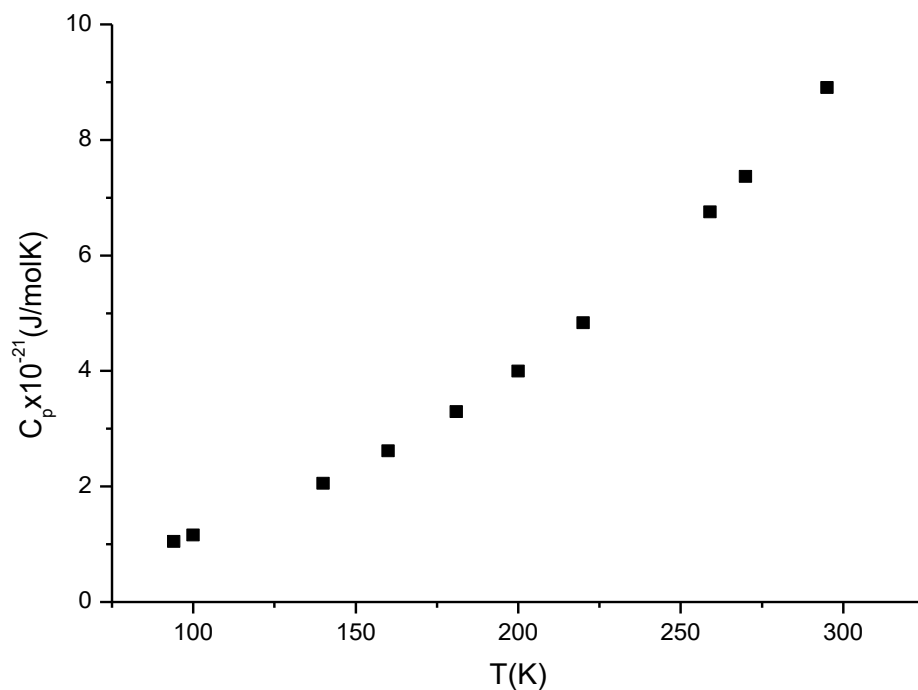


Figure 3. 39 Heat capacity determined as a function of temperature at zero pressure ( $P=0$  GPa) using the Raman frequencies of the total nine vibron modes of solid anthracene.

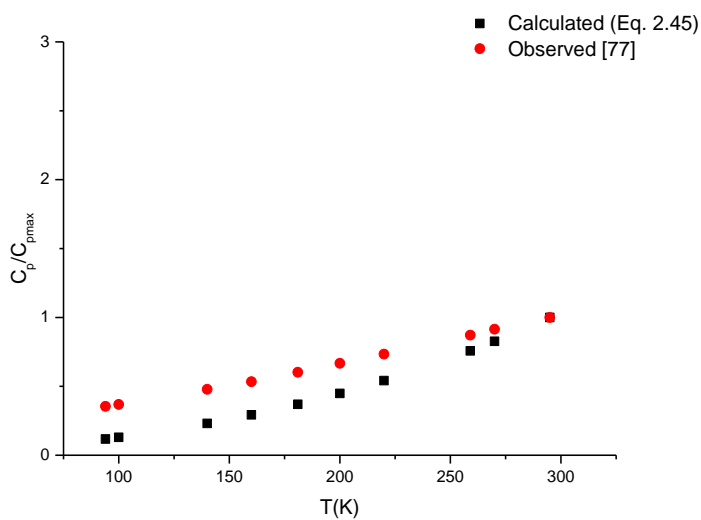


Figure 3. 40 The determined heat capacity due to the six phonon and nine vibron modes of solid naphthalene ( $P=0$  GPa) according to Equation (2.45). Observed data [77] are also given here for comparison.

Heat capacity due to the contributions of six phonon and nine vibron modes of solid anthracene was calculated according to Equation (2.45) by using the experimental volume data [48] through the isobaric ( $\gamma_p$ ) and the isothermal ( $\gamma_T$ ) mode Grüneisen parameter. We plot the heat capacity as a function of temperature in Figures 3.38 and 3.39, which increase as the temperature increases. Calculations were carried out at zero pressure and room temperature conditions. In Figure 3.40, both calculated and observed [77] heat capacity of six phonon and nine vibron modes of solid anthracene are represented for comparison. Heat capacities were normalized with respect to the maximum heat capacity value. Calculated data gets well agreement through the higher temperature values up to 300 K with the observed data [77]. Discrepancy between the calculated and observed [77] data can be attributed to the isobaric compression.

### **3.4 Calculation of the Specific Heat Under Pressure by Using the Raman Frequency Shifts for Hydrocarbons**

#### **3.4.1 Benzene**

Heat capacity of solid benzene under various pressures at room temperature ( $T=300\text{K}$ ) is calculated from an integral expression as given below:

$$C_p(T, p) = C_p(T, 0) + \int_0^p \left( \frac{\partial C_p}{\partial p'} \right)_T dp' = C_p(T, 0) - T \int_0^p \left( \frac{\partial^2 V}{\partial T^2} \right)_{p'} dp' \quad (3.11)$$

Heat capacity of all six modes of solid benzene was calculated by using Equation (3.11) and a graph of total heat capacity of six modes versus pressure is given in Figure 3.41.



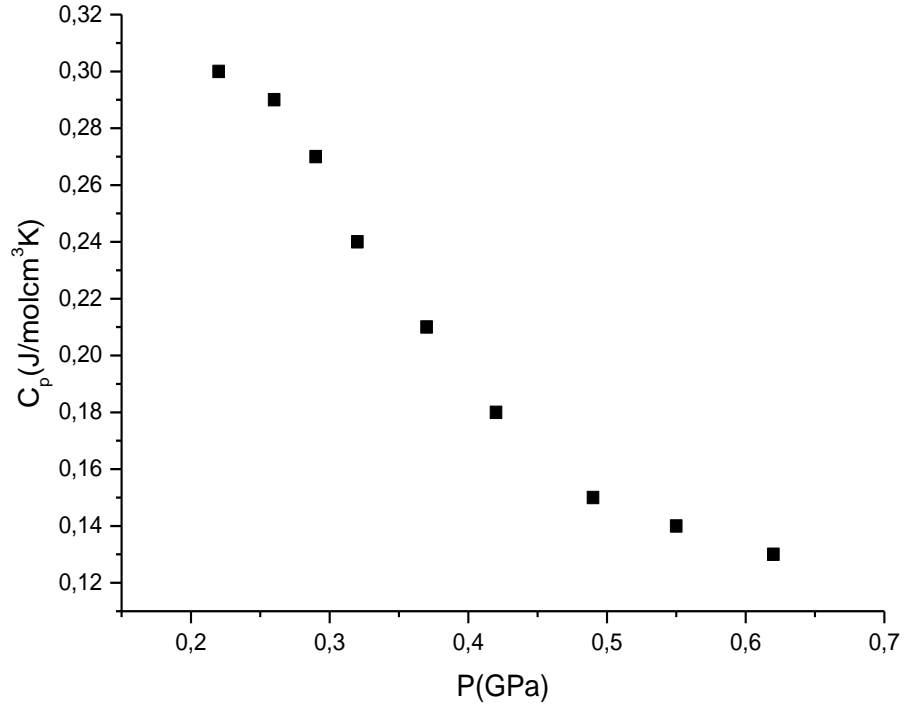


Figure 3. 41 Total heat capacity due to the six modes of solid benzene which was calculated at various pressures at room temperature (T=300K).

The specific heat  $C_P$  determined as a function of pressure at room temperature ( $T = 300$  K) decreases as the pressure increases (Figure 3.41). As mentioned above, the pressure dependence of the specific heat  $C_P$  was also calculated ( $T = 300$  K) from the frequency shifts  $\left(\partial\vartheta/\partial T\right)_P$  and  $\left(\partial\vartheta/\partial P\right)_T$  due to the contributions of the six lattice modes (A, B, C and X, Y, Z) according to Equation (3.11) for the phases I–II of benzene.

### 3.1.1.3 Pressure Dependence of the Heat Capacity for Benzene Close to the I-II Phase Transition

Heat capacity due to each mode in phase I-II of solid benzene is calculated as a function of pressure according to Equation (2.54) by using constant values of critical exponent for the thermal expansion and for the thermal compressibility. Critical exponent for the thermal expansion  $\phi$  which was obtained from Equation (2.24), was

assumed to be constant value of 0.8 for each mode in solid phases I-II of benzene. In the same way, critical exponent for the thermal compressibility  $\phi$  which was obtained from Equation (2.32), was assumed to be constant value of -0.3 for the six modes of benzene. A constant molar volume of benzene (at zero pressure and at room temperature), isobaric mode Grüneisen parameter ( $p=0\text{GPa}$ ) and isothermal mode Grüneisen parameter ( $T=300\text{K}$ ) (Equations (2.9) and (2.10)) were used for this calculation. Finally, total heat capacity due to six modes in benzene was calculated close to the I-II phase transition. The heat capacity as a function of pressure for benzene is given in Figure 3.42.

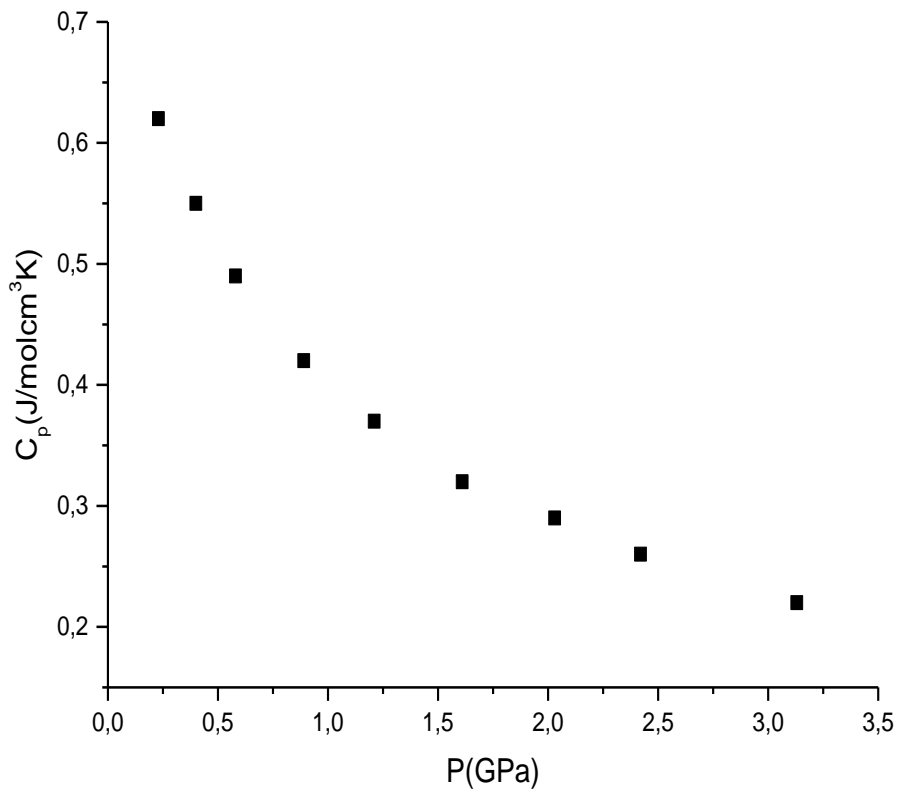


Figure 3. 42 Calculated heat capacity as a function of pressure according to Equation (2.55) for the I-II transition ( $p_C=1.3\text{GPa}$ ,  $T_C=300\text{K}$ ) in benzene.

The pressure dependence of the specific heat  $C_p$  was determined from the frequency shifts  $\left(\frac{\partial\vartheta}{\partial T}\right)_p$  and  $\left(\frac{\partial\vartheta}{\partial P}\right)_T$  due to the contributions of the six lattice modes (A, B, C and X, Y, Z) according to Equation (2.55) for the phases I–II of benzene at

critical conditions ( $p_c=1.3\text{GPa}$ ,  $T_c=300\text{K}$ ). Calculated heat capacity (Equation (2.55)) for the six phonon modes in the I-II transition of solid benzene decreases with the increasing pressure range up to 3.5 GPa. Up to our knowledge, there is no experimental data for the I-II transition in benzene to compare with this calculation in the literature.

#### **3.4.1.1 Pressure Dependence of Heat Capacity for Benzene Close to the I-II Phase Transition at Room Temperature**

Similar to Section 3.1.1.2, total heat capacity for benzene in the solid phases I-II is calculated at a constant temperature ( $T=300\text{K}$ ) according to Equation (2.54) with a correction in the critical exponent  $\phi$  for the isothermal compressibility which was fitted to Equation (2.32). Critical exponent for the isothermal compressibility for benzene was renormalized with the renormalized exponent  $\alpha_R$  according to the Fisher renormalized critical behavior [78],

$$\alpha = -\frac{\alpha_R}{1-\alpha_R} \quad (3.6)$$

which gives  $\phi_R=0.23$  for the I-II transition in benzene. Figure 3.43 defines the behavior of total heat capacity as a function of pressure.

$$\phi_R = -\frac{\phi}{1-\phi} \quad (3.7)$$

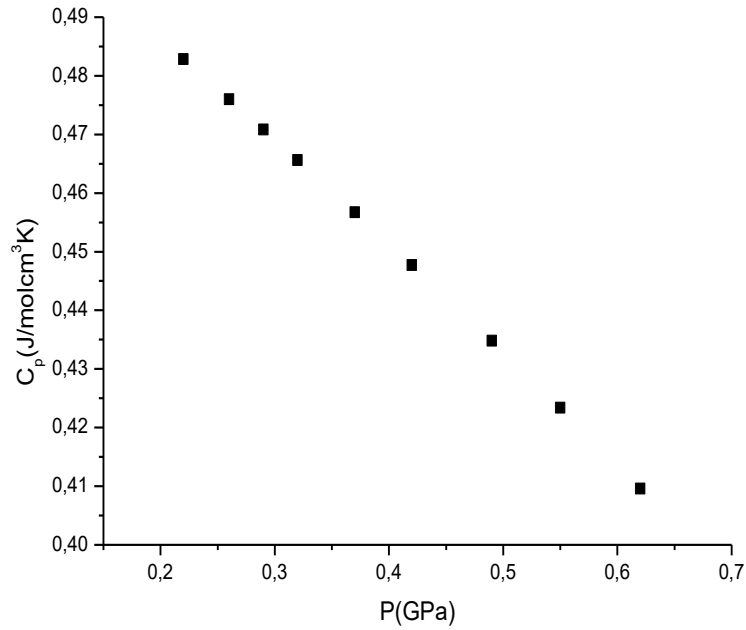


Figure 3. 43 Calculated total heat capacity due to the six modes of benzene using the critical exponent ( $\phi_R=0.23$ ) as a function of pressure according to Equation (2.54) at room temperature ( $T=300K$ ).

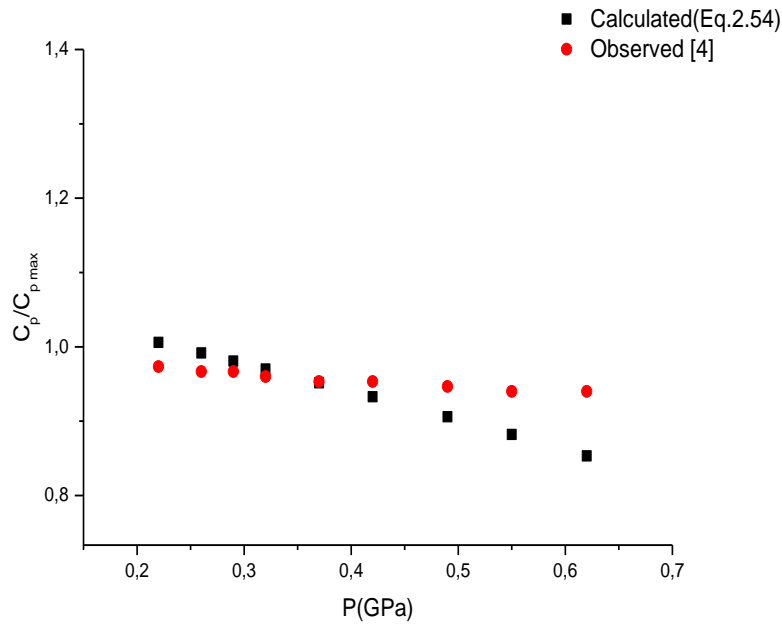


Figure 3. 44 Calculated total heat capacity  $C_p$  due to the six lattice modes as a function of pressure in the solid phases I-II of benzene at room temperature according to Equation (2.54). Observed  $C_p$  data [4] for benzene are also plotted here for comparison.

Heat capacity  $C_p$  due to the six lattice modes as a function of pressure in the solid phases I-II of benzene at room temperature according to Equation (2.54), was calculated with the renormalized critical exponents through the Grüneisen parameter. Pressure dependence of the calculated total heat capacity close to the I-II transition in solid benzene as given in Figure 3.43, shows the decreasing values with increasing pressures ranging up to 0.65 GPa, as observed with the section 3.4.1.1. In Figure 3.44, calculated and observed data close to the I-II transition in solid benzene are given for comparison as normalized with respect to the maximum value. Calculated data exhibits the same behavior with the observed data [77]. The discrepancy in Figure 3.44 between calculated and observed data [77] for the six phonon modes close to the I-II transition in solid benzene, gets sharper through the higher pressure ranges. This can be attributed to the lattice rearrangement in crystal close to the I-II transition in solid benzene.

### 3.4.2 Naphthalene

Heat capacity of all six modes of solid naphthalene was calculated by using Equation (3.11), a graph of total heat capacity of six modes versus pressure is given in Figure 3.45.

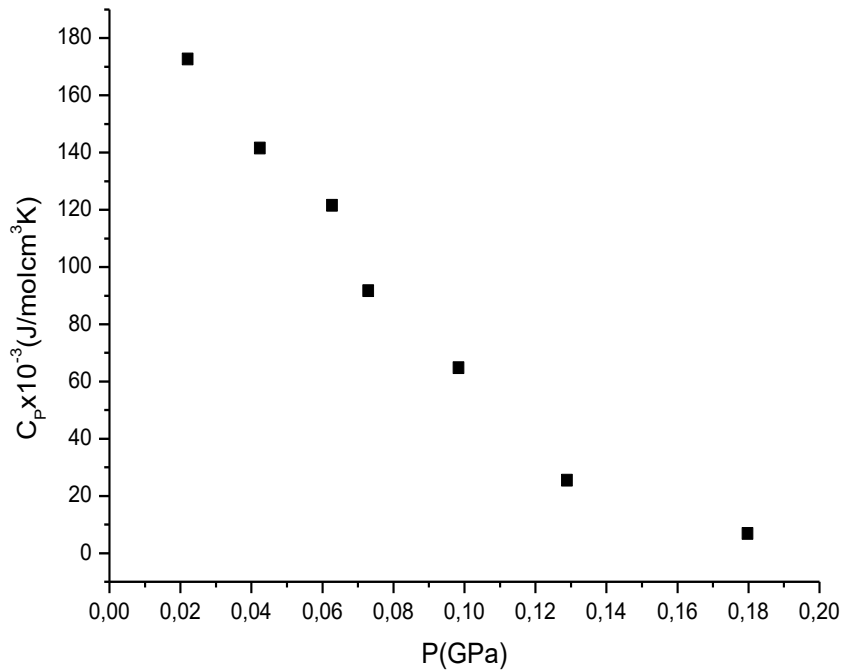


Figure 3. 45 Total heat capacity due to the six modes of solid naphthalene which was calculated at various pressures at room temperature (T=300K).

The pressure dependence of the specific heat  $C_P$  was calculated from the temperature dependence of the crystal volume due to the contributions of the six lattice modes according to Equation (3.11) for solid naphthalene up to 0.2 GPa at room temperature. Calculated heat capacity (Equation (3.11)) for the six phonon modes of solid naphthalene decreases with the increasing pressure range up to 0.2 GPa. Up to our knowledge, there is no experimental data for mentioned modes of solid naphthalene to compare with this calculation in the literature.

### 3.4.3 Anthracene

The heat capacity  $C_P$  due to the six phonon and nine vibron modes of solid anthracene was calculated using Equation (3.11). Graphs of the total heat capacity  $C_P$  using the contributions of the six phonon and nine vibron modes as a function of pressure are given in Figures 3.46 and 3.47.

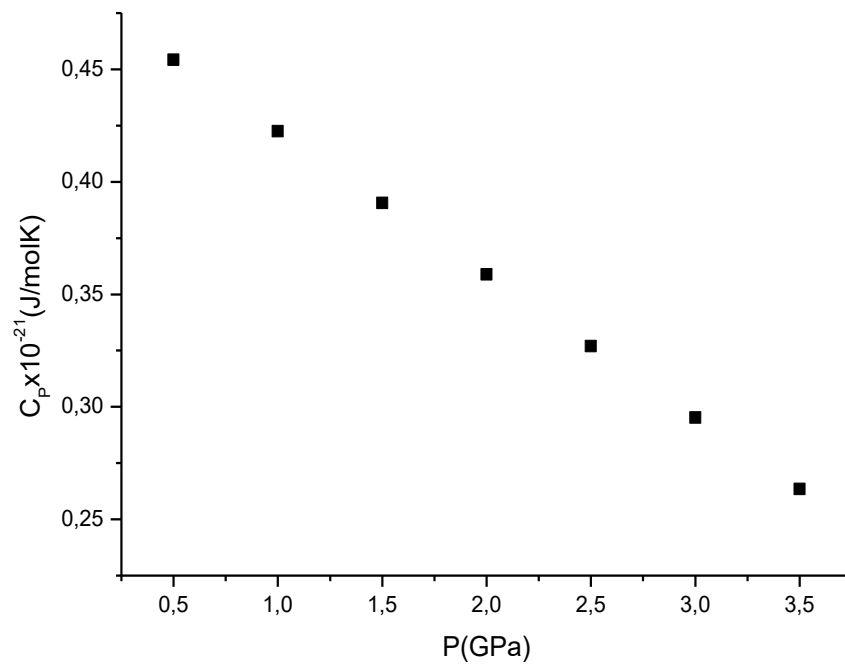


Figure 3. 46 Total heat capacity due to the six phonon modes of solid anthracene, which was found as a function of pressure at room temperature ( $T=300K$ ).

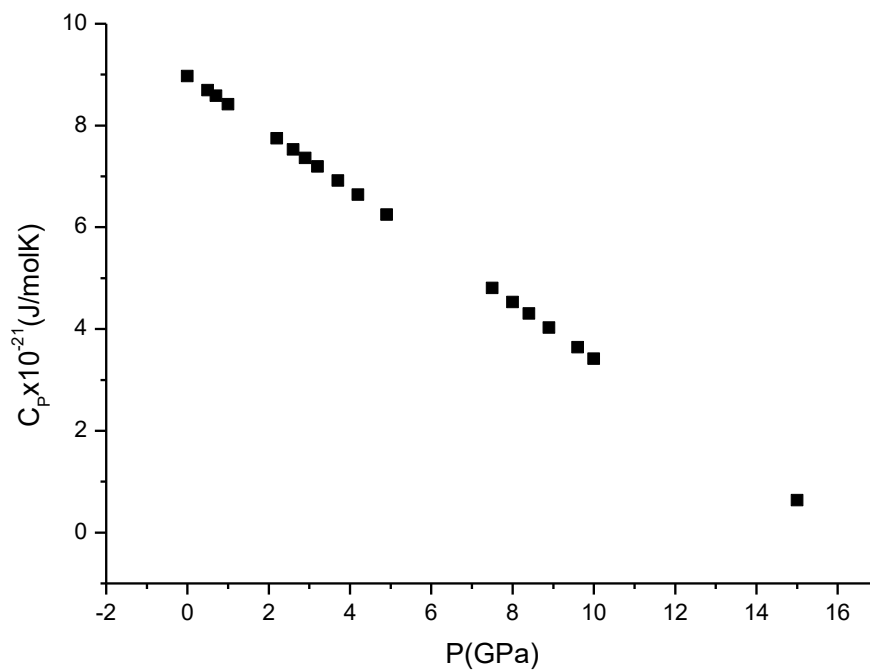


Figure 3. 47 Total heat capacity due to the six vibron modes of solid anthracene, which was found as a function of pressure at room temperature ( $T=300K$ ).

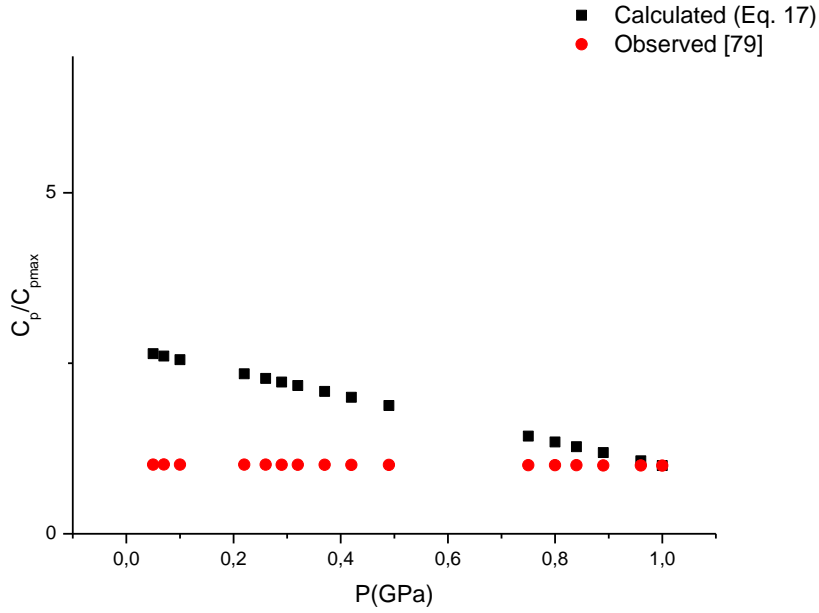


Figure 3. 48 Change in the heat capacity  $C_P$  due to the six lattice modes of solid anthracene as a function of pressure at room temperature ( $T=300$  K).

The pressure dependence of the specific heat  $C_P$  was calculated from the temperature dependence of the crystal volume due to the contributions of the six phonon and nine vibron modes according to Equation (3.11) for solid anthracene up to 1 GPa at room temperature. Calculated heat capacity (Equation (3.11)) for the six phonon and nine vibron modes of solid anthracene decreases with the increasing pressure range up to 1 GPa as shown in Figures 3.46 and 3.47. Calculated heat capacity agrees well with the observed data [79] through the higher pressures.



### 3.5 Calculation of Change in Entropy Under Temperature

#### 3.5.1 Benzene

Change in entropy ( $\Delta S = S_2 - S_1$ ) of the phases I-II of solid benzene due to the contributions of the six modes was calculated by using an integration over temperature from the minimum to a maximum temperature, according to:

$$s(T, 0) = s(T_{min}, 0) + \int_{T_{min}}^T C_p(T', 0) d\ln T' \quad (3.12)$$

$C_p(T, 0)$  is known over the temperature range from  $T_{min}$  to  $T_{max}$  using our earlier calculation in section 3.3. for six modes of the phases I-II of solid phases. Figure 3.49 shows the behaviour of change in entropy of total six modes of solid benzene under different temperatures.

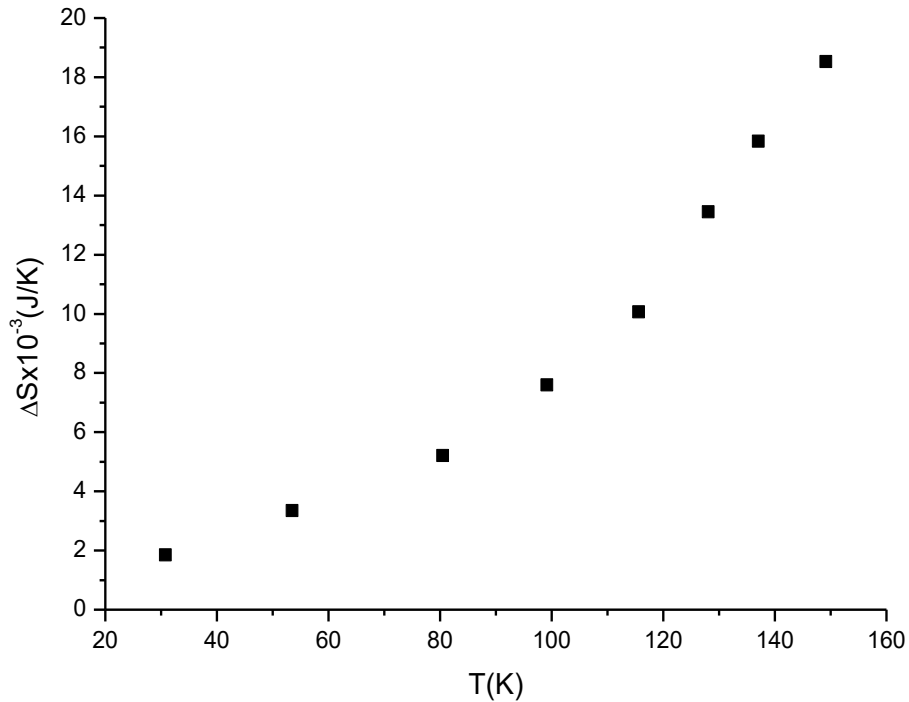


Figure 3. 49 Change in entropy due to the total six modes of the phases I-II of solid benzene (Equation (3.12)) from  $T_{min}$  to  $T_{max}$  at various temperatures.

Change in entropy due to the total six phonon modes of the phases I-II of solid benzene was calculated according to Equation (3.12) through the heat capacity at  $P=0$  GPa over a temperature integral up to 160 K. Change in entropy due to the total six phonon modes (Equation (3.12)) increases with the increasing temperature range up to 160 K, as expected.

### 3.5.2 Naphthalene

$C_p(T,0)$  is known over the temperature range from  $T_{\min}$  to  $T_{\max}$  using our earlier calculation in section 3.3.2. for six modes of naphthalene. Values of  $\Delta S$  were calculated according to Equation (3.12) and Figure 3.50 shows the behaviour of change in entropy of total six modes of solid naphthalene under different temperatures.

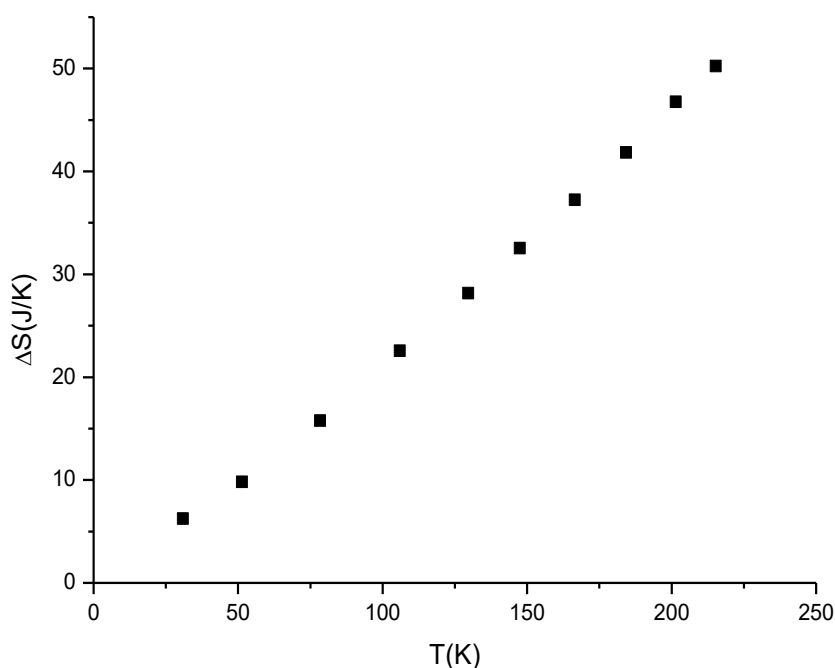


Figure 3. 50 Change in entropy due to the total six modes of solid naphthalene (Equation (3.12)) from  $T_{\min}$  to  $T_{\max}$  at various temperatures.

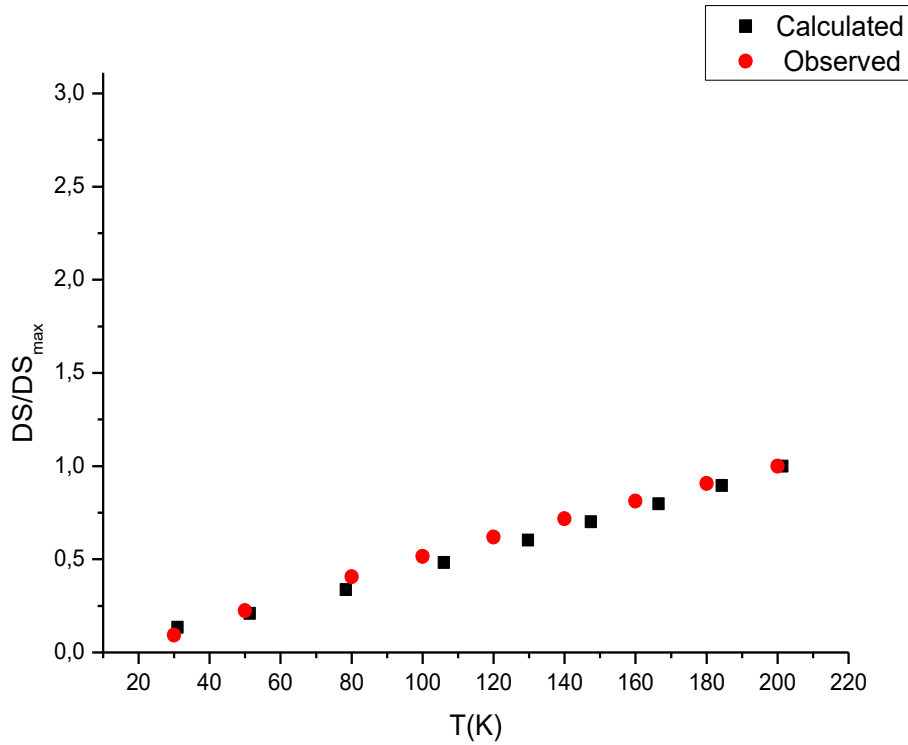


Figure 3. 51 Change in entropy due to the total six modes of solid naphthalene (Equation (3.12)) is given in comparison with the observed data [25].

Change in entropy due to the total six phonon modes of solid naphthalene was calculated according to Equation (3.12) through the heat capacity at  $P=0$  GPa over a temperature integral up to 250 K. Change in entropy due to the total six phonon modes (Equation (3.12)) increases with the increasing temperature range up to 250 K (Figure 3.50). There is a high agreement between the computed and the observed data [25] with the normalization due to maximum value in entropy range as seen in Figure 3.51. There is a discrepancy between 80 and 190 K decreasing through the higher temperatures up to 220 K.

### 3.5.3 Anthracene

$C_p(T,0)$  was obtained for the temperature range in our earlier calculation in section 3.3.3 for six phonon and nine vibron modes of anthracene. Figures 3.52 and 3.53 show, respectively, the behaviour of the change in entropy contributed by the six phonon and nine vibron modes of solid anthracene as a function of temperature.

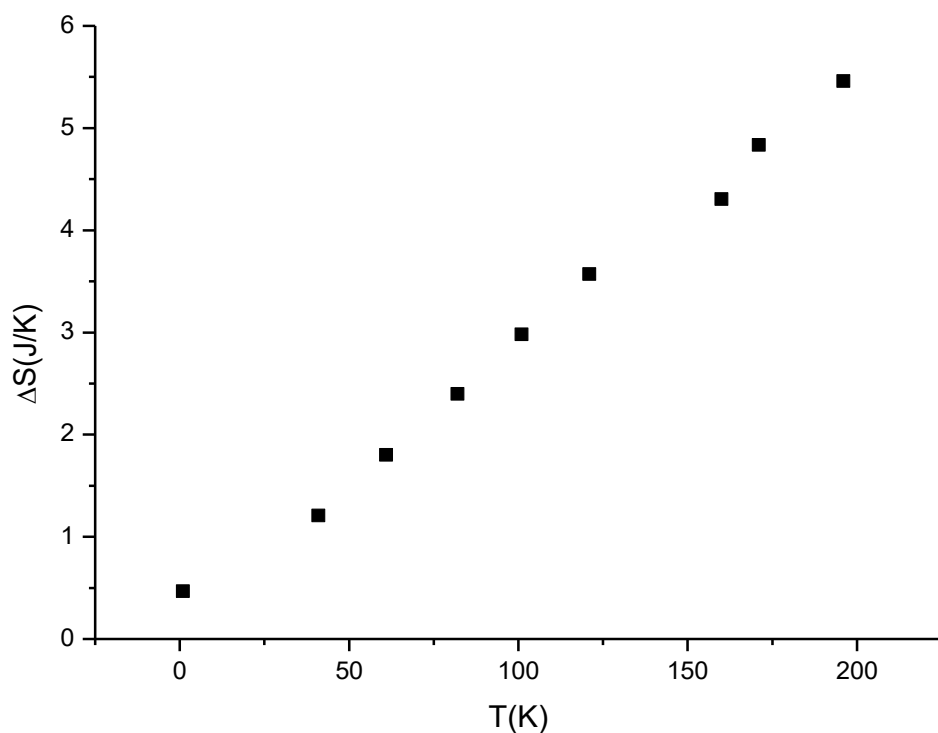


Figure 3. 52 Change in the entropy ( $\Delta S$ ) due to the six phonon and nine vibron modes of solid anthracene (Equation (3.12)) at various temperatures ( $P=0$ ).

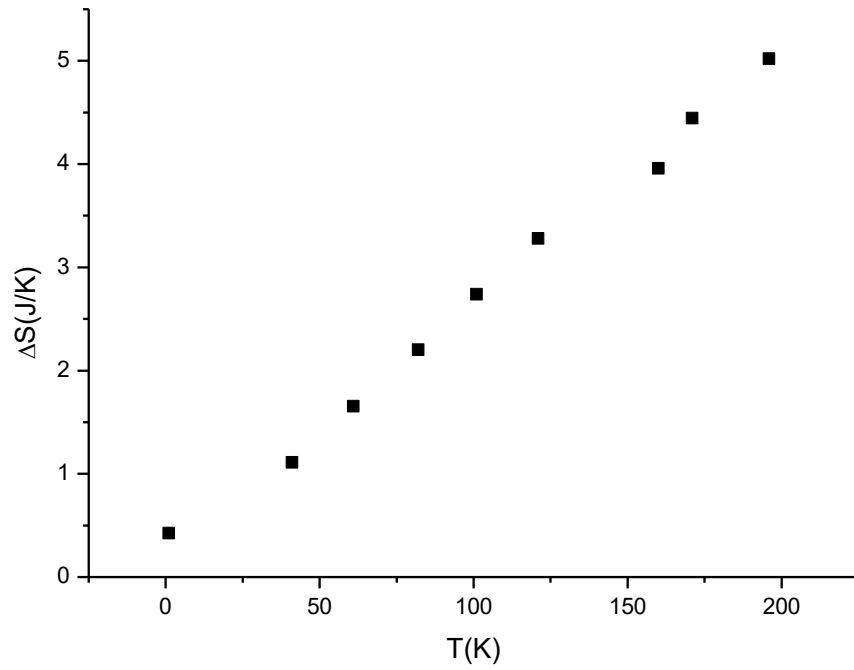


Figure 3. 53 Change in the entropy ( $\Delta S$ ) due to the six vibron modes of solid anthracene (Equation (3.12)) at various temperatures ( $P=0$ ).

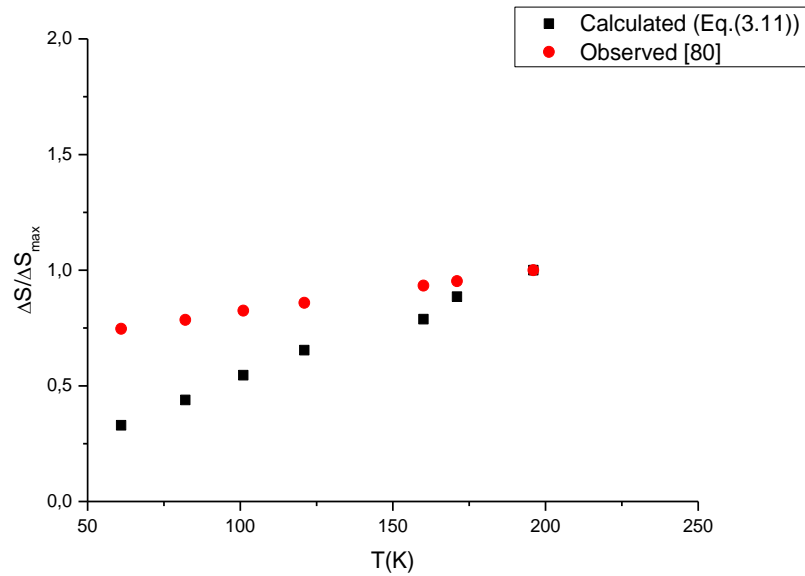


Figure 3. 54 Change in the entropy calculated (Equation (3.12)) due to the total six modes of solid anthracene. The observed data [80] are also shown for comparison.

Change in the entropy due to the total six phonon and nine vibron modes of solid naphthalene was calculated according to Equation (3.12) through the heat capacity at  $P = 0$  GPa over a temperature integral up to 200 K. Change in entropy due to the total six phonon modes (Equation (3.12)) increases with the increasing temperature range up to 200 K (Figures 3.52 and 3.53). In Figure 3.54, both calculated and observed data [80] are given in comparison as normalized with respect to the maximum value of change in entropy. There is a sharp discrepancy between the calculated and the observed data [80] which is decreasing through the high temperatures.

### **3.6 Derived Thermodynamic Quantities by Quasi Harmonic Free Energy of Solid Benzene, Naphthalene and Anthracene as Hydrocarbon**

The approximation of ignoring the population driven anharmonic changes corresponds to the quasi-harmonic (QH) description of crystals [37]. In this section, theory is held for benzene, naphthalene and anthracene comparatively as hydrocarbons. Benzene, naphthalene and anthracene are assumed as a system of harmonic oscillators and the Helmholtz free energy of this system is given by

$$F = U + \sum_i \frac{h\nu_i}{2} + k_B T \sum_i \ln \left[ 1 - \exp \left( -\frac{h\nu_i}{k_B T} \right) \right] \quad (3.13)$$

where  $i$  defines the modes of benzene, naphthalene and anthracene.  $k_B$  is the Boltzmann constant with the value of  $1.38 \times 10^{-23}$  J/K,  $h$  is the Planck constant,  $6.63 \times 10^{-34}$  Js and  $U$  is the total potential energy. Second term denotes zero point energy and the last term represents the thermal energy of crystal which depends on frequency of crystal. The last two terms define the vibrational contribution. The last two terms as vibrational were calculated in sub-sections, as given by

$$F_{vib} = \frac{1}{2} \sum_i h\nu_i + k_B T \sum_i \ln \left( 1 - \exp \left( -\frac{h\nu_i}{k_B T} \right) \right) \quad (3.14)$$

### 3.6.1 Calculation of the Vibrational Free Energy for Benzene

Frequency as a function of temperature is fitted to experimental data [12] to define the constants of  $d_0$ ,  $d_1$  and  $d_2$  of different six lattice modes of benzene as given in Table 3.9 in Section 3.2.1. Using the definition of free energy as a function of temperature (Equations (3.13)-(3.14)), free energy of solid benzene was calculated for all six lattice modes and their values are close to each other due to the six modes in benzene. At the end, total free energy was found at various temperatures for benzene. Figure 3.55 represents the behaviour of free energy of solid benzene under temperature.

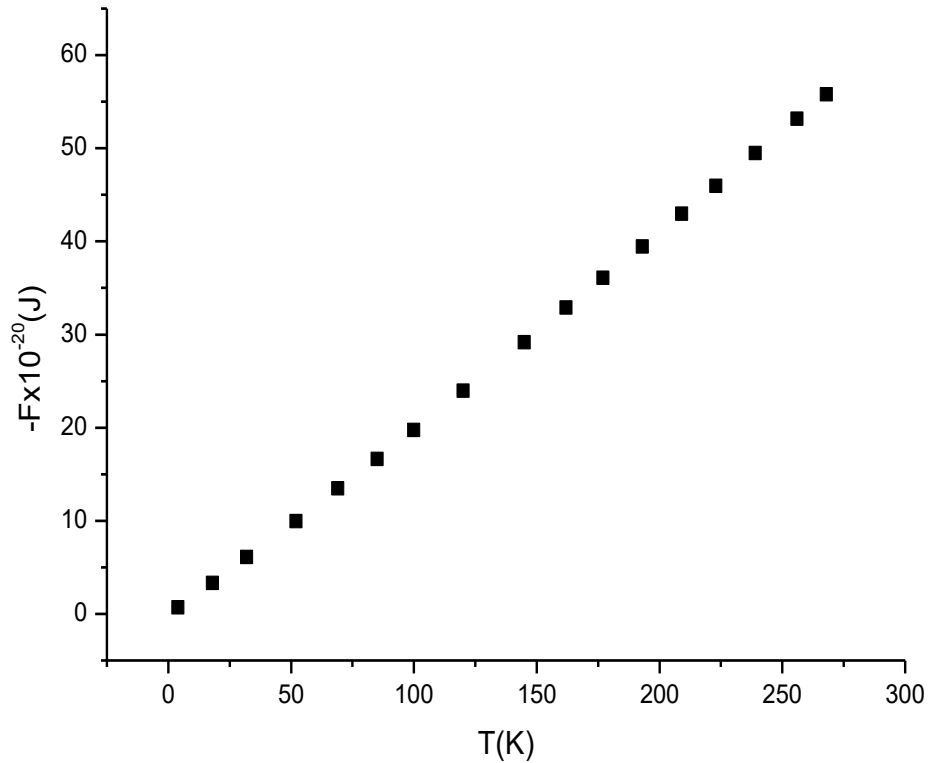


Figure 3. 55 Calculated total free energy of six lattice modes (A,B,C and X,Y,Z) of solid benzene under temperature.

### 3.6.2 Entropy Derived from the Vibrational Free Energy for Benzene

As is known from the thermodynamic relations entropy can be derived by using derivative of free energy (Equation (3.15)). In this section, first derivative of the temperature dependent free energy (Equation (3.16)) gets access to entropy of solid benzene. For six lattice modes total entropy of solid benzene was calculated at various temperature, as shown in Figure 3.56.

$$S = - \left( \frac{\partial F}{\partial T} \right)_V \quad (3.15)$$

$$S = -\frac{1}{2} h(b + 2cT)_i + \frac{e^{-\frac{h(a+bT+cT^2)_i}{k_B T}} k_B T \left( -\frac{h(b+2cT)_i}{k_B T} + \frac{h(a+bT+cT^2)_i}{k_B T^2} \right)}{1 - e^{-\frac{h(a+bT+cT^2)_i}{k_B T}}} - k_B \sum_i \ln \left( 1 - e^{-\frac{h(a+bT+cT^2)_i}{k_B T}} \right) \quad (3.16)$$

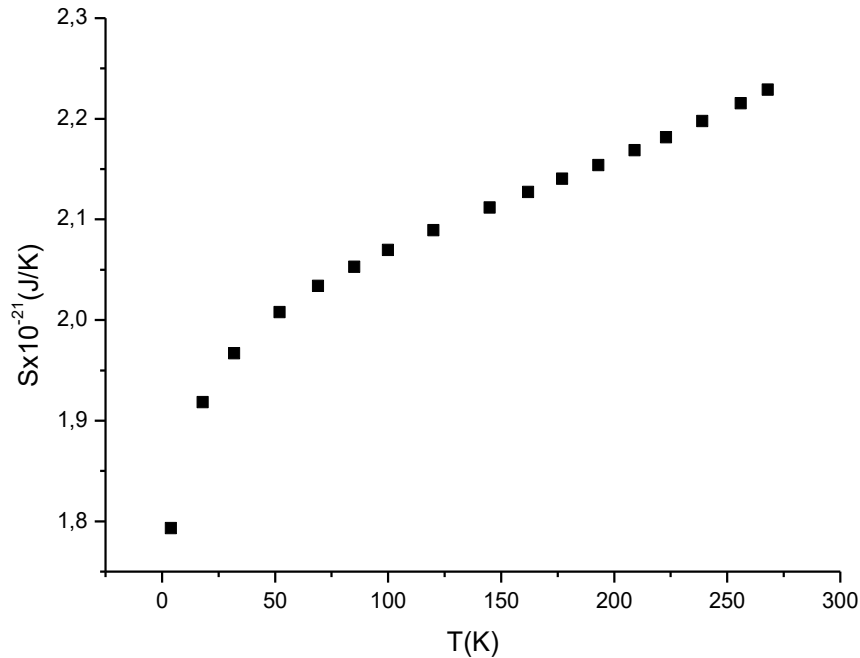


Figure 3. 56 Total entropy (Equation (3.16)) due to the six lattice modes (A,B,C and X,Y,Z) of solid benzene as a function of temperature.



### 3.6.3 The Heat Capacity at Constant Volume Derived from the Vibrational Free Energy for Benzene

It is possible to get heat capacity from the free energy using the thermodynamic relations as given in Equation (3.47). Using Equation (3.47) we obtained the heat capacity as a function of temperature as a new relation (Equation (3.48)). By using Equation (3.18), the heat capacity can be found as a function of temperature under various temperatures. Behaviour of the heat capacity of total six modes of solid benzene is given in Figure 3.57.

$$C_V = T \left( \frac{\partial S}{\partial T} \right)_V \quad (3.47)$$

$$C_V = -ch + \frac{e^{-\frac{h(a+bT+cT^2)_i}{k_B T}} k_B T \left( -\frac{2ch}{k_B T} + \frac{2h(b+2cT)_i}{k_B T^2} - \frac{2h(a+bT+cT^2)_i}{k_B T^3} \right)}{1 - e^{-\frac{h(a+bT+cT^2)_i}{k_B T}}} + \frac{2e^{-\frac{h(a+bT+cT^2)_i}{k_B T}} k_B \left( -\frac{h(b+2cT)_i}{k_B T} + \frac{h(a+bT+cT^2)_i}{k_B T^2} \right)}{1 - e^{-\frac{h(a+bT+cT^2)_i}{k_B T}}} + \frac{e^{-\frac{2h(a+bT+cT^2)_i}{k_B T}} k_B T \left( -\frac{h(b+2cT)_i}{k_B T} + \frac{h(a+bT+cT^2)_i}{k_B T^2} \right)^2}{\left( 1 - e^{-\frac{h(a+bT+cT^2)_i}{k_B T}} \right)^2} + \frac{e^{-\frac{h(a+bT+cT^2)_i}{k_B T}} k_B T \left( -\frac{h(b+2cT)_i}{k_B T} + \frac{h(a+bT+cT^2)_i}{k_B T^2} \right)^2}{1 - e^{-\frac{h(a+bT+cT^2)_i}{k_B T}}} \quad (3.48)$$

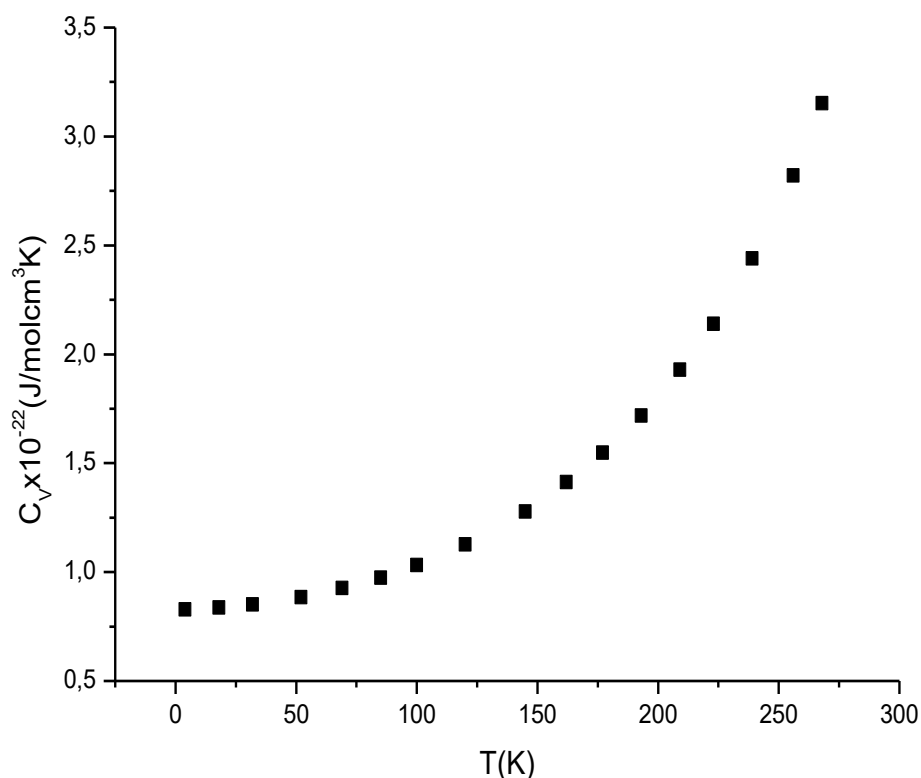


Figure 3. 57 Calculated total heat capacity (Equation (3.48)) of six lattice modes (A,B,C and X,Y,Z) of solid benzene as a function of temperature.

### 3.6.4 Analysis of Free Energy for Naphthalene

Frequency as a function of temperature was fitted to experimental data [37] to define the constants of  $d_0$ ,  $d_1$  and  $d_2$  of different six lattice modes of naphthalene as given in Table 3.11 in Section 3.2.2. Once the frequency of crystal was defined as a function of temperature, it is possible to calculate vibrational free energy (Equation (3.14)) of solid naphthalene at various temperatures. For all six lattice modes of solid naphthalene were analysed identically and at the end total vibrational free energy of six lattice modes of solid naphthalene was found out. Behaviour of free energy of six lattice modes of solid naphthalene as a function of temperature under temperature is given in Figure 3.58.

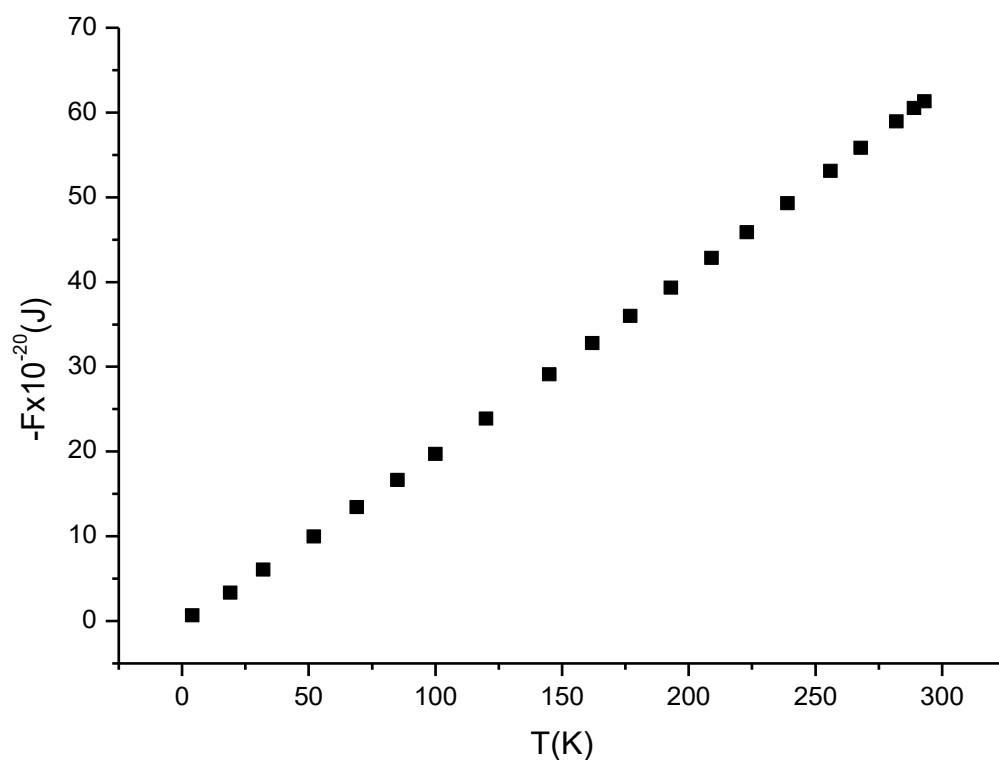


Figure 3. 58 Free energy due to the six lattice modes of solid naphthalene at various temperatures.

### 3.6.5 Derived Entropy by Free Energy for Naphthalene

After calculation of entropy according to Equation (3.16) individually, total entropy of six lattice modes of solid naphthalene was found. These values of total free energy of naphthalene are drawn graphically in Figure 3.59.

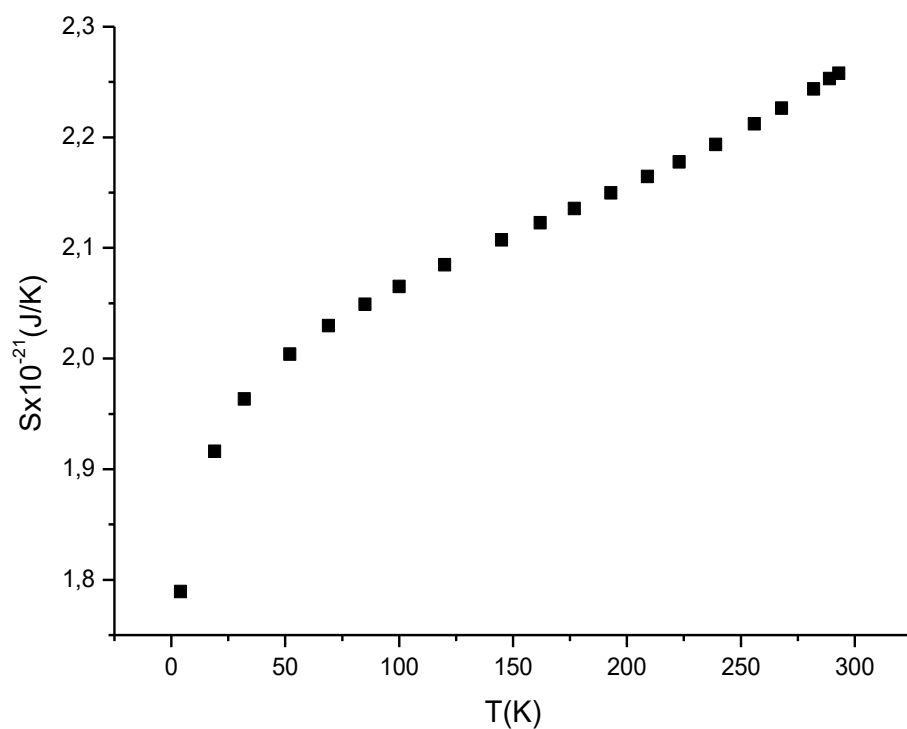


Figure 3. 59 Derived total entropy (Equation (3.16)) due to the six lattice modes of solid naphthalene as a function of temperature.

### 3.6.6 The Heat Capacity at Constant Volume Derived from the Vibrational Free Energy for Naphthalene

Total heat capacity was calculated due to the six lattice modes by using Equation (3.48) and its graph for naphthalene is given in Figure 3.60.

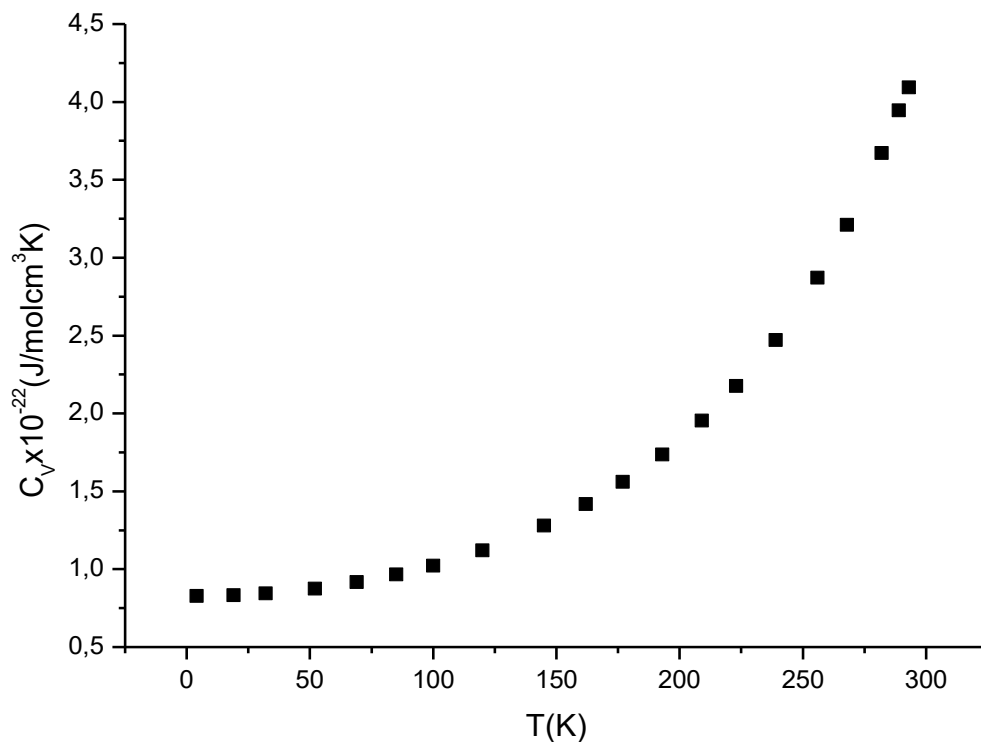


Figure 3. 60Calculated heat capacity as a function of temperature (Equation (3.48)) of solid naphthalene.

### 3.6.7 Calculation of the Vibrational Free Energy for Anthracene

The vibrational frequency was fitted to experimental data [43] to determine the constants of  $d_0$ ,  $d_1$  and  $d_2$  for six lattice modes of anthracene ( $P=0$ ) as given in Table 3.14 in Section 3.2.3.

Once the vibrational frequency of crystal was obtained as a function of temperature, it is possible to find the temperature dependence of the vibrational free energy (Equation 3.14) of solid anthracene. The six phonon and nine vibron modes of solid anthracene were analyzed identically and the total vibrational free energy due to the six phonon and nine vibron modes of solid anthracene was obtained. Behaviour of free energy due to the six phonon and nine vibron modes of solid anthracene is given as a function of temperature in Figure 3.61.

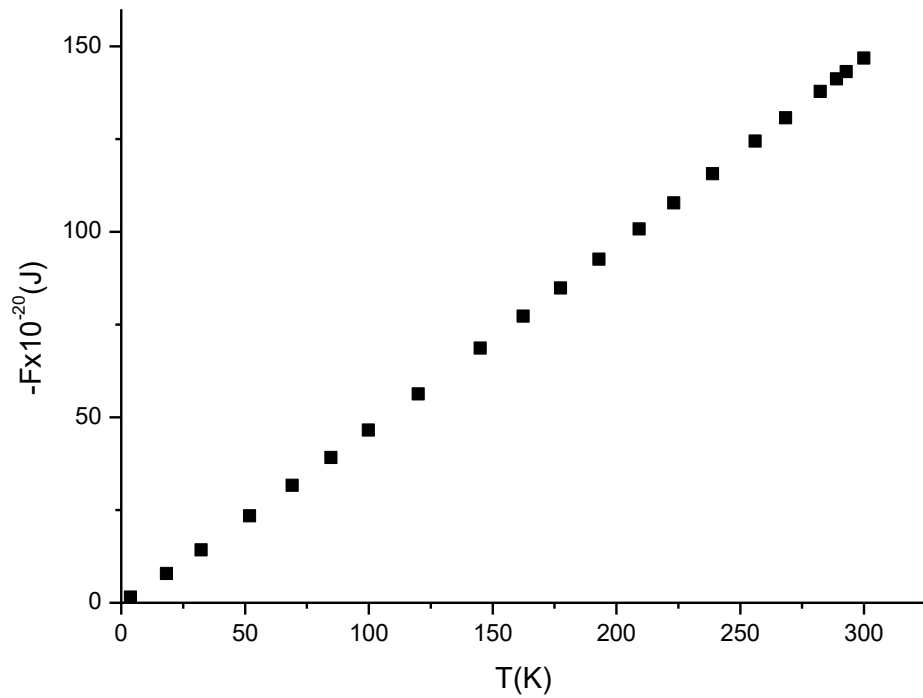


Figure 3.61 Vibrational free energy due to the six phonon and nine vibron modes of solid anthracene as a function of temperature according to Equation (3.14).

### 3.6.8 Entropy Derived from the Vibrational Free Energy for Anthracene

Total entropy of six lattice modes of solid anthracene was calculated (Equation (3.16)). In this section, we derive the entropy due to the six phonon and nine vibron modes of solid anthracene using the vibrational free energy. These values of total free energy of anthracene are shown graphically in Figure 3.62.

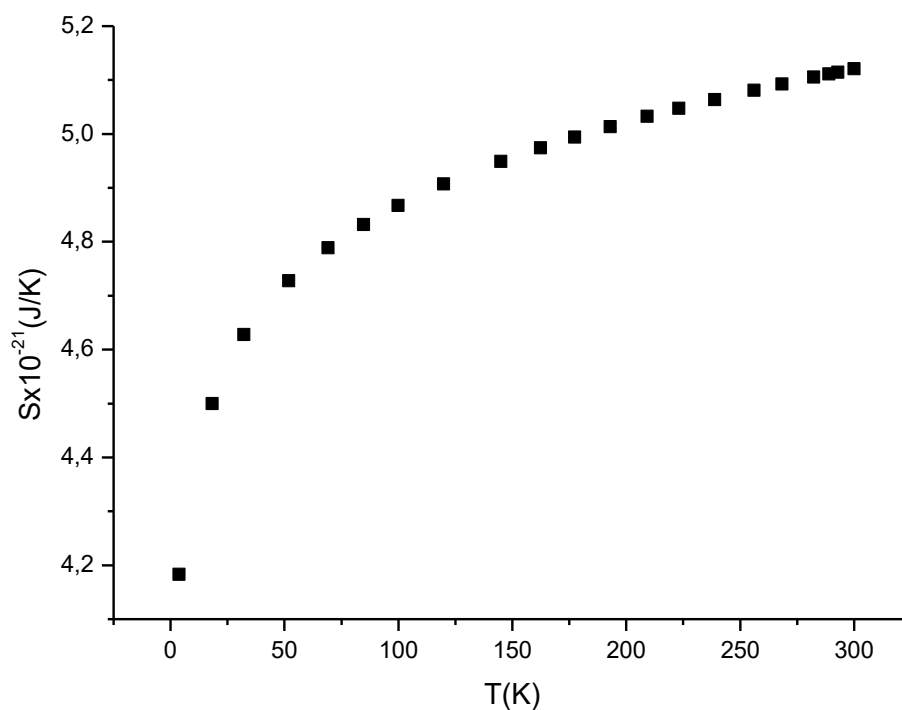


Figure 3. 62 The total entropy derived (Equation 3.16) due to the six phonon and nine vibron modes of solid anthracene as a function of temperature.

### 3.6.9 The Heat Capacity at Constant Volume ( $C_V$ ) Derived from the Vibrational Free Energy for Anthracene

Total heat capacity was calculated due to the six phonon and nine vibron modes of solid anthracene by using Equation (3.48) and a graph of total heat capacity of anthracene is given in Figure 3.63.

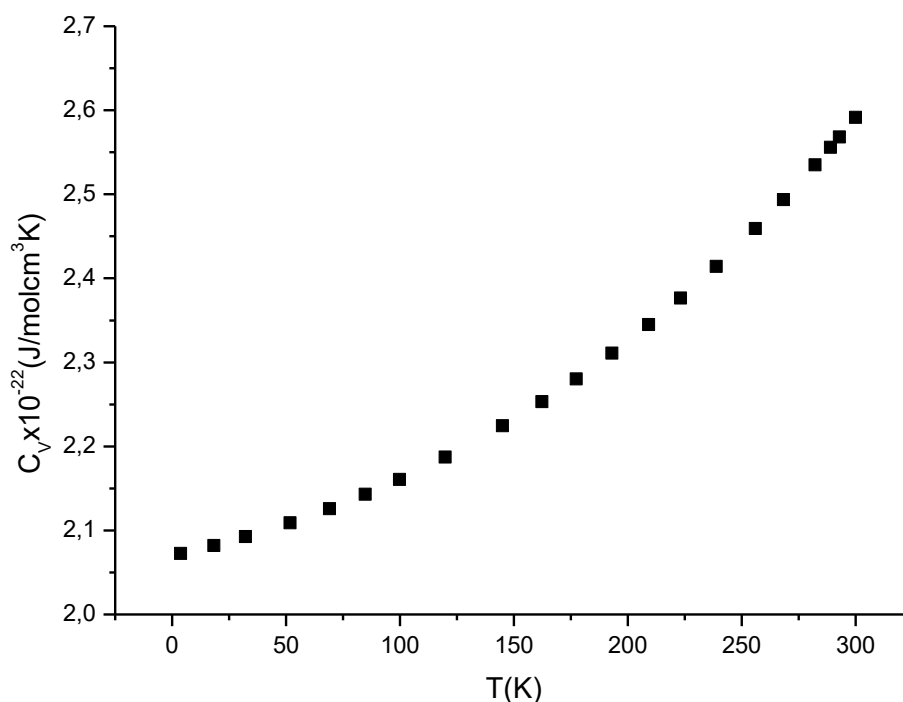


Figure 3. 63 The heat capacity  $C_V$  calculated as a function of temperature (Equation 3.48) due to six phonon and nine vibron modes of solid anthracene.

In this section thermodynamic properties of benzene, naphthalene and anthracene as in the same hydrocarbon groups were calculated through the quasi-harmonic approximation to the experimental data as a function of temperature and pressure. Quasi-harmonic free energy was discussed with the vibrational contribution to those hydrocarbons. In this approximation, anharmonic shifts population was neglected in the crystals of mentioned hydrocarbons. Vibrational free energy was calculated according to Equation (3.14) at zero pressure through the Raman frequency shifts as a function of temperature (Equation (3.4), Tables 3.13, 3.16 and 3.20). Vibrational free energy increases linearly with the increasing temperature or solid benzene, naphthalene and anthracene.

We derived the vibrational entropy (Equation 3.16) and it was calculated for solid benzene contributed and solid naphthalene contribution due to the six phonon modes and solid anthracene contributed due to the six phonon and nine vibron modes. The entropy behaves the same as solid anthracene, naphthalene and benzene. It increases



with increasing temperature for both (solid naphthalene and benzene) (Figures 56 and 59).

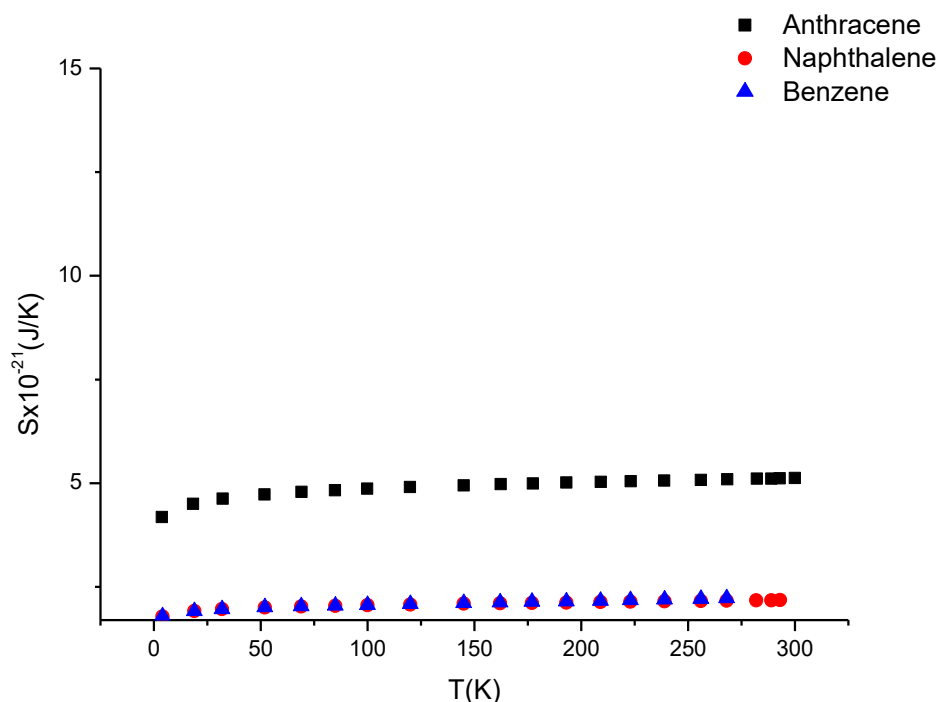


Figure 3. 64 The total entropy derived (Eq. 23) due to the six phonon and nine vibron modes of solid anthracene as a function of temperature. Solid naphthalene and benzene are also given in this figure for comparison. Squares are used for solid anthracene due to the six phonon and nine vibron modes, circles are used for solid naphthalene due to six lattice modes and triangles are used for solid benzene due to the six lattice modes.

As an another thermodynamic quantity, the heat capacity at constant volume ( $C_v$ ) was calculated according to Equation (3.48) through the temperature dependency of Raman frequency shifts for solid benzene, naphthalene and anthracene by considering contributions due to modes studied. The total heat capacity  $C_v$  of solid anthracene exhibits the same behaviour as a function of temperature in solid naphthalene and benzene (Figures 57,60) and also behaviour of the calculated vibrational heat capacity (Equation (3.48)) is consistent with the calculated heat capacity.

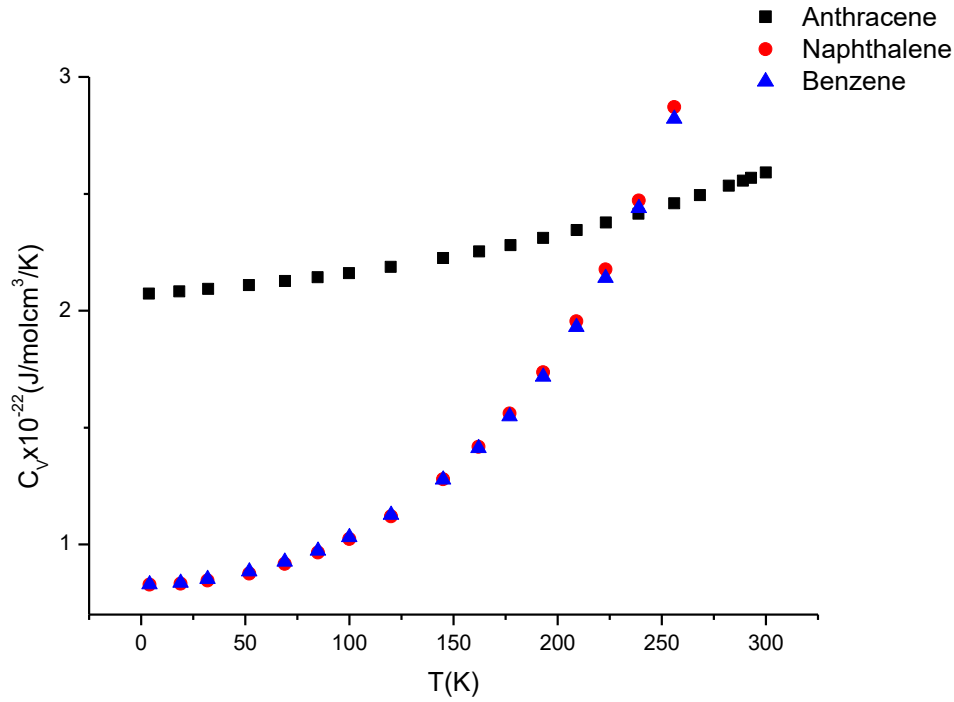


Figure 3. 65 Heat capacity calculated (Equation (3.48)) as a function of temperature for solid anthracene, naphthalene and benzene. Squares are used for solid anthracene due to the six phonon and nine vibron modes, circles are used for solid naphthalene due to six lattice modes and triangles are used for solid benzene due to the six lattice modes.

### 3.7 Application of Vinet Equation of State for Benzene at Constant Temperatures

Vinet equation of state is used to define the equation of state of molecular crystals, as given below:

$$P = 3B_0 \frac{(1-f_\theta)}{f_\theta^2} \exp \left[ \frac{3}{2} (C_0 - 1)(1 - f_\theta) \right] \quad (3.49)$$

where  $f_{\theta} = \left(V/V_0\right)^{1/3}$ . This equation depends on four quantities evaluated at zero pressure, the cell volume at ambient pressure  $V_0$ , the isothermal bulk modulus  $B_0$  and  $C_0$  which defines the derivative of the isothermal bulk modulus with respect to the pressure.

In this section, we first analyzed the observed data according to Equation (3.49). These data have been analyzed [11] previously for benzene at 540 K [11]. The observed data [11] has also been analyzed here using Vinet equation of state, as plotted in Figure 3.66.

By using Vinet equation of state with the experimental values of the pressure and volume at 540 K [11], the fitted values were obtained for the cell volume at ambient pressure  $V_0$ , the isothermal bulk modulus  $B_0$  and  $C_0$  which is the derivative of the isothermal bulk modulus with respect to the pressure.

Table 3. 18 Values of the cell volume at ambient pressure  $V_0$ , the isothermal bulk modulus  $B_0$  and  $C_0$  which is the derivative of the isothermal bulk modulus with respect to the pressure at 450 K.

BENZENE	$V_0 \left( \text{\AA}^3 \right)$	$B_0$ (GPa)	$C_0$
T= 540 K	$246.49 \pm 5.40$	$5.40 \pm 1.11$	$8.62 \pm 0.36$

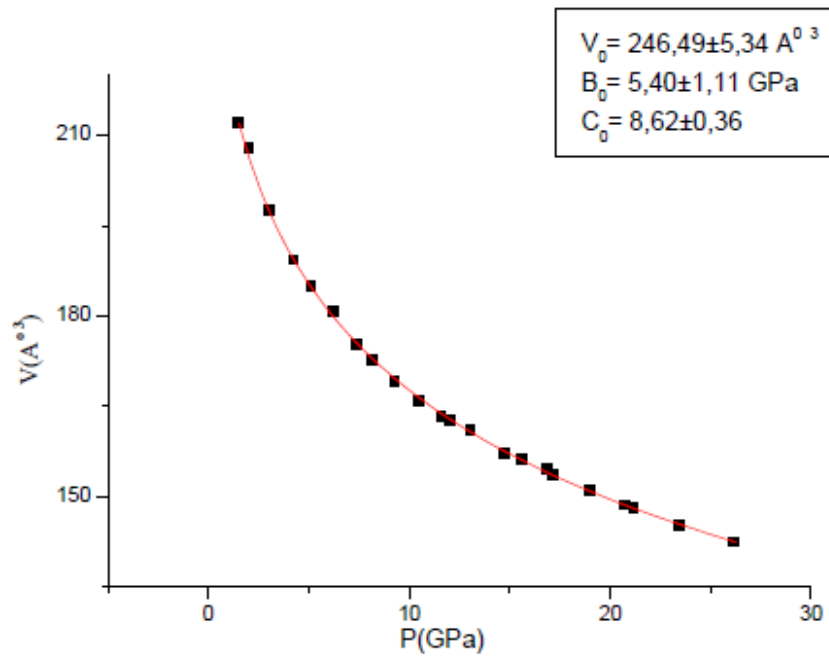


Figure 3. 66 Calculated equation of state according to Equation (3.49) of crystalline benzene at 540 K. Calculated equation of state (Equation (3.49)) is given with the solid line, experimental data [11] are given with the squares.

The fitted values of the cell volume at ambient pressure  $V_0$ , the isothermal bulk modulus  $B_0$  and  $C_0$  (the derivative of the isothermal bulk modulus with respect to the pressure) using the observed data [5] at room temperature are given in Table 3.22. Figure 3.67 gives our fit (Equation (3.49)) to the experimental data [15].

Table 3. 19 Values of the cell volume at ambient pressure  $V_0$ , the isothermal bulk modulus  $B_0$  and  $C_0$  (derivative of the isothermal bulk modulus with respect to the pressure at room temperature).

BENZENE	$V_0 \left( \text{\AA}^3 \right)$	$B_0 \text{ (GPa)}$	$C_0$
T= 300 K	$66.64 \pm 2.70$	$27.99 \pm 11.02$	$3.53 \pm 1.34$

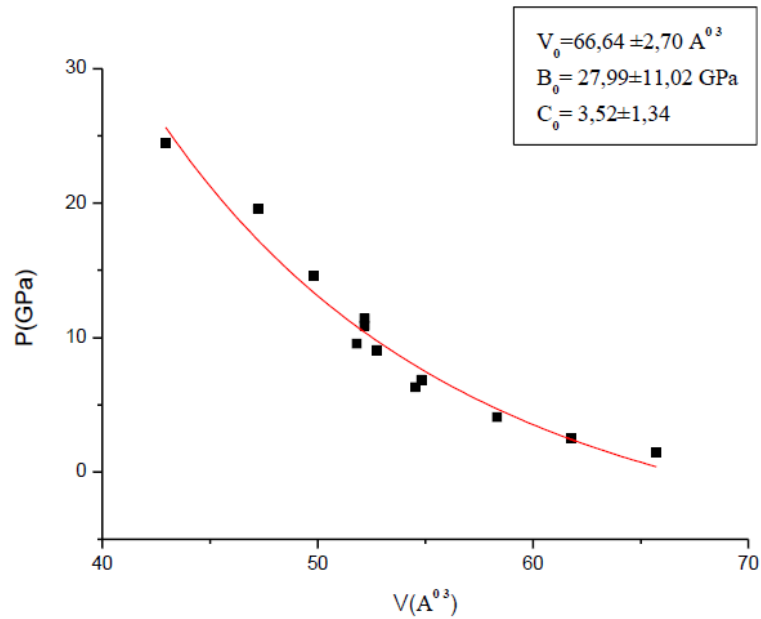


Figure 3. 67 Calculated equation of state according to Equation (3.49) of crystalline benzene at 300 K. Calculated equation of state (Equation (3.49)) is given with the solid line, experimental data [15] are given with the squares.

The change with pressure of the volume has been fitted by Vinet equation using the experimental data [11] at 540 K. This shows that the Vinet equation describes the observed [11] equation of state (P-V) for benzene at 540 K.

Similarly, the change with pressure of the volume has been fitted by Vinet equation using the experimental data [15] at room temperature. There is a good match between the observed [15] and calculated (Eq. 35) values for benzene at room temperature.

### 3.7 Suggested Phase Diagram in Phase I and Phase I' in Solid Benzene

A phase diagram is constructed through the Raman frequencies as a function of temperature and pressure in solid benzene between phase I and phase I'. Raman frequencies as a function of pressure were calculated according to Equation (3.3) at various pressures and similarly temperature dependence of the Raman frequencies were obtained according to Equation (3.4) for benzene. To define the T-P relations between phase I and phase I' we used a functional form in terms of Raman frequencies, temperature and pressure (Equation 3.50).

$$\vartheta_p(T) = \Delta\vartheta_0 + e_0\vartheta_T(P) + e_1T + e_2P \quad (3.50)$$

$\Delta\vartheta_0$  defines the difference between Raman frequency at zero pressure and room temperature. The coefficients  $e_0$ ,  $e_1$  and  $e_2$  in Equation 3.50 are given in Table 3.23 for six phonon modes of solid benzene. Using Equation 3.50, we calculated the temperature values corresponding to the various pressure ranges up to 1.48 GPa to describe the phase transition between phase I-I' as given in Figure 3.68.

Table 3.67 Coefficients  $e_0$ ,  $e_1$  and  $e_2$  as determined according to Equation (3.50) by using observed data [12] for six phonon modes of solid benzene. We also give here the difference between the calculated Raman frequency at zero pressure and room temperature.

BENZENE	$e_0$	$e_1$	$e_2$	$\Delta\vartheta_0$
Mode A	-0.28	0.61	-155.33	4.02
Mode B	0.73	0.25	-97.58	5.94
Mode C	-107.17	106.19	-19667.50	5.87
Mode X	0.063	0.42	-122.35	15.11
Mode Y	0.45	0.42	-139.80	13.45
Mode Z	0.44	0.45	-150.91	15.43

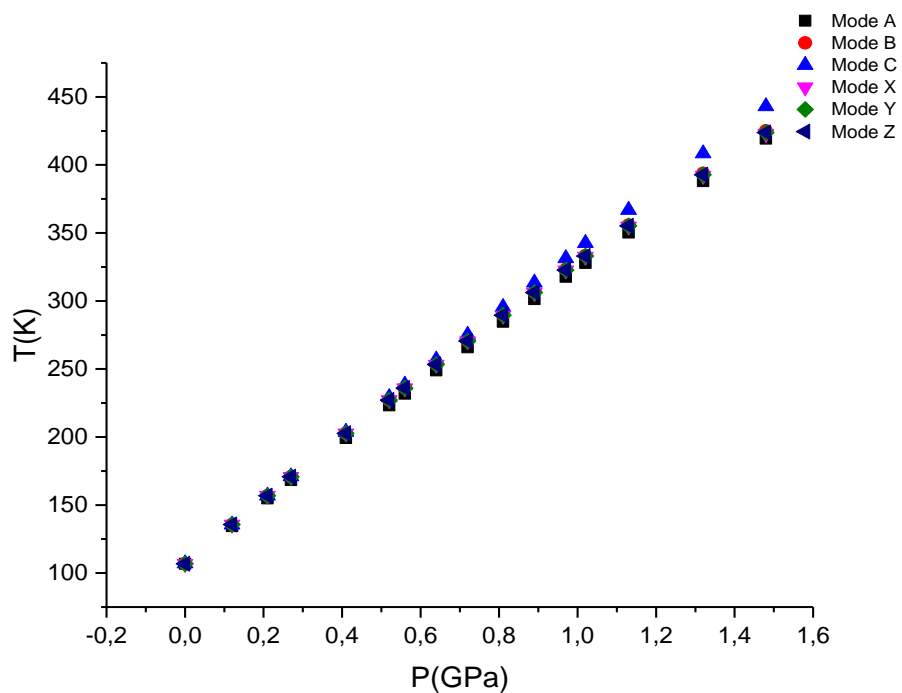


Figure 3.68 Suggested phase diagram due to Equation (3.50) for six phonon modes in phases I-I' in solid benzene.

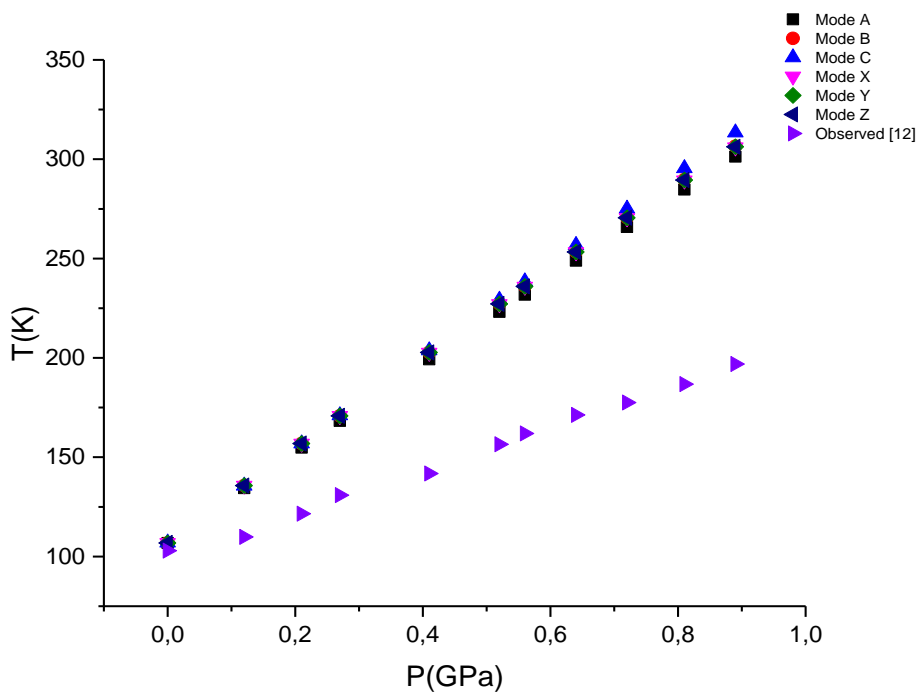


Figure 3.69 Calculated temperature as a function of pressure according to Equation (3.50) for six phonon modes in phases I-I' of solid benzene. Observed data [12] is also given comparison in here.

Temperature range was investigated as a function of pressure according to Equation 3.50 for six phonon modes (A,B,C and X,Y,Z) close to the phase transition between phases I and I' in solid benzene in Figure 3.68. Temperature values increase with increasing pressure contrary to the expected result. This is a special case for the transition between phase I and phase I', which is observed in the study of M. M. Thiery et. al. [12] as defined with a change in the structure of phase I upon relaxation 0 K. Our calculations exhibit the same behaviour with the observed data [12]. There is an increasing discrepancy through the higher pressures between the calculated and observed data. This can arise from the calculations using experimental data carried out through the experimental structure instead of released structure. Phase I' was predicted by a metadynamics method [81] and dft calculations [65] in literature which is in agreement with our calculations. Phase I' is not well-defined and it is not obvious that phase I' is an established phase or not. So phase I' needs to be supported by the experimental studies.



## CHAPTER 4

### CONCLUSIONS

The Raman frequency shifts were determined as functions of pressure and temperature through the isobaric and isothermal mode Grüneisen parameters at zero pressure and room temperature. The observed volume data were used in this calculation at various pressures and temperatures ( $P=0$ ) from the literature. This calculation was carried out for hydrocarbons of benzene, naphthalene and anthracene. Modes I, II ( $T= 300$  K) and III ( $T= 450$  K) in solid phase II of benzene were analyzed through the isothermal mode Grüneisen parameter at various pressures up to 16 GPa. The isothermal mode Grüneisen parameter decreases with the increasing pressure at constant temperature for phase II of benzene. Both pressure and temperature dependences of Raman frequencies were obtained for the six lattice modes (A,B,C and X,Y,Z) of solid benzene I using the volume data through the mode Grüneisen parameters. The isothermal mode Grüneisen parameter decreases with the increasing pressure for the lattice modes of solid benzene I. Six phonon modes ( $A_g$  and  $B_g$  modes) of solid naphthalene were obtained Raman frequency shifts as a function of pressure and temperature through the isobaric and isothermal mode Grüneisen parameters using the observed volume. The isothermal mode Grüneisen parameter has the value of 2.5 to 4 at room temperature whereas isobaric mode Grüneisen parameter is about 3 at zero pressure. The Raman frequency shifts were calculated through the Grüneisen parameter for six phonon and nine vibron modes for solid anthracene. Grüneisen parameter varies from 3 to 4 for phonon modes and they vary between 0.03 and 0.2 for vibron modes of solid anthracene. Calculated Raman frequencies as functions of pressure increase with the increasing pressure for benzene, naphthalene and anthracene, as expected. Calculated Raman frequencies decrease with increasing temperature for benzene, naphthalene and anthracene. Our calculated Raman frequencies with the pressure and temperature are in high agreement with the experimental data in general. Uncertainties in these

calculations are also given through the pressure and temperature dependence of observed Raman frequency shifts and volume data. Our calculating method of the Raman frequencies from the volume data, offers the thermal expansion  $\alpha_p$  and the isothermal compressibility  $\kappa_T$ , which can be estimated from the Raman frequency shifts  $\left(\partial\vartheta/\partial T\right)_p$  and  $\left(\partial\vartheta/\partial P\right)_T$  for the anharmonic hydrocarbon crystals studied here for as naphthalene, benzene and anthracene.

Heat capacity was calculated as a function of pressure and temperature through the isothermal and isobaric mode Grüneisen parameters by relating crystal volume to the frequencies of benzene, naphthalene and anthracene. Pressure dependence of heat capacity for benzene was carried out for six lattice modes (A,B,C and X,Y,Z) (T= 300 K) of solid benzene I. Calculated heat capacity contributed from the modes of solid benzene reduces with increasing pressure. There is a inconsistency between calculated and observed data through the higher pressure values. Calculated heat capacity can be compared with the experimental data when available in the literature for the phonon modes close to the I-II transition ( $P_C=1.3$  GPa and  $T_C=300$  K) for phonon modes of solid benzene. There is a discrepancy between the temperature dependence of calculated heat capacity and the observed data at low temperatures and at the higher temperatures calculated values almost follow the observed data. For the six phonon modes ( $A_g$  and  $B_g$ ) of solid naphthalene, heat capacity was calculated as functions of pressure and temperature. Our calculated data for solid naphthalene has a discrepancy at lower temperature range as compared with the observed data and it decreases at higher temperatures. Heat capacity was calculated for the six phonon and nine vibron modes of solid anthracene. Calculated values also give discrepancy as compared with the observed data at low pressures and temperatures and at the higher pressure and temperature ranges, this discrepancy decreases. Calculated heat capacity for benzene, naphthalene and anthracene as a function of pressure decreases with the increasing pressure. Calculated heat capacity increases with the increasing temperature for benzene, naphthalene and anthracene. This indicates that heat capacity can be calculated through the Raman frequency shifts in relation to the crystal volume. This method of calculating the heat capacity can be applied to other hydrocarbons.

Change in entropy ( $\Delta S = S_2 - S_1$ ) for benzene, naphthalene and anthracene was calculated by using an integration over temperatures from minimum to a maximum temperature. Calculated entropy increases as the temperature increases for benzene, naphthalene and anthracene. Calculated data are in a high agreement with the observed ones for the six phonon modes of solid naphthalene. There is a distinct discrepancy between the calculated and the observed data at low temperatures for the six phonon and nine vibron modes of solid anthracene and, they get closer at higher temperatures. Calculated data can be compared with experimental data when available for solid benzene.

In addition, heat capacity under various pressures at room temperature was calculated as an integral over pressures for benzene, naphthalene and anthracene. Calculated data agree well with the observed data and we find that the benzene, naphthalene and anthracene exhibit the same behaviour decreasing with the increasing pressures. This method of calculating entropy can also be applied to some other hydrocarbons.

Thermodynamic properties of benzene, naphthalene and anthracene were calculated through the quasi-harmonic approximation using experimental data as a function of temperature and pressure. Quasi-harmonic free energy was discussed with the vibrational contribution of hydrocarbons studied. Vibrational free energy was calculated for benzene, naphthalene and anthracene as a function of temperature and we find that the vibrational free energy increases with increasing temperature. Entropy was derived through the vibrational energy for benzene, naphthalene and anthracene. Entropy derived from the vibrational frequency exhibits an increasing behaviour with respect to the increasing temperature. Similarly, heat capacity was obtained by taking the derivative of vibrational frequency over temperatures for benzene, naphthalene and anthracene. Heat capacity increases with the increasing temperature range. We get similar behaviour in our all calculations for benzene, naphthalene and anthracene. When the experimental data are available in the literature, our calculations can be compared with the observed data for benzene, naphthalene and anthracene. It can then be generalized to all hydrocarbons.

The change with pressure of the volume has been fitted by Vinet equation using the experimental data at different temperatures. There is a good match between the observed and calculated values for benzene at various temperatures. This method can be applied to other hydrocarbons to obtain the equation of state of different crystals.

A phase diagram between phases I and I' is suggested for the six phonon modes of solid benzene using the pressure and temperature dependence of the Raman frequencies by means of the experimental data. For six phonon modes close to the phase transition between phase I and phase I' of solid benzene, we find that the temperature increases with pressure. Phase I' was suggested with a different structure (Cmca, Z=4) from phase I in the literature using the X-ray diffraction method as a second order phase transition. Our calculations show the same behavior as compared to the observed data and some other calculated data from the literature. Phase I' is not well characterized phase and need more detailed study for the transformation between the phases I and I'. When more experimental data are available in the literature, our calculations can be compared again. This calculations can be carried out for the other phase transitions in solid benzene to construct a phase diagram. Also, this method could be applied to some other hydrocarbons (naphthalene and anthracene).

The predictions and calculations are carried out in this thesis work is adequate to describe the thermodynamical quantities through the Raman frequency shifts for solid benzene, naphthalene and anthracene. All calculations can be applied for various modes and also for other phases of benzene, naphthalene and anthracene. More generally, a similar analysis can be applied to other hydrocarbons.

## REFERENCES

- [1] G. A. Olah and Á. Molnár, Hydrocarbon Chemistry (Wiley Interscience, Hoboken, NJ, 2003).
- [2] J. O. Sofo, A. S. Chaudhari, G. D. Barber, Phys. Rev. B 75 (2007) 153401.
- [3] F. Cansell, D. Fabre, J.P. Petitet, J. Chem. Phys. 99 (1993) 7300.
- [4] P. Figuiere, A.H. Fuchs, M. Ghelfenstein, H. Szwarc, J. Phys. Chem. Solids 39 (1978) 19.
- [5] R.G. Ross, P. Anderson, G. Backstrom, Mol. Phys. 38 (1979) 377.
- [6] Ph. Pruzan, D.H. Lienbenberg, R.L. Mills, J. Phys. Chem. Solids 47 (1986) 949.
- [7] H. Yurtseven, T. Unsal, Tsinghua Sci. Technol. 12 (2007) 624.
- [8] H. Yurtseven, T. Unsal, High Temp. Mater. Proc. 26 (2007) 365.
- [9] A.B. Pippard, The Elements of Classical Thermodynamics, Cambridge University Press, New York, 1957.
- [10] H. Yurtseven, A.S. Karakus, Int. J. Phar. Chem. Bio. Sci. 2 (2012) 729.
- [11] L. Ciabini, F.A. Gorelli, M. Santoro, R. Bini, V. Schettino, M. Mezovar, Phys. Rev.B72 (2005) 094108.
- [12] M.M. Thiery, J.M. Leger, J. Chem. Phys. 89 (1988) 4255.
- [13] M. Ghelfenstein, H. Szwarc, Mol. Crys. Liq. Cryst. 14 (1971) 273.
- [14] M. Ghelfenstein, H. Szwarc, Chem. Phys. Lett. 32 (1975) 93.
- [15] M.M. Thiery, J.M. Besson, J. Chem. Phys. 96 (1992) 2633.

- [16] Y.A. Sataty, A. Ron, M. Brith, Chem. Phys. Lett. 23 (1973) 500.
- [17] L. Ciabini, M. Santoro, R. Bini, V. Schettino, J. Chem. Phys. 115 (2001) 3742.
- [18] H. Özdemir and H. Yurtseven, J. Mol. Struc. 1080 (2015) 117.
- [19] A. J. Pertsin, A.I. Kitaigorodsky, The Atom–Atom Potential Method, Springer, Berlin, 1987.
- [20] M. El Hamamsy, S. Elnahwy, A.C. Damask, H. Taub, W.B. Daniels, J. Chem. Phys. 67 (1977) 5501.
- [21] E.L. Bokhenkov, E.M. Rodina, E.F. Sheka, I. Natkaniec, Phys. Status Solidi 85 (1978) 331.
- [22] E. Baharie, G.S. Pawley, Acta Crystallogr. A38 (1982) 803.
- [23] J.F.J. Jordan, A. Axmann, H. Egger, J. Kalus, Phys. Status Solidi (a) 71 (1982) 457.
- [24] J.P. McCullough, H.L. Finke, J.F. Messerly, S.S. Todd, T.C. Kincheloe, G. Waddington, J. Phys. Chem. 61 (1957) 1105.
- [25] R.D. Chirico, S.E. Knipmeyer, W.V. Steele, J. Chem. Thermodyn. 34 (2002) 1873.
- [26] D.A. Dows, L. Hsu, S.S. Mitra, O. Brafman, M. Hayek, W.B. Daniels, R.K. Crawford, Chem. Phys. Lett. 22 (1973) 595.
- [27] M. Hinenno, H. Yoshinaga, Spectrochim. Acta 31A (1975) 617.
- [28] E.F. Sheka, E.L. Bokhenkov, B. Dorner, J. Kalus, G.A. Mackenzie, I. Natkaniec, G.S. Pawley, U. Schmelzer, J. Phys. C: Solid State Phys. 17 (1984) 5893.

- [29] M. Nicol, M. Vernon, J.T. Woo, J. Chem. Phys. 63 (1975) 1992.
- [30] M. Backer, W. Hafner, W. Kiefer, J. Raman Spectrosc. 13 (1982) 247.
- [31] S.C. Capelli, A. Albinati, S.A. Mason, B.T.M. Willis, J. Phys. Chem. A 110 (2006) 11695.
- [32] D.E. Williams, J. Chem. Phys. 47 (1967) 4680.
- [33] T.L. Star, D.E. Williams, Acta Crystallogr. A 33 (1977) 771.
- [34] G. Filippini, A. Gavezzotti, Acta Crystallogr. B 49 (1993) 868.
- [35] H. Özdemir and H. Yurtseven, J. Mol. Struct. 1090 (2015) 65.
- [36] D.W.J. Cruickshank, Acta Crystallogr. 10 (1957) 504.
- [37] R.F. Della Valle, E. Venuti, A. Brillante, Chem. Phys. 198 (1995) 79.
- [38] J. M. Robertson, Proc R Soc A 140 (1933) 79.
- [39] A. I. Kitaigorodsky, Molecular crystals and molecules, (Academic, New York), 1973.
- [40] J. R. Ferraro, Vibrational spectroscopy at high external pressures, (Academic Press Inc, New York), 1984.
- [41] R. H. Warnes, J Chem Phys, 53 (1970) 1088.
- [42] V.K. Jindal, J. Kalus, J. Phys. C: Solid State Phys. 16 (1983) 3061.
- [43] L. Zhao, B. J. Baer, E. L. Chronister, J Phys Chem A 103 (1999) 1728.
- [44] H. Özdemir and H. Yurtseven, Ind. J. Pure App. Phys 54 (2016) 489.

- [45] R. Mason, *Acta Cryst*, 17 (1964) 547.
- [46] C. M. Gramaccioli, G. Flippini, M. Simonetta, S. Ramdos, G. M. Parkinson, J. M. Thomas, *J Chem Soc Faraday* 76 (1980) 1336.
- [47] M. Fukuhara, A. H. Matsui, M. Takeshima, *Chem Phys*. 258 (2000) 97.
- [48] C. P. Brock, J. D. Dunitz, *Acta Cryst B* 46 (1990) 795.
- [49] J. M. Leger, H. Aloualiti, *Solid State Commun*. 79 (1991) 901.
- [50] M. Oehzelt, R. Resel, A. Nakayana, *Phys Rev B* 66 (2002) 174104.
- [51] M. Oehzelt, G. Heimel, R. Resel, P. Puschnig, K. Hummer, C. A. Draxl, K. Takemura K, A. Nakayama, *J Chem Phys* 119 (2003) 1078.
- [52] S. N. Vaidya, G. C. Kennedy, *J Chem Phys* 55 (1971) 987.
- [53] K. Hummer, P. Puschnig, C. A. Draxl, *Phys Rev B* 67 (2003) 184105.
- [54] H. Yurtseven and H. Özdemir, *J. Mol. Struc.* 1090 (2015) 53.
- [55] M. Fujimoto, *The Physics of Structural Phase Transitions*, Springer Press, 2003.
- [56] J. Akella, G.C. Kennedy, *J. Chem. Phys.* 55 (1971) 793.
- [57] S. Block, C.E. Weir, G.J. Piermarini, *Science* 169 (1970) 586.
- [58] E.R. Andrew, R.G. Eades, *Proc. R. Soc.* 218A (1953) 537.
- [59] G.E. Bacon, N.A. Cury, S.A. Wilson, *Proc. R. Soc.* A279 (1964) 98.
- [60] E.G. Cox, *Rev. Mod. Phys.* 30 (1958) 159.



- [61] D.M. Adams, R. Appleby, Proc. R. Soc. London Ser. A 296 (1977) 1896.
- [62] Ph. Pruzan, J.C. Chervin, M.M. Thiery, J.P. Itie, J.M. Besson, J.P. Forgerit, M. Revault, J. Chem. Phys. 92 (1990) 6910.
- [63] L. Ciabini, M. Santoro, R. Bini, V. Schettino, Phys. Rev. Lett. 88 (2002) 085505.
- [64] <http://www.crystallography.net>, Last visited on 19 February 2017.
- [65] X. D. Wen, R. Hoffmann, N. W. Ashcroft, J. Am. Chem. Soc. 133 (2011) 9023.
- [66] A. Anderson, The Raman Effect, Marcel Dekker, Inc., New York, 1971 (Chapter 1 and Chapter 3).
- [67] C. Kittel, Introduction to the Solid State Physics, 2005 (Chapter 11).
- [68] S. Blundell, J. Katherine, M. Blundell, Concepts in Thermal Physics. Oxford University Press, (2008).
- [69] S. Kumar, S. K. Sharma and O. P. Pandey, J. Phys. 87 (2016) 21.
- [70] E. Grüneisen, Annals Physik, 12 (1912) 257.
- [71] F Birch, J. Geophys. Res. 91 (1986) 4949.
- [72] A.P. Ryzhenkov, V.M. Kozhin, Sov. Phys. Crystallogr. 12 (1968) 943.
- [73] C.P. Brock, J.D. Dunitz, Acta Crystallogr. B 38 (1982) 2218.
- [74] H. C. Alt, J. Kalus, Acta Crystallogr. B 38 (1982) 2595.

- [75] U. Schmelzer, E.L. Bokhenkov, B. Dorner, J. Kalus, G.A. Mackenzie, I. Natkaniec, G.S. Pawley, E.F. Sheka, J. Phys. C: Solid State Phys. 14 (1981) 1025.
- [76] R.F. Della Valle, E. Venuti, A. Brillante, Chem. Phys. 198 (1995) 79.
- [77] T. Aree and H. B. Burgi, J. Phys. Chem B 110 (2006) 26129-26134.
- [78] M. E. Fisher, Phys. Rev. 176 (1968) 257.
- [79] R. G. Ross, P. Andersson and G. Backstrom, Mol. Phys. 38 (1979) 527-533.
- [80] S. A. Kudchadker, A. P. Kudchadker and B. J. Zwolinski, J. Chem. Thermodynamics 11(1979) 1051-1059.
- [81] L Voadlo, J P Poirer and G D Price, Am. Miner. 85(2000) 390.

## CURRICULUM VITAE

### PERSONAL INFORMATION

Surname, Name: Özdemir, Hilal

Nationality: Turkish (TC)

Date and Place of Birth: 26 October 1981, Kayseri

Phone: +90 312 210 43 28

email: [mhilal@metu.edu.tr](mailto:mhilal@metu.edu.tr)

### EDUCATION

Degree	Institution	Year
B.S.	Selçuk University Physics Education	2006

### WORK EXPERIENCE

Year	Place	Enrollment
2008-Present Assistant	METU Department of Physics	Research
2014-2015 Researcher	University of Groningen,  Department of Chemistry	Visiting

## PUBLICATIONS

1. H. Özdemir and H. Yurtseven, “ Pressure dependence of the Raman frequencies for the modes I, II and III at constant temperatures in phase II of benzene”, Journal of Molecular Structure, 2015, doi: 10.1016/j.molstruc.2014.09.057
2. H. Yurtseven and H. Özdemir, “ Calculation of the specific heat using the Raman frequency shifts for the solid I-II transition in benzene”, Journal of Molecular Structure, 2015, doi:10.1016/j.molstruc.2014.12.016
3. H. Özdemir and H. Yurtseven, “ Raman frequency shifts calculated from the volume data in naphthalene”, Journal of Molecular Structure, 2015, doi: 10.1016/j.molstruc.2014.12.035
4. H. Özdemir and H. Yurtseven, “ Temperature and pressure dependence of the Raman frequency shifts in anthracene”, Indian Journal of Pure & Applied Physics, 2016, Vol. 54, 489-494.